# DYNAMICS OF JOSEPHSON JUNCTION ARRAYS

# A DISSERTATION SUBMITTED TO THE DEPARTMENT OF APPLIED PHYSICS AND THE COMMITTEE ON GRADUATE STUDIES OF STANFORD UNIVERSITY IN PARTIAL FULFILLMENT OF THE REQUIREMENTS FOR THE DEGREE OF DOCTOR OF PHILOSOPHY

By Peter Hadley March 1989

## Acknowledgements

I would like to acknowledge Mac Beasley, Kurt Wiesenfeld, and Bernardo Huberman who provided the advice and assistance necessary to complete this thesis.

I would also like to thank my wife Silvia for her patience and support. Thanks Schatzl.

#### **Abstract**

The dynamics of Josephson junction arrays is a topic that lies at the intersection of the fields of nonlinear dynamics and Josephson junction technology. The series arrays considered here consist of several rapidly oscillating Josephson junctions where each junction is coupled equally to every other junction. The purpose of this study is to understand phaselocking and other cooperative dynamics of this system. Previously, little was known about high dimensional nonlinear systems of this sort. Numerical simulations are used to study the dynamics of these arrays. Three distinct types of periodic solutions to the array equations were observed as well as period doubled and chaotic solutions. One of the periodic solutions is the symmetric, in-phase solution where all of the junctions oscillate identically. The other two periodic solutions are symmetry-broken solutions where all of the junctions do not oscillate identically. The symmetry-broken solutions are highly degenerate. As many as (N-1)! stable solutions can coexist for an array of N junctions. Understanding the stability of these several solutions and the transitions among them is vital to the design of useful devices.

From the technological point of view the most useful dynamical state of the junction arrays is the in-phase state where all of the junctions oscillate identically. A detailed analysis of the stability of the in-phase state is given and the fluctuations about the in-phase state are described. Using this analysis a proposal is made for the design of a generator of millimeter wave radiation that maximizes the stability of the in-phase state. The other technological application that is discussed is parametric amplification. The relation between the instabilities of this system and the process of

parametric amplification is described and a proposal is made for the design of a high gain parametric amplifier that exploits a previously undocumented instability of this system.

# Table of Contents

1. Introduction	1
2. Review	6
3. The Dynamical States	18
4. Stability Analysis of the In-phase Solution	32
5. Transitions Between Solution	<b>4</b> 5
6. Noise Driven Fluctuations of the In-phase Solution	54
7. Parametric Amplifiers	65
8. Nonidentical Junctions	70
9. Coupled 1-d Arrays, 2-d Arrays, and 3-d Arrays	74
10. Conclusions	86
Appendices	
A: The nature of chaos	88
B: Stability of N-dimensional solutions	95
C: Some mathematical details	98
Poforongos	101

# List of Figures

2.1	Schematic of a Josephson junction	7
2.2	Circuit Diagram for a single shunted junction	7
2.3	Snapshots of the phase of a junction	10
2.4	Current-Voltage curves for two exact solutions	11
2.5	Current-Voltage curves for a junction with an rf bias current .	13
2.6	Circuit diagram for a series array of Josephson junctions	14
3.1	Sets of snapshots of the phases of N junction arrays	21
3.2	Time series of the supercurrents	22
3.3	Power spectra of the voltage oscillations	23
3.4	Movies of the Split solution	28
3.5	Phase portraits of a two junction array	30
<b>4</b> .1	Contours of the largest real part of the Floquet exponents	37
4.2	Coherence plotted against time	42
5.1	The three generic, codimension-one bifurcations	46
5.2	Current-Voltage curves for three junction arrays	48
5.3	Phase portraits of the dynamics	49
5.4	Current-Voltage curve for a three junction array	51
6.1	Representation of the in-phase solution in phase space	57
6.2	Power spectrum of the total voltage	63
7.1	Circuit diagram of a parametric amplifier	68
8.1	Movie of the solution foe arrays with 100 junctions	71
9.1	More complex Josephson junction arrays	75
9.2	A coupled 1-d array with a shunt impedance	78
9.3	A 2-d array of Josephson junctions	80
9.4	Current-Voltage curve showing steps in the voltage	84
<b>A</b> 1	Random number generators use stretching and folding	90
A2	Chaotic solution of a two junction array	91
А3	Poincare section of a chaotic solution	92

#### §1. Introduction

In 1962 Josephson<sup>1</sup> first considered the tunnelling of Cooper pairs of electrons between superconductors as a perturbation to the conventional description of superconductivity. Based on that calculation he predicted two startling new effects.

- (i) For zero voltage difference between two weakly coupled superconductors a dc current can flow, up to a maximum current,  $I_{C}$ .
- (ii) When a finite voltage is maintained between the superconductors, an oscillating current appears of amplitude  $I_C$  and frequency 2eV/h. Here V is the voltage, e is the charge of an electron, and h is Planck's constant.

These are now known as the dc and ac Josephson effects. Shortly after Josephson predicted these effects their existence was verified experimentally.<sup>2</sup> Researchers now routinely construct devices (called Josephson junctions) that exploit these effects.

Several mathematical models have been developed to describe the dynamics of Josephson junctions. In the simplest model a single junction obeys the same equations as those for a pendulum. In the seventies it was discovered that this deceptively simple looking model could exhibit complicated and sometimes bizarre dynamics. Because of the rich dynamics that the Josephson junctions can exhibit, they became an experimental testing ground for the new concepts that were being developed in the field of low dimensional nonlinear dynamics.<sup>3</sup>

In recent years the understanding of the nonlinear dynamics of low dimensional systems has greatly increased and the focus of the research in

nonlinear dynamics has turned to high dimensional systems. Traditionally, the high dimensional systems that have been studied were constructed by coupling many low dimensional systems together. Groundbreaking work along these lines was done in 1955 by Fermi, Pasta, and Ulam<sup>4</sup> who studied a system of sixty-four harmonic oscillators with cubic coupling. They intended to show that the anharmonicity would cause an even distribution of the energy among the oscillators. This was to be used to justify the ergodic hypothesis of statistical mechanics. The computer experiments showed that the energy was not evenly distributed but rather the system acted more like uncoupled harmonic oscillators. This puzzling result was eventually explained by Kolmogorov, Arnold, and Moser who showed that weak anharmonic coupling would not distribute the energy evenly among a set of oscillators.<sup>5</sup> This early work foreshadowed the complexity that was later observed in other coupled oscillator systems such as coupled pendula, anharmonic oscillators, coupled logistic maps, and coupled circle maps.6 Here we continue in this tradition by considering arrays of many coupled Josephson junctions. These are systems of identical, driven, dissipative oscillators which are highly connected. Here every junction is coupled equally to every other junction of the array.

Like its predecessors the system studied here exhibits several interesting dynamical features. For example, we will show that instabilities in the dynamics of the junction arrays arise in which many symmetries of the equations are simultaneously broken. After this instability as many as (N-1)! stable solutions appear, where N is the number of junctions in the array. With this tremendous number of solutions crowded into phase space, these systems are highly sensitive to external noise. Even for relatively modest sized arrays of 100 junctions, the 99! stable solutions would be far too many to detect using a conventional computer. This

shows that care must be taken in interpreting numerical simulations of high dimensional systems.

Apart from the fundamental aspects of high dimensional systems, Josephson junction arrays need to be understood because they are used in practical applications. For instance, the National Bureau of Standards uses series arrays of up to 1500 Josephson junctions to define the U. S. standard volt. Josephson junction arrays have also been considered in applications as oscillators, mixers, and amplifiers. In these applications the arrays generate and manipulate millimeter wave radiation. There is a program now underway in Europe to build a receiver for far infrared astronomy based on Josephson junction arrays. In the U. S. arrays are being developed for use as local oscillators in terahertz analog circuitry. In order to design a high dimensional system, such as a junction array, it is important to understand the dynamics of that system and especially to understand the dynamical instabilities that can occur.

In this work most of the discussion focuses on series arrays of Josephson junctions. Series arrays have a potential application as millimeter wave generators. In this application the oscillating supercurrents which arise from the ac Josephson effect are the source of the radiation. Each junction must oscillate identically so that the radiation from each junction adds coherently. Consequently, the phaselocking of the junctions and the stability of this coherent state will be discussed in detail.

This thesis is organized as follows. In section 2 the equations that model Josephson junction arrays are introduced and the limitations of this model are discussed. This work is also contrasted with previous work on Josephson junction arrays, most notably that of Likharev and his coworkers.

In section 3 the dynamics of series arrays coupled to various loads are described. Three distinct types of periodic solutions are observed as well as period doubled solutions and chaotic solutions. One of the dynamical states that is observed is the in-phase state in which all of the junctions oscillate identically. In section 4, a stability analysis of the in-phase state is presented. This analysis demonstrates the existence of the in-phase state in a broader parameter range than had been appreciated previously. This result is already being applied by groups designing and constructing practical arrays. The numerical results of this analysis also extend the previous work by providing a quantitative measure of the stability of the in-phase solution. This section concludes with specific recommendations for designing arrays which maximize the stability of the in-phase state.

Section 5 discusses the observed transitions between the dynamical states using the language of bifurcation theory. The high symmetry of the arrays causes some unusual bifurcations in which many Floquet exponents cross the imaginary axis simultaneously. After one of these bifurcations occur, there are many coexisting stable solutions. Building on the results of the two sections preceding it, section 6 discusses the fluctuations to the in-phase state. Here it is shown that there are two fundamentally different types of fluctuations and that both types increase near a bifurcation. Section 7 discusses parametric amplification from a modern perspective. This point of view helps explain why parametric amplifiers made out of Josephson junctions arrays have had only limited success in the past. A proposal is made on how to construct a high gain parametric amplifier using one of the new bifurcations discovered here.

Throughout most of this work each junction of an array was assumed to be identical. Section 8 discusses modifications to these results that must be made when all of the junctions are no longer identical. It is shown that the in-phase state still exists when the junctions are no longer identical. Section 9 discusses the in-phase oscillations of coupled 1-d arrays, 2-d arrays, and 3-d arrays. Ironically it is often easier to determine the stability for the in-phase solution to the more complex arrays than it is for the series arrays. This is because a symmetry of the in-phase solution prevents it from being stable. We suggest ways to stabilize the in-phase solution in these arrays by altering the system. Finally, some of the results presented in sections 3,4,5,6, and 8 can be found in our previously published work.<sup>9-13</sup>

#### § 2. Review

Josephson junctions are constructed by arranging two superconductors so that they are weakly coupled. Typically the two superconductors are separated by some nonsuperconducting material or barrier (see Fig. 2.1). The simplest approximation for the supercurrent between weakly coupled superconductors is  $I_S=I_C\sin(\phi)$ . Here  $I_C$  is the critical current which depends on the temperature, the magnetic field applied, the geometry of the superconductors and of the barrier, and on the materials used. The quantity  $\phi$  is the difference in the phases of the quasiclassical superconducting wave functions of the two superconductors. Because  $\sin(\phi)$  is limited to the range,  $-1 < \sin(\phi) < 1$ , the supercurrent flowing through the barrier can never be less than  $-I_C$  and can never be greater than  $I_C$ .

A statement of the ac Josephson effect is that the supercurrent oscillates with an angular frequency of 2eV/ħ. Mathematically this statement relates the voltage across the junction to the phase difference,

where the dot denotes a derivative with respect to time. In addition to the supercurrent there may also be a normal current passing through the barrier. Assuming that this current is proportional to the voltage, (Ohm's law) the normal current flowing through the barrier is  $I_n = V/R_N = \hbar \dot{\phi}/(2eR_N)$ , where  $R_N$  is the normal resistance of the barrier. Finally, because of the geometry of the junction, there is a capacitance, C. The charge collecting on this capacitor corresponds to a current of  $I_{cap} = C\dot{V} = \hbar C\dot{\phi}/(2e)$ . By Kirchhoff's laws, these three currents must equal the bias current applied to the junction,  $I_S + I_n + I_{cap} = I$ . Thus the dynamics of a single junction can be modeled by the differential equation,

$$\frac{\hbar C \ddot{\phi}}{2e} + \frac{\hbar \dot{\phi}}{2eR_N} + I_c sin(\phi) = I$$
 2.2

This equation is called the shunted junction model which was first discussed by Stewart and McCumber. 14 The circuit diagram that represents this equation is shown in Fig. 2.2. Here the X represents the superconductive tunnelling channel. More sophisticated models can be constructed by including corrections to the supercurrent or by using a more realistic, voltage dependent, resistance for the normal current.

Nevertheless, the shunted junction model is a good approximation for a Josephson junction and it will be used throughout this work. For a more complete discussion of Josephson junctions see the books by Likharev 15 and by Van Duzer and Turner. 16

It is convenient to normalize Eqn. 2.2 to reduce the number of constants. Dividing the equation by  $I_C$  and rescaling time so that it is measured in units of  $\hbar/2eI_CR_N$ , puts this equation into the form,

$$\beta_c \ddot{\phi} + \dot{\phi} + \sin(\phi) = I_B(t)$$
 2.3

where  $I_B$  is the normalized bias current,  $I_B=I/I_C$ , and  $\beta_C$  measures the ratio of inertia to dissipation in the system,  $\beta_c=(2eI_cR_N^2C)/\hbar$ . In this form it is clear that the model for a Josephson junction is equivalent to a damped driven pendulum with a mass of  $\beta_C$  and damping coefficient equal to 1.

The simplest solution to Eqn. 2.3 is the stationary solution. This solution can only occur when the bias current,  $I_B$ , is a constant less than one. In this case the junction reaches a time independent steady state,  $\sin(\phi)=I_B$ , corresponding to a motionless pendulum. In this solution,  $\dot{\phi}=0$  so there is no voltage across the junction even though there is a current,  $I_B$ , flowing through it. This solution represents the dc Josephson effect. As  $I_B$  is

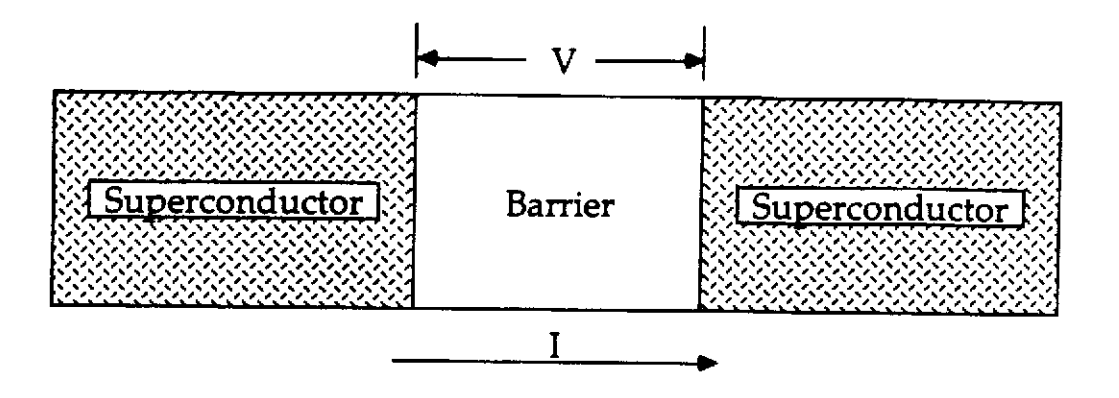


Fig. 2.1 - Schematic of a Josephson junction.

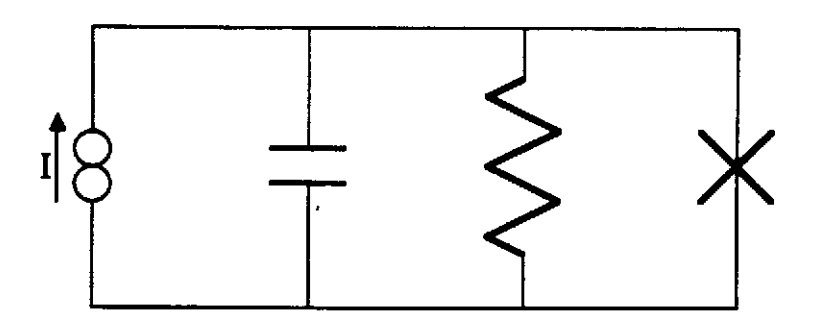


Fig. 2.2 - Circuit diagram for the shunted junction model of a single Josephson junction driven by a bias current, I.

increased above one the stationary state loses stability and a periodic solution appears.

In terms of the pendulum analogy a periodic solution corresponds to a rotating pendulum. Figure 2.3 shows a sequence of snapshots of the phase of a junction exhibiting a periodic solution. The phase is measured as the angle from vertical as it would be for a pendulum. Viewed successively from left to right these snapshots form a movie of the phase motion.

For a constant bias current, exact solutions for the periodic states are known in the two extremes,  $\beta_C=0$  and  $\beta_C\to\infty$ . For  $\beta_C=0$  the solution is,

$$\varphi(t) = 2 \tan^{-1} \left[ \frac{\xi \tan(\xi t/2)}{I_B} + 1 \right]; \qquad \xi = \sqrt{I_B^2 - 1}$$
 2.4

and in the limit of very large  $\beta_{C}$ ,

$$\varphi(t) = I_B t 2.5$$

For other values of  $\beta_C$  and  $I_B$  approximate solutions can be determined numerically or by perturbation theory. In some cases more than one solution is stable for the same parameter values. For example, when  $\beta_C>>1$  and  $I_B<1$  both the periodic solution and the stationary solution are stable. Which solution appears depends on the initial conditions of the junction. Multiple stable solutions such as this often manifest themselves as hysteresis loops in a plot of the observables. Figure 2.4a shows the voltage plotted against the current for a junction with  $\beta_C>>1$ . Notice that there are two possible voltages for every current less than  $I_C$ . For comparison Fig. 2.4b shows the nonhysteretic current-voltage characteristics (I-V) of a junction with  $\beta_C=0$ . Plots of the I-V curves are a common way of viewing experimental data on Josephson junctions. In this work the results of the calculations will sometimes be presented as I-V curves to in order to facilitate comparison with experiments.

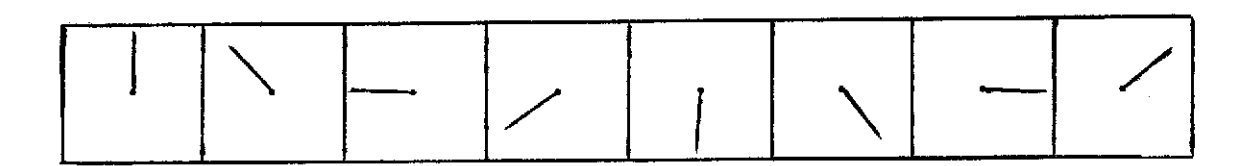
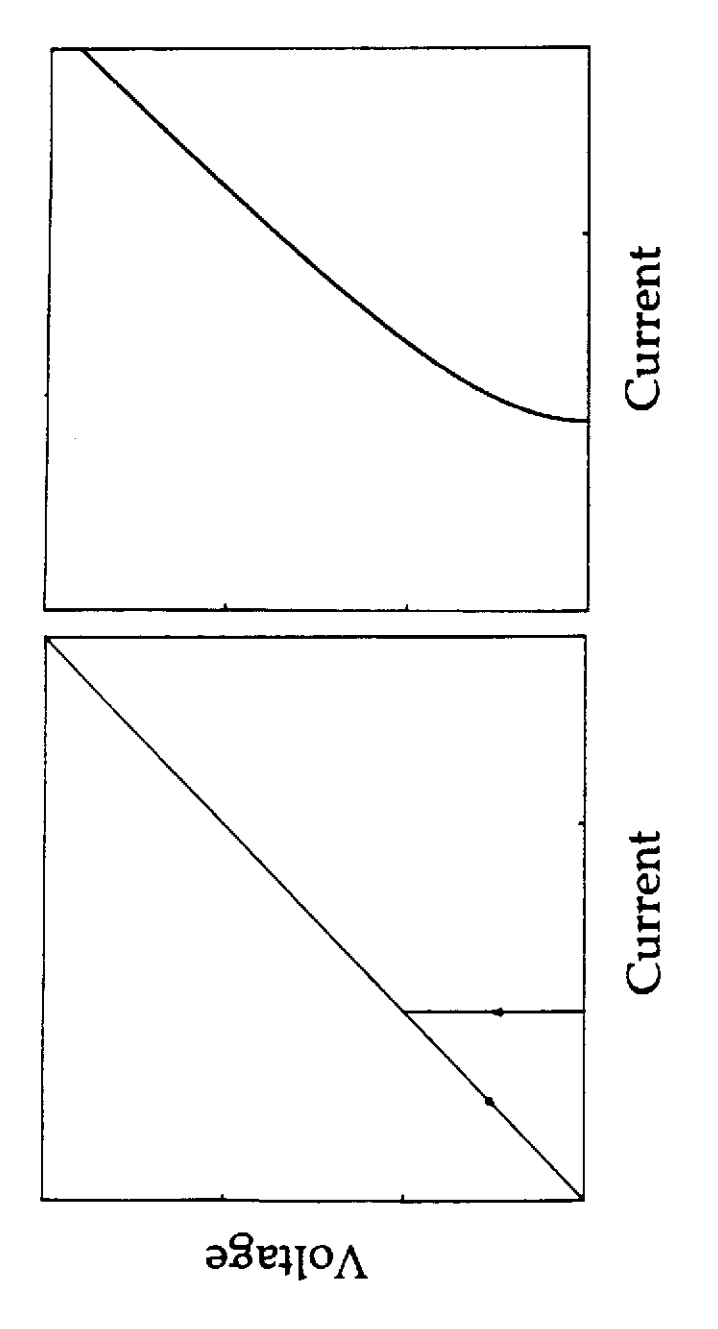


Fig. 2.3 - Snapshots of the phase of a junction at eight points in the cycle. Viewed successively form left to right they form a movie of the phase motion.



nonhysteretic solution for  $\beta_c$ =0.

As the parameters are further varied all periodic solutions to Eqn. 2.3 can lose stability and a chaotic solution may appear. When this happens any perturbative approach breaks down and the solutions must be calculated by numerical integration. Chaos and the breakdown of perturbation theory are discussed in appendix A.

Another interesting phenomena that Josephson junctions exhibit is phaselocking. External phaselocking is the synchronization of the oscillating supercurrent with a periodic bias current. Figure 2.5 is an experimental I-V curve which shows the phaselocking of a Josephson junction to an external ac drive. When the junction is phaselocked, its frequency, and therefore its voltage, remain constant. This results in the flat steps that appear in the I-V curve.<sup>17</sup> These are called Shapiro steps and are used to define the U. S. standard volt. This type of external phaselocking is discussed in standard texts on synchronous motors and phaselocked loops.<sup>18</sup> The existence of external phaselocking suggests that it may be possible for the junctions to mutually phaselock. In this case there is no externally fixed frequency but the interactions among the oscillators cause them to synchronize. It is the mutual phaselocking among the junctions of an array that we will be concerned with here.

#### <u>Arrays</u>

Many different arrays can be constructed by connecting Josephson junctions together but for most of this work our attention will be focused on series arrays of junctions shunted by a load impedance. Only simple passive loads are considered here such as resistors, capacitors, and inductors, or combinations of these. The general circuit diagram of the array we are considering is shown in Fig. 2.6. When the constant bias current exceeds the

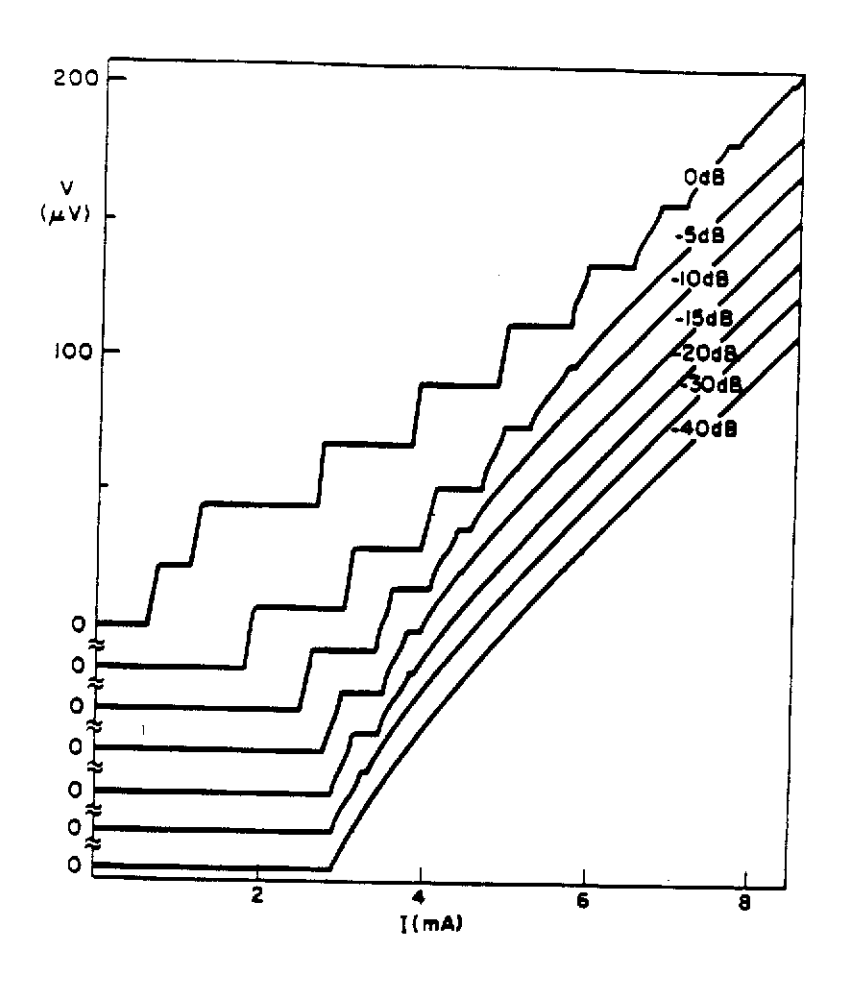


Fig. 2.5 Current-Voltage curves of a single Josephson junction with an external rf bias current. The flat steps in the voltage correspond to the ranges where the junction is phaselocked to the drive frequency. (From A. de Lozanne, Ph. D. Thesis, Stanford University, 1982).

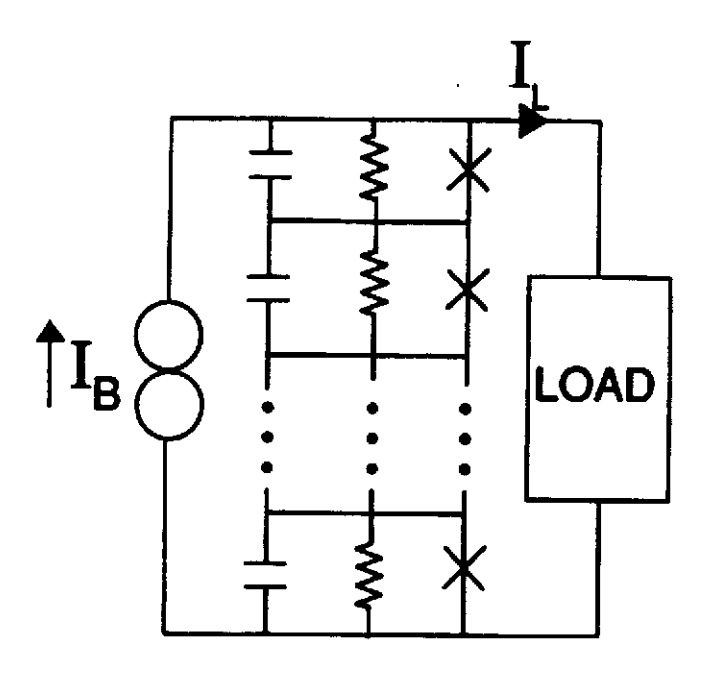


Fig. 2.6 - Circuit diagram for a series array of Josephson junctions shunted by a load.

critical current, oscillations arise causing the voltage across each junction to oscillate. The oscillating voltages generate a high frequency current through the load. This load current flows through all of the junctions and serves to couple them. Under certain conditions the interaction between the oscillating load current and the oscillating supercurrent flowing through the junctions leads to mutual phaselocking and coherent oscillation of the junctions in the array.

In this work the shunted junction model is used to calculate the dynamics of the array. This model does not include propagation delays so it is only valid for arrays small compared to the wavelength of radiation and for distributed arrays. The equations that describe the behavior of the circuit in Fig. 2.6 are,

$$\beta_{c}\ddot{\phi}_{k}(t) + \dot{\phi}_{k}(t) + \sin(\phi_{k}(t)) + I_{L}(t) = I_{B}$$
 k=1,2,...,N 2.6a 
$$V(t) = \sum_{k=1}^{N} \dot{\phi}_{k}(t) = F(I_{L}(t))$$
 2.6b

The first equation is a statement of the conservation of current and the second that the voltage across the array of junctions equals the voltage across the load. Every junction is coupled equally to every other junction through the load current,  $I_L$ . We have used the usual reduced units, measuring current in units of the critical current,  $I_C$ , voltage in units of  $I_CR_N$ , resistance in units of  $R_N$ , capacitance in units of  $\hbar/(2eI_cR_N^2)$ , inductance in units of  $\hbar/(2eI_c)$ , and time in units of  $\hbar/(2eI_cR_N)$ . Here N is the number of junctions,  $I_L$  is the load current,  $I_B$  is the applied bias current, and  $F(I_L)$  is the functional that relates the load current,  $I_L$ , to the total voltage, V, across the array. (For instance when the load in Fig. 2.6 is a capacitor  $F(I_L)=(1/C)\int I_L dt$ .)

The reason for studying this particular array is that it may have practical applications. It was long ago suggested that the high frequency oscillations of the supercurrent that appear due to the ac Josephson effect could be exploited to construct a rapidly tunable rf generator.<sup>8</sup> The simplest generator of this type consists of a single Josephson junction. Unfortunately single junction generators have the practical limitations that their impedance and output power are impractically small. For this reason there has been interest in fabricating rf generators from series arrays of Josephson junctions. If all of the junctions of an N junction array oscillate coherently, then the array will have N times the impedance, N<sup>2</sup> times the output power, and 1/N times the linewidth as a single junction.<sup>19</sup> These potential benefits of arrays of junctions are well understood but determining the conditions under which the junctions mutually phaselock has remained a problem.

Groundbreaking work in the understanding of the phaselocking of series arrays of Josephson junctions was made by Jain, Likharev, Lukens, and Sauvageau. They used a multiple time scale technique to calculate an approximate solution for the in-phase state. This calculation used the exact solution of an array of junctions with  $\beta_C$ =0 and no load as its starting point (Eqn. 2.4). Two times were then introduced: a fast time for the Josephson oscillations, and a slow time for the changes in the frequency of the oscillations. By solving the equations selfconsistently in these two time domains they obtained an approximate solution for junctions with  $\beta_C$ =0 and various loads. Among their many results was that the in-phase solution is stable when the load is inductive and that it is unstable when the load is capacitive. We use a more general numerical approach to study systematically the stability of the in-phase state and found that their results are only valid for a narrow range of  $\beta_C$ . The reason is that for most loads

there is a line of bifurcations near  $\beta_{C}$ =0. One would not expect the results of a perturbation calculation to be valid past a bifurcation. Our results show that the phaselocking is strongest when  $\beta_{C}$ =1 independent of the type of load. We now turn to a numerical study of the dynamical states of the series arrays.

## §3. The Dynamical States

In this section the dynamical states of series arrays of Josephson junctions observed in our study are described. The dynamical states were determined by using a computer to simulate the dynamics of the the array shown in Fig. 2.6. Six different loads were examined: a resistor (R), a capacitor (C), an inductor (L), a series RL load, a series LC load, and a parallel LC load. This is a representative sample of the loads that might be encountered in applications. In each case the bias current was adjusted so that the junctions were oscillating and then the simulation calculated the time evolution of all of the junctions in the array. In these calculations the normalized parameters,  $\beta_C$  and  $I_B$ , were varied in the range from 0 to 5. Within this range three distinct types of periodic solutions were observed as well as period doubled solutions and chaotic solutions. Other periodic or quasiperiodic solutions may exist but were not observed in the simulations described here. The three periodic solutions, which were observed over fairly large parameter ranges, are called the in-phase solution, the antiphase solution, and the split solution. These are each described below.

A variety of numerical integration routines (Euler's method, predictor-correctors, Runge-Kutta) were used to simulate the dynamics, all of which gave essentially the same results. All of the data presented here was calculated by either a second order or a fourth order Runge-Kutta routine.<sup>20</sup> To check that these routines were accurately simulating the dynamics, the integration step size was halved and the simulations were run again to see if the same results were produced. Ironically, it is easier to simulate dissipative systems such as these junction arrays than it is to simulate a conservative system such as the harmonic oscillator. The reason is that dissipative systems have stable attractors and when the numerical

integration routine makes an error the dynamics tends to correct the error and drives the simulation back towards the real solution. This self-correcting action does not take place in conservative systems.

#### The in-phase solution

The simplest type of periodic solution is the in-phase solution. In this case each junction oscillates with the same frequency and phase, that is  $\phi_k = \phi_j$ . Experimental evidence for the existence of this state was first presented in the sixties.<sup>21</sup> The in-phase solution is the most important to understand from the technological point of view because it is the most suitable state for generator, mixer, and parametric amplifier applications. Because of its importance, the stability and fluctuations of the in-phase state will be discussed in detail in later sections. When all the junctions oscillate identically, Eqn. 2.6 for the dynamics of the array reduces to a single equation which is equivalent to that for a single junction.

$$\beta_c \ddot{\varphi}_o(t) + \dot{\varphi}_o(t) + \sin(\varphi_o(t)) + I_L(t) = I_B$$
 3.1

Thus, in the in-phase state, the entire array acts like a single junction. Each junction oscillates with the same frequency and phase. The equivalence of the in-phase state and the corresponding single junction problem greatly reduces the amount of computation required to calculate the in-phase solution. The in-phase solution was observed to be stable roughly in the parameter range  $\beta_C I_B > 1$  for resistive and capacitive loads, and was stable for inductive loads roughly in the range  $\beta_C > 1$ . A detailed discussion of the stability of the in-phase state is given in section 4.

#### The antiphase solution

The antiphase solution is a periodic solution in which all of the junctions oscillate with the same frequency but each has a distinct phase. In the antiphase state we find that the phases of all of the junctions arrange

themselves such that the fundamental Fourier component of the oscillations is absent in any observable measured across the entire array. This is a phaselocked solution in the sense that all of the junctions have a definite phase relationship but their phases are not identical like they are in the in-phase solution. Figure 3.1a-3.1f shows snapshots of the phases,  $\phi_k$ , of two, three, four, five, six, and ten junction arrays in a typical antiphase solution at eight points in a cycle. The phases are measured as angles from vertical as they would be in the pendulum analogy to Josephson junctions. Viewed successively from left to right the snapshots form a movie of the antiphase solution. Note how the phases are spread out, tending to add destructively in this solution. For comparison, Fig. 3.1g shows a movie of the in-phase state which looks the same for any number of junctions.

Another way to visualize these solutions is to plot the supercurrents of all of the junctions as a function of time. Such time series for the in-phase and antiphase solutions of a three junction array are shown in Fig. 3.2. In the in-phase state all of the supercurrent oscillations are the same so the total voltage oscillations across the array scales with the number of junctions in the array. In the antiphase state the supercurrent oscillations are staggered so that the total voltage oscillations across the array are nearly zero. The power spectra of the voltage oscillations across the array are shown in Fig. 3.3. Notice that due to the staggering in the antiphase state, the fundamental of the voltage oscillations vanishes in this state. The disappearance of the fundamental in two junction series arrays was observed experimentally by Finnegan and Wahlsten.<sup>22</sup> They could not measure the relative phases of the junctions but they proposed that this was evidence for the existence of an antiphase state. One way the different antiphase solutions could be distinguished experimentally would be by beating together the oscillations of two different junctions with a mixer.

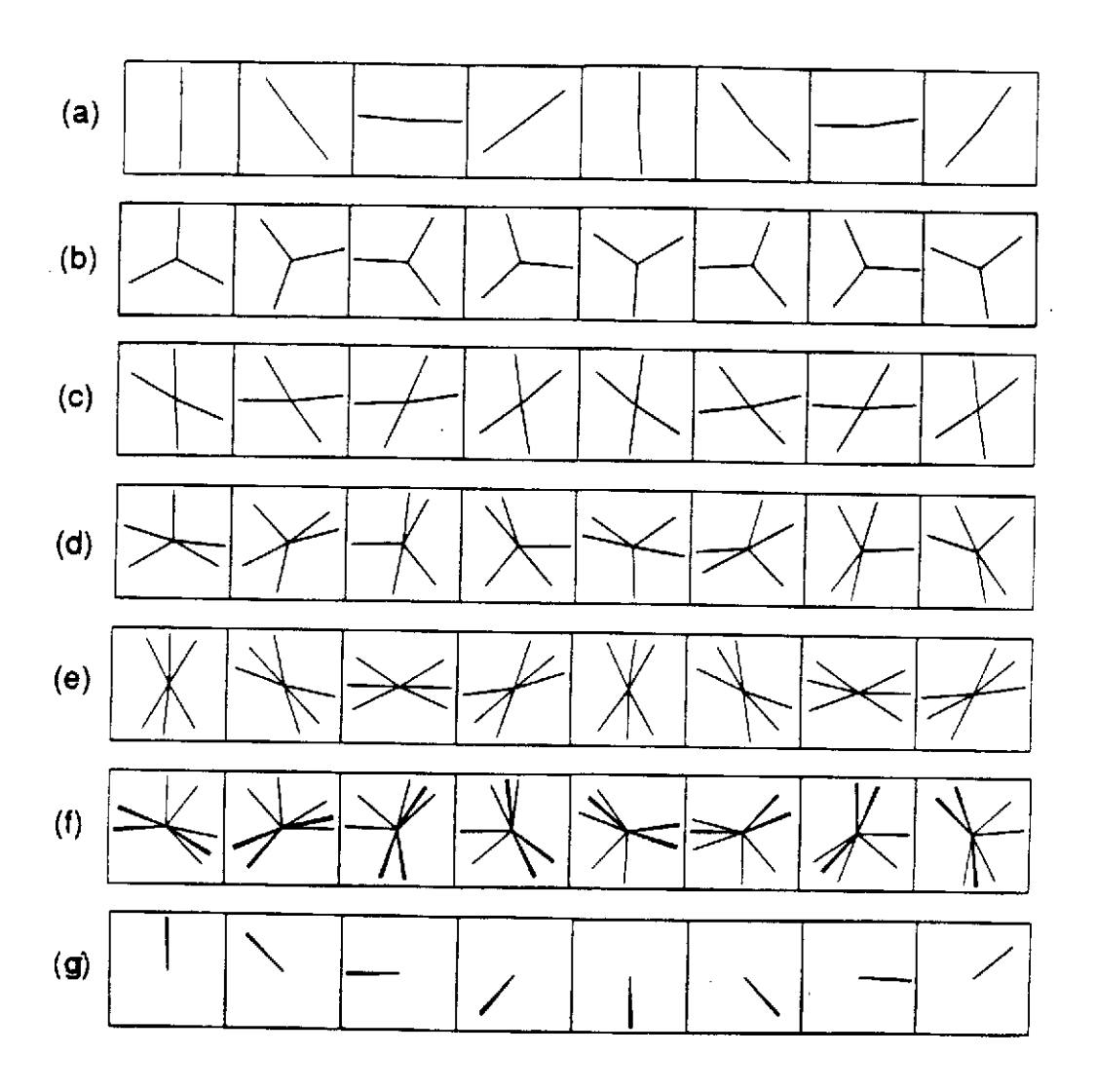
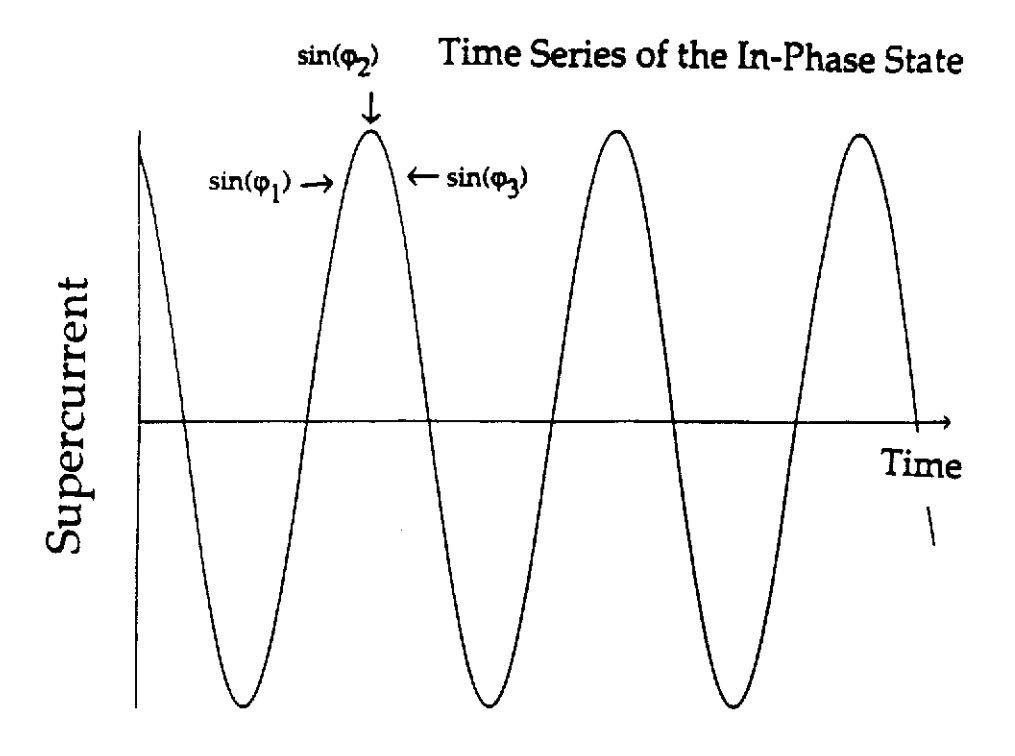


Fig. 3.1 - Six sets of snapshots of the phases,  $\varphi_k$ , of an N junction array in the antiphase solution at eight points in a cycle. The phases are measured as angles from vertical as they would be in the pendulum analogy to Josephson junctions. Viewed successively from left to right the snapshots form a movie of the antiphase solution. Note that the phases tend to add destructively in this solution. The load in each case was a series inductor-capacitor where L=N/2, C=1/(2N), I<sub>B</sub>=2.5,  $\beta_c$ =2.5, where N is the number of junctions. (3.1a) - N=2. (3.1b) - N=3. (3.1c) - N=4. (3.1d) - N=5. (3.1e) - N=6. (3.1f) - N=10. Figure 3.1g is a movie of the in-phase solution. Movies of the in-phase solution look the same no matter how many junctions are involved.



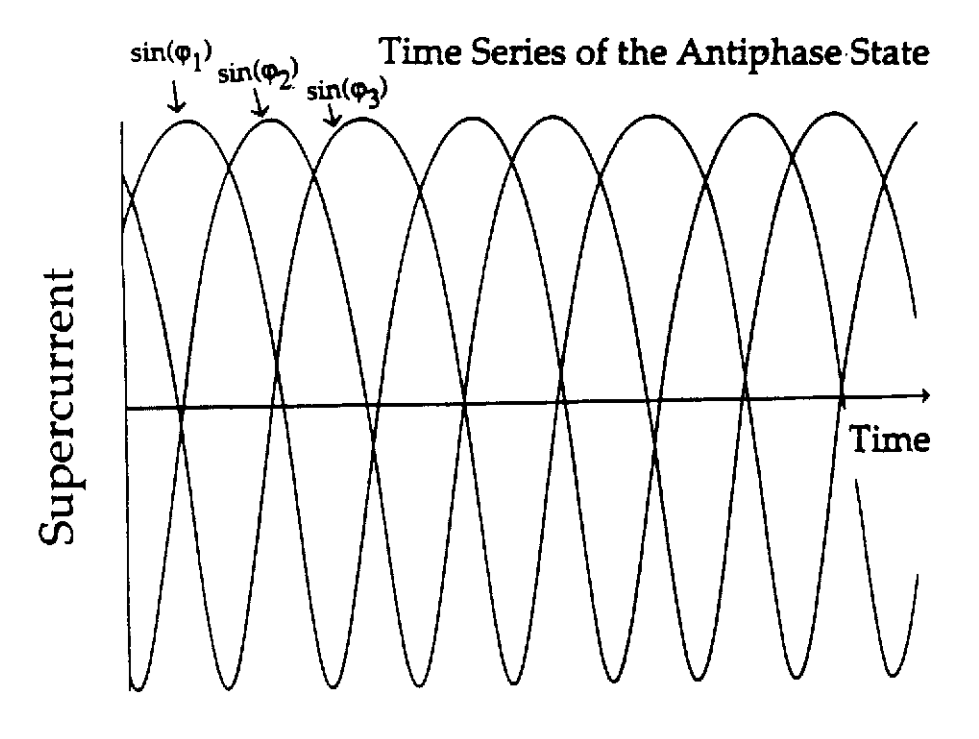
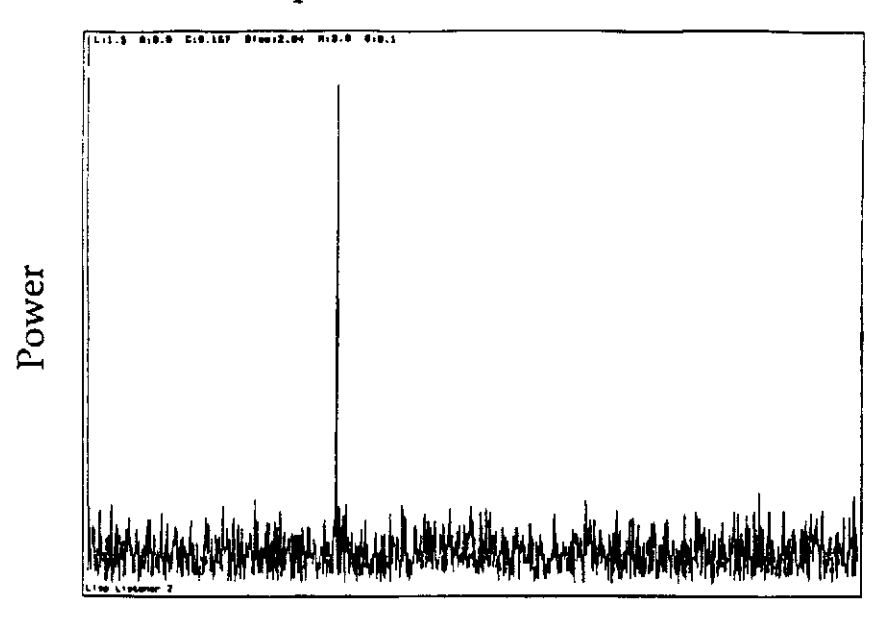


Fig. 3.2 - Time series of the supercurrents of the in-phase state and the antiphase state for arrays with three junctions. The supercurrent oscillations are the same for each junction in the in-phase state but they are staggered in the antiphase state.

## Power Spectrum of the In-Phase State



# Power Spectrum of the Antiphase State

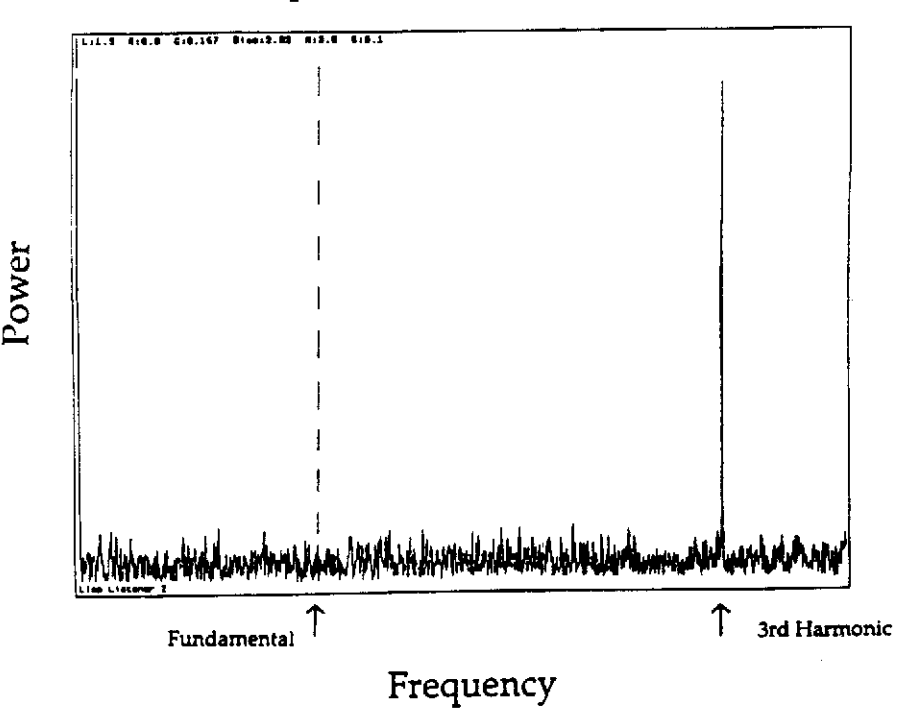


Fig. 3.3 - The power spectra of the voltage oscillations across a three junction array for the in-phase state and the antiphase state. The staggering of the oscillations in the antiphase state results in the disappearance of the fundamental.

The response at dc would tell you the relative phase of the two junctions. A number of such measurements would specify the antiphase state.

Although we observe no fundamental Fourier component in the antiphase state, higher harmonics of the voltage oscillations are present. The amplitudes of these harmonics decrease with increasing bias current, so for high bias currents only small voltage oscillations appear across the array. Since it is these voltage oscillations that generate the currents that couple the junctions, at high bias current there is only weak coupling among the junctions. In the limit of vanishingly small ac load current, the equations for the array of junctions decouple into N independent equations, each identical to the equation for a single junction with no external load. The actual behavior of an array in the antiphase state approaches this limiting solution as the bias current is increased and the ac Josephson oscillations have less harmonic content. Thus a good approximation for the antiphase solution of a series array of Josephson junctions can be constructed by describing each junction in the array by the solution of a single junction without an external load, and then distributing the phases of the junctions between zero and  $2\pi$ , so that the fundamental Fourier component on the single junction oscillation vanishes.

There is only one way that the conditions for the antiphase solution can be met by arrays of two or three junctions. In order that each junction have a distinct phase and that the fundamental Fourier component vanish, each junction must oscillate with the same waveform, but the waveforms must be spaced in time by T/2 in the two junction case and by T/3 in the three junction case, where T is the period of the oscillations. For more than three junctions there are many ways to satisfy the conditions for the antiphase state. For instance, one might imagine that for a four junction array the

junctions could break into two pairs and the waveforms of the junctions within a pair could be spaced by T/2. The spacing between the pairs could be anything at all and still satisfy the condition that the amplitude of the fundamental oscillations be zero. The simulations show, however, that this is not the case. (see Fig. 3.1) It is not understood why the antiphase solutions for more than three junctions have the exact form that they do.

If the junctions in a series array are assumed to be identical then the system possesses a permutation symmetry: any junction can be exchanged with any other junction. A solution breaks this symmetry if the result of permuting two junctions does not give the same solution back again. The antiphase solution is such a symmetry broken solution. Any transformation that permutes two of the junctions will usually generate another antiphase solution. For this reason the antiphase solution should really be thought of as a set of solutions. Each member of this set can be generated by permuting the junctions of a single example of the set. Since each junction has a distinct phase in the antiphase solution, it follows that there are at least (N-1)! distinct antiphase solutions of an N junction array. The number of solutions grows so quickly that for N>100 it would be impossible to simulate all of the antiphase solutions even on the most powerful computer. Here is an example of where just running a simulation without understanding how many solutions may exist in phase space, could lead to an incorrect conclusion. One expects that this is a generic problem for dynamical systems of many degrees of freedom and high symmetry.

When any of the antiphase solutions is stable then we know by symmetry that they are all stable. This means for large N that there can be very many stable, coexisting antiphase solutions. For large N, phase space becomes so crowded with these stable solutions that one would expect that

even the tiniest amount of noise would cause the system to hop from one antiphase solution to another. This situation has been studied in a related system that has the same symmetry and connectivity.<sup>23</sup> The noise sensitivity of coupled circle maps was studied numerically for several different noise levels. These coupled maps also exhibit antiphase solutions that crowd phase space. In this study the noise was held at a constant level and the number of maps was increased. When a critical number of attractors was reached the system began to wander from one antiphase solution to another. When this happened the many antiphase solutions effectively merged into one pseudoattractor and the system wanders diffusively on that pseudoattractor. An observed consequence of this hopping is the appearance of low frequency noise when the diffusive motion among the antiphase attractors begins. There is also evidence that the many antiphase solutions crowd the in-phase solution decreasing the basin of attraction for the in-phase solution. This makes the in-phase solutions more sensitive to noise as the number of maps increases. One expects that the same sort of behavior will occur for the Josephson junction arrays.

For all current applications the antiphase solution is undesirable. Since the phases of the junctions conspire to eliminate the fundamental Fourier component of the oscillations an array operating in this state would not be a good rf generator. In mixer or amplifier applications each junction would interact with the signal with a different phase so the net result would cancel out. Furthermore the crowding of stable antiphase attractors in phase space may lead to the undesirable appearance of low frequency noise.

#### The split solution

The third type of periodic solution that was observed is the split solution. In this case the phases of the junctions divide into a small number of coherent subgroups. Arrays with even numbers of junctions form two groups where half of the junctions oscillate with one phase and half oscillate with another. Odd numbered arrays with greater than three junctions also form two groups, dividing themselves as evenly as possible. The case of three junctions seems to be a special one, with all three junctions out of step. Figures 3.4a-3.4e illustrate the behavior for arrays of two, three, four, five, and fifty junctions. Notice that for arrays of four or more junctions the solutions look very much like the two junction case, even for as many as fifty junctions.

The split solution must also be considered to be a set of solutions since it has lower symmetry than the full permutation symmetry of the equations. In this case there are  $N!/(\alpha!(N-\alpha)!)$ , symmetry related solutions in the set, where  $\alpha$  is the integer part of N/2. In the large N limit there are  $2^N$  split solutions. This solution has the same disadvantages as the antiphase solutions for any technical applications.

#### Period doubled states, chaos

As the bias current flowing through the array is varied these periodic states can lose stability. When this happens symmetry broken states, period doubled states, or chaotic states sometimes appear. A detailed description of what happens at the instabilities when the periodic states lose stability will be given in the section 5. Here some examples of the more exotic solutions that appear are presented.

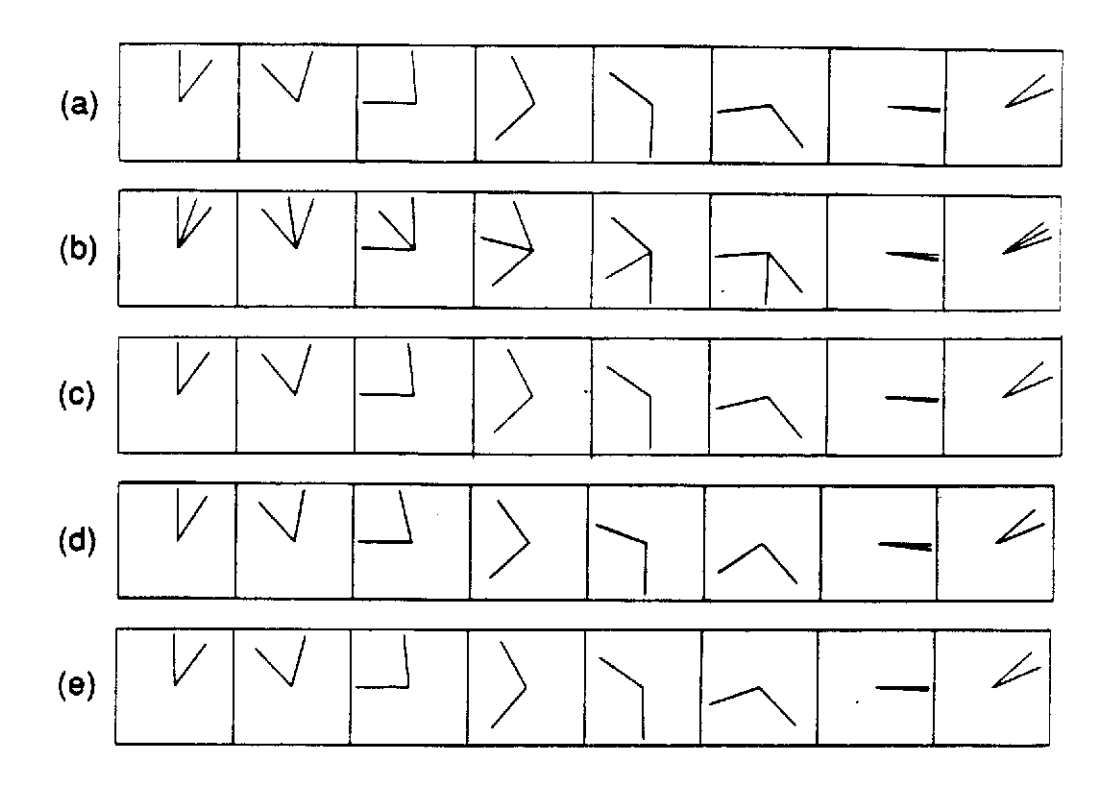


Fig. 3.4 - Movies of the split solution. This solution has twice the period of the in-phase solution. For more than three junctions the phases form coherent subgroups and half of the junctions oscillate with one phase while half oscillate with another. The load in this case is a resistor, R=N,  $I_B=1.7$ ,  $\beta_C=1$ . (3.4a) - N=2. (3.4b) - N=3. (3.4c) - N=4. (3.4d) - N=5. (3.4e) - N=50.

One way to visualize these states is by looking at phase portraits of the dynamics. Figure 3.5 is a collection of phase portraits constructed from the dynamics of two junction arrays. These phase portraits are projections of the circuit's phase space trajectories onto the  $\sin(\phi_1)$  -  $\sin(\phi_2)$  plane. Physically, the phase portraits can be interpreted as plots of the supercurrent of one of the junctions plotted against the supercurrent of the other junction. The phase portrait should be thought of as two dimensional windows looking into phase space that allow us to infer the symmetry and topology of the solutions.

In Fig. 3.5a the phase portrait is a diagonal line stretching from [-1,-1] to [1,1], corresponding to an in-phase solution ( $\phi_1 = \phi_2$ ). Phase portraits such as this are observed whenever the in-phase solution is stable. When the bias current is decreased the in-phase state loses stability and a period-doubled solution appears (see Fig.3.5b). Notice that this solution makes two loops in phase space before repeating itself and thus has twice the period of the inphase solution. (The curve can intersect itself since it is only a projection of the true, nonintersecting trajectory onto the plane.) This solution is coherent in the sense that there is a definite (time dependent) phase relationship between the oscillations of the two junctions but they do not oscillate identically as they do in the in-phase solution. After another period-doubling bifurcation occurs, a the new solution that appears has four times the period of the (now unstable) in-phase state (see Fig. 3.5c). Further decreasing the bias current leads to a cascade of period-doubling bifurcations. Each new solution that appears has twice the period of the preceding solution. Eventually this sequence of periodic doublings leads to a chaotic solution (see Fig. 3.5d). A complete description of the period doubling route to chaos can be found in Feigenbaum's work.<sup>24</sup> Chaotic behavior is mostly observed for arrays with capacitive loads, biased in the vicinity of the

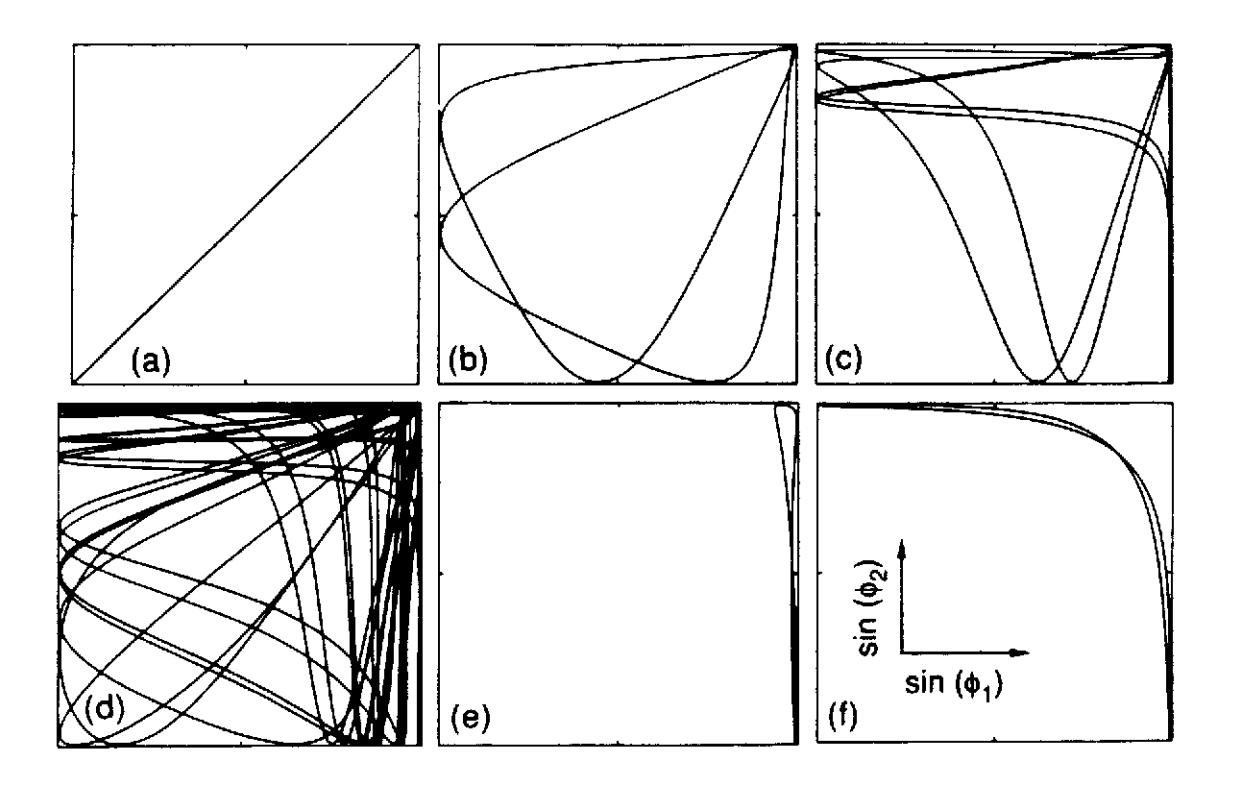


Fig. 3.5 - These phase portraits are projections of the two junction array trajectory in phase space onto the  $\sin(\phi_1)$ - $\sin(\phi_2)$  plane. (3.5a) - In-phase solution observed at  $I_B$ =2.3,  $\beta_C$ =.75. (3.5b) - Solution with twice the period of the in-phase oscillations observed at  $I_B$ =1.7,  $\beta_C$ =1. (3.5c) - Solution with four times the period of the in-phase oscillations observed at  $I_B$ =1.5,  $\beta_C$ =1. (3.5d) - Chaotic solution observed at  $I_B$ =1.45,  $\beta_C$ =1. (3.5e) - Symmetry-broken solution observed at  $I_B$ =1.2,  $\beta_C$ =1. (4f) - Antiphase solution observed at  $I_B$ =1.2,  $\beta_C$ =0.1. In each case the load was a resistor where R=N in the normalized units.

critical current. Finally Fig. 3.5e shows an example of a symmetry broken solution. This solution does not share the permutation symmetry of the governing equations; indeed  $\phi_1(t)$  and  $\phi_2(t)$  have different waveforms altogether, though they do have the same period.

### §4. Stability Analysis of the In-phase Solution

Since the in-phase state is probably the most useful from the technological point of view, the next three sections are devoted to a detailed analysis of this state. Section 5 examines the transitions from the in-phase solution to the other solutions and section 6 discusses the fluctuations about the in-phase solutions. In this section a generalized linear analysis is used to calculate the stability of the in-phase solution. Here we calculate not only where the in-phase solution loses stability, but we also determine quantitatively how stable the in-phase solution is, whenever it is stable. Unfortunately, even in this linear analysis, numerical methods must be used. The numerical results of this analysis are presented for series arrays shunted by six representative loads. This section concludes with specific recommendations for the design of arrays that maximize the stability of the in-phase solution.

To determine the stability of the in-phase solution consider small perturbations about that solution, ( $\phi_k = \phi_0 + \eta_k$ ,  $I = I_L + i$ ). Linearizing Eqn. 2.6 around the in-phase solution results in a set of linear differential equations with periodic coefficients,

$$\beta_c \ddot{\eta}_k(t) + \dot{\eta}_k(t) + \cos(\phi_0(t)) \eta_k(t) + i(t) = 0 \qquad k=1,2,...,N \qquad 4.1a$$
 
$$\sum_{k=1}^N \dot{\eta}_k(t) = F'(I_L(t)) i(t) \qquad \qquad 4.1b$$

where  $\phi_{O}(t)$  and  $I_{L}(t)$  represent the in-phase solution, and are functions of period T that solve Eqn. 3.1.  $F'(I_{L}(t))$  is the derivative of the load functional, F(I), evaluated at the in-phase current. This functional is different for each type of load. For instance, for a resistive load the functional is simply,  $F(I_{L})=(I_{L})/R$ .

The linearized equations can be simplified greatly by taking advantage of the permutation symmetry of the system. (Any permutation,  $\eta_j \leftrightarrow \eta_k$ , leaves Eqn. 4.1 unchanged.) We transform to the natural coordinates of this system, which are the mean coordinate  $\vartheta=(1/N)\Sigma$   $\eta_k$ , and the N-1 relative coordinates,  $\zeta_k = \eta_k - \eta_{k+1}$ . This transformation was suggested by Kurt Wiesenfeld. The equations (4.1) then become,

$$\begin{array}{lll} \beta_{c}\ddot{\zeta}_{k}(t) + \dot{\zeta}_{k}(t) + \cos(\phi_{o}(t))\zeta_{k}(t) = 0 & k=1,2,...,N-1 & 4.2a \\ \beta_{c}\ddot{\vartheta}(t) + \dot{\vartheta}(t) + \cos(\phi_{o}(t))\vartheta(t) + i(t) = 0 & 4.2b \\ N\dot{\vartheta}(t) = F'(I_{o}(t))i(t) & 4.2c \end{array}$$

This transformation decouples all N coordinates in the problem. Further simplification results because all of the relative coordinates obey the same equation. Thus, because of symmetry, the stability analysis of the original N+1 equations reduces to solving the above set of three equations. The mean coordinate describes the average motion of the perturbations and the relative coordinates describe the difference in the dynamics of the individual junctions. The in-phase solution,  $\phi_0$ , will remain stable as long as the relative coordinates do not grow. We therefore focus our attention on Eqn. 4.2a.

Equation 4.2a arises in many physical problems and can be analyzed using Floquet theory.<sup>25</sup> The analysis shows that any solution to this equation can be expressed as a linear combination of two fundamental solutions,  $\zeta_a(t)$  and  $\zeta_b(t)$ , which are specified by the initial conditions:  $\zeta_a(0)=1$ ,  $\dot{\zeta}_a(0)=0$ ,  $\zeta_b(0)=0$ ,  $\dot{\zeta}_b(0)=1$ . Since  $\cos(\phi_0)$  is a periodic function,  $\zeta_a(t+T)$  and  $\zeta_b(t+T)$  must also be solutions to Eqn. 4.2a, which can be expressed in terms of  $\zeta_a(t)$  and  $\zeta_b(t)$ . This leads to the vector equation,

$$\begin{pmatrix} \zeta_{a}(t+T) \\ \zeta_{b}(t+T) \end{pmatrix} = \begin{pmatrix} \zeta_{a}(T) & \dot{\zeta}_{a}(T) \\ \zeta_{b}(T) & \dot{\zeta}_{b}(T) \end{pmatrix} \begin{pmatrix} \zeta_{a}(t) \\ \zeta_{b}(t) \end{pmatrix}$$
 4.3

The eigensolutions of Eqn. 4.3 are called the Floquet solutions and can be put in the form  $\zeta_1 = e R^t \chi_1(t)$ ,  $\zeta_2 = e R^t \chi_2(t)$ , where  $\chi_1(t)$  and  $\chi_2(t)$  are periodic functions of period T and  $\rho_1 + \rho_2 = -1/\beta_C$ . The p's are called the Floquet exponents and their real parts determine the stability of the perturbations. They are related to the eigenvalues,  $\lambda_j$ , of the matrix in Eqn. 4.3 by  $\rho_j = \ln(\lambda_j)/T$ . If both  $Re(\rho_1)$  and  $Re(\rho_2)$  are negative, then any initial perturbation decays and the in-phase solution is linearly stable. If either exponent has a positive real part, the perturbations grow and the in-phase solution is linearly unstable. Finally if either  $Re(\rho_1) = 0$  or  $Re(\rho_2) = 0$ , then the perturbations to Eqn. 4.2 neither grow nor decay: we then say that the in-phase state is (linearly) neutrally stable, and nonlinear terms omitted in writing Eqn. 4.1 determine the ultimate stability of  $\phi_0(t)$ . Note that the imaginary part of the Floquet exponents are determined only up to an integer multiple of  $2\pi i/T$ . To avoid any ambiguity we will pick  $-\pi/T < Im(\rho) \le \pi/T$ .

### Limiting cases

Before discussing the numerical solutions to these equations we consider approximate solutions for the Floquet exponents in various limits. The approximate solutions give physical insight and they also provide a check on the numerical work. First consider the large  $\beta_C$  limit. We know from Floquet theory that,

$$\rho_1 + \rho_2 = -1/\beta_C. 4.4$$

Let  $\rho_+$  represent the greater of the two exponents and  $\rho_-$  the lesser. Whenever  $\rho_+>0$  the in-phase solution is unstable. Using this notation Eqn. 4.4 can be written as the inequality,  $\rho_+\geq -1/(2\beta_C)$ . For large  $\beta_C$ ,  $\rho_+$  can either be a tiny negative number or a positive number. Thus the in-phase state is either barely stable or unstable for large  $\beta_C$ .

Next consider the large  $I_B$  limit. For large bias currents,  $\cos(\phi_O)$  oscillates with a period much shorter than any other time in the problem. We can therefore employ the averaging method<sup>26</sup> to find an approximate solution to Eqn. 4.2a. In this approximation, which is valid for  $\beta_C >> T \approx 2\pi/I_B$ , we replace  $\cos(\phi_O)$  with its average value,  $\overline{\cos(\phi_O)}$ . The solutions to the averaged equation are

$$e^{\rho_{+}t}$$
 and  $e^{\rho_{-}t}$  where  $\rho_{\pm} = \frac{-1 \pm \sqrt{1 - 4\beta_{c}\cos(\phi_{o})}}{2\beta_{c}}$  4.5

For  $I_B>>1$ ,  $\cos(\phi_O)$  is nearly sinusoidal and  $\rho_+\approx -\overline{\cos(\phi_O)}\to 0$ . Hence the inphase solution is stable for  $\overline{\cos(\phi_O)}>0$  and approaches neutral stability as the bias current increases. In the pendulum analogy the condition,  $\overline{\cos(\phi_O)}>0$ , can be interpreted as saying that the in-phase state is stable when the pendula hang down on average. From this analysis we conclude that arrays of junctions with  $I_B>>1$  will either be unstable or barely stable.

In the highly damped limit one can take  $\beta_C$ =0 and the equation for the relative coordinate can be solved exactly. Direct integration of Eqn. 4.2a in this case yields,

$$\zeta(t) = \exp\left(-\int_0^1 \cos(\varphi_0(t'))dt'\right)$$
 4.6

From this solution we see that such an array will once again phase-lock when  $\overline{\cos(\phi_0)}>0$ . By differentiating Eqn. 3.1 in this case one finds

$$\overline{\cos(\varphi_0)} = \frac{1}{T} \int_0^T \frac{\dot{I}_L(t)}{\dot{\varphi}_0(t)} dt$$
 4.7

Except for bias currents close to the critical current both  $I_L(t)$  and  $\dot{\phi}_O(t)$  are nearly sinusoidal, periodic functions. Here  $\dot{\phi}_O(t)$  is the voltage across the

load and  $I_L(t)$  is the current through the load so  $I_L(t)$  leads  $\mathring{\phi}_O(t)$  by  $\pi/2$  when the load is capacitive,  $I_L(t)$  lags  $\mathring{\phi}_O(t)$  by  $\pi/2$  when the load is inductive, and  $I_L(t)$  has the same phase as  $\mathring{\phi}_O(t)$  when the load is resistive. These phase relationships taken together with Eqn. 4.7 dictate the sign of  $\overline{\cos(\phi_O)}$  and show that in this limit ( $\beta_C$ =0,  $I_B$ >>1) the junctions will phase-lock with an inductive load, will not phase-lock with a capacitive load, and will be neutrally stable with a resistive load. This agrees with the earlier perturbation calculation of Jain, Likharev, Lukens, and Sauvageau, and with our numerical results in this limit which are presented below.

#### Numerical results of the stability analysis

For the general case the Floquet exponents have to be calculated numerically. This has been done for six representative array circuits which include a resistive load, a capacitive load, two inductive loads, and series and parallel resonant LC loads. The Floquet exponents were calculated in each case by numerically determining  $\zeta_a(t)$ ,  $\zeta_b(t)$ , and  $\phi_0(t)$  by means of a Runge-Kutta algorithm and then using these results to diagonalize the matrix of Eqn. 4.3. Each time the matrix was diagonalized, a check was performed to insure that  $|\lambda_1\lambda_2-e^{-T/\beta}|$  was less than 0.05. The condition,  $\lambda_1\lambda_2-e^{-T/\beta}=0$ , is equivalent to  $\rho_1+\rho_2=-1/\beta_C$  which is an exact result of Floquet theory. When the period of the oscillation gets long (T>>1), as it does for bias currents near the critical current, longer numerical integrations are required and it becomes more difficult to calculate the Floquet exponents. In fact for low bias currents the condition,  $\rho_+<-1/(2\beta_C)$ , is violated in Fig. 4.1a and 4.1b although the numerical results are within the limits stated above.

In Fig. 4.1a- 4.1f we plot contours of the largest real part of the Floquet exponents associated with the relative coordinate as a function of the junction capacitance,  $\beta_C$ , and the bias current,  $I_B$  for each of these loads.

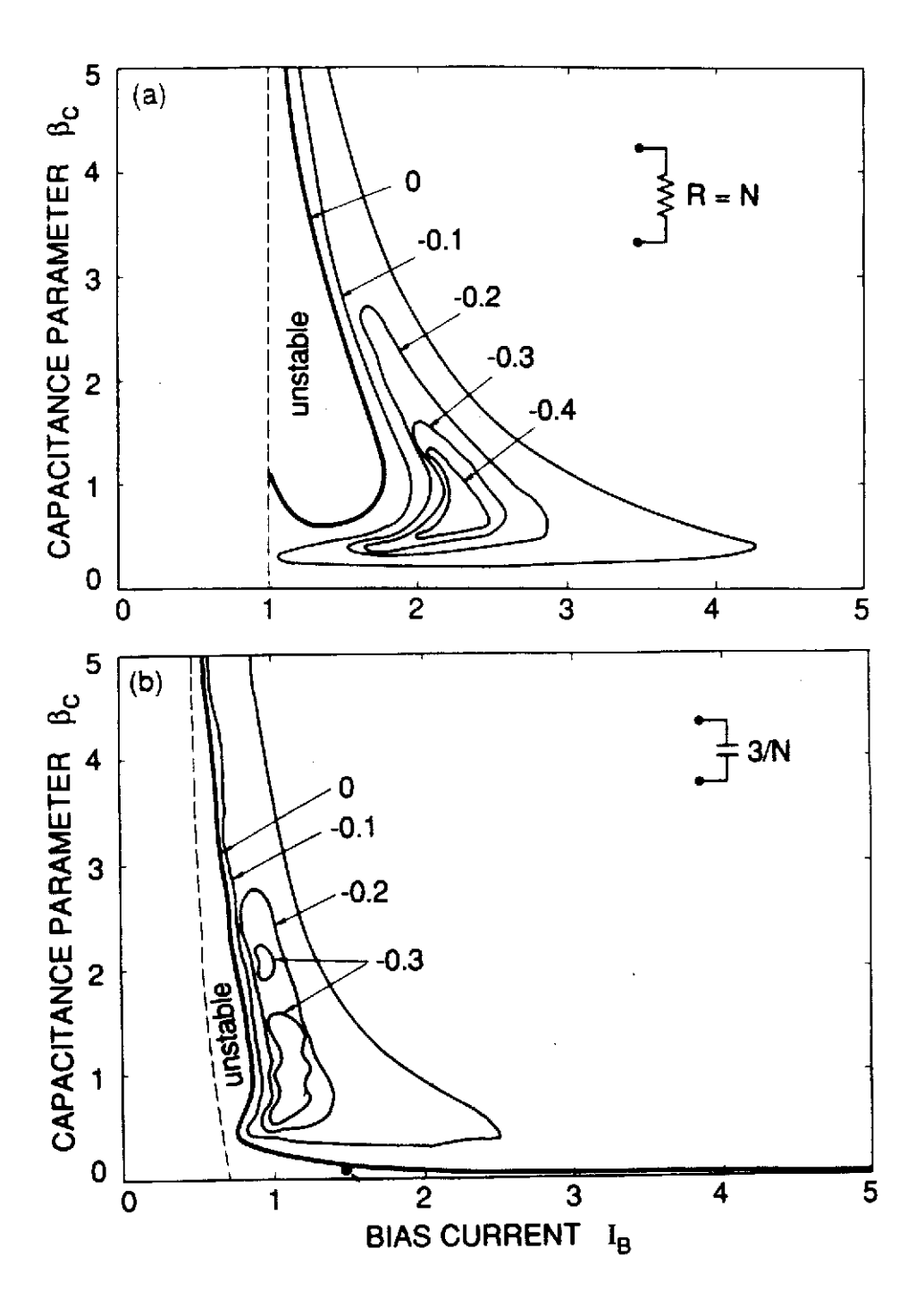


Fig. 4.1 - Contours of the largest real part of the Floquet exponents are plotted as a function of the junction capacitance,  $\beta_C$ , and the bias current,  $I_B$ . The in-phase solution is unstable for  $Re(\rho)>0$  and is most stable for the most negative exponents. These plots relate the stability of arrays with an arbitrarily large number of junctions where the impedance of the load scales with the number of junctions. (4.1a) - Resistive load with an impedance matched to the impedance of the array, R=N. (4.1b) - Capacitive load, C=3/N.

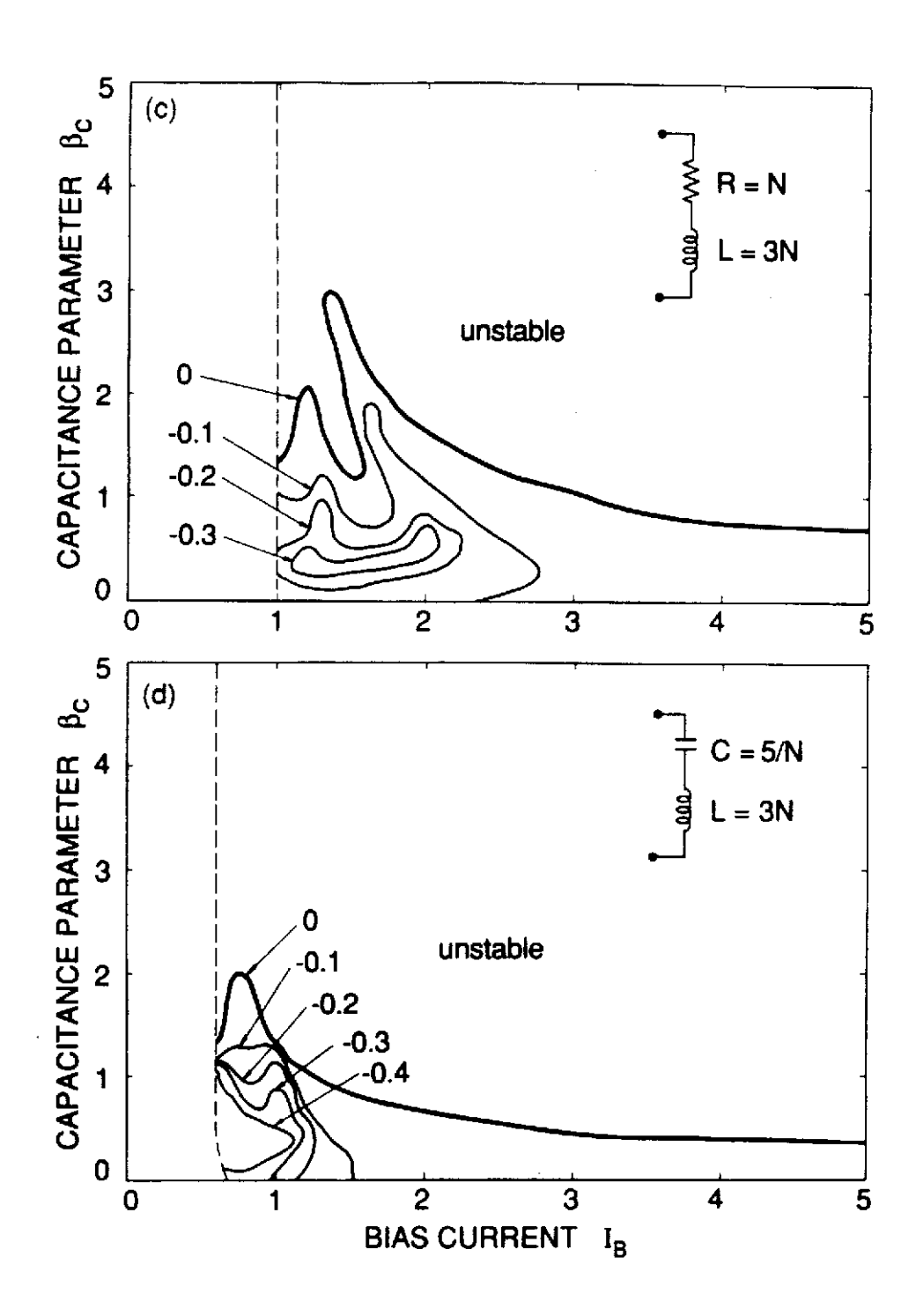


Fig. 4.1 continued - Contours of the largest real part of the Floquet exponents are plotted as a function of the junction capacitance,  $\beta_{\text{C}}$ , and the bias current,  $I_{\text{B}}$ . (4.1c) - Load is a series resistor-inductor, R=N, L=3N. (4.1d) - Load is a series inductor-capacitor, L=3N, C=5/N. Here a large capacitor is used to block dc currents which would short the junctions. The load has an inductive impedance at all relevant frequencies.

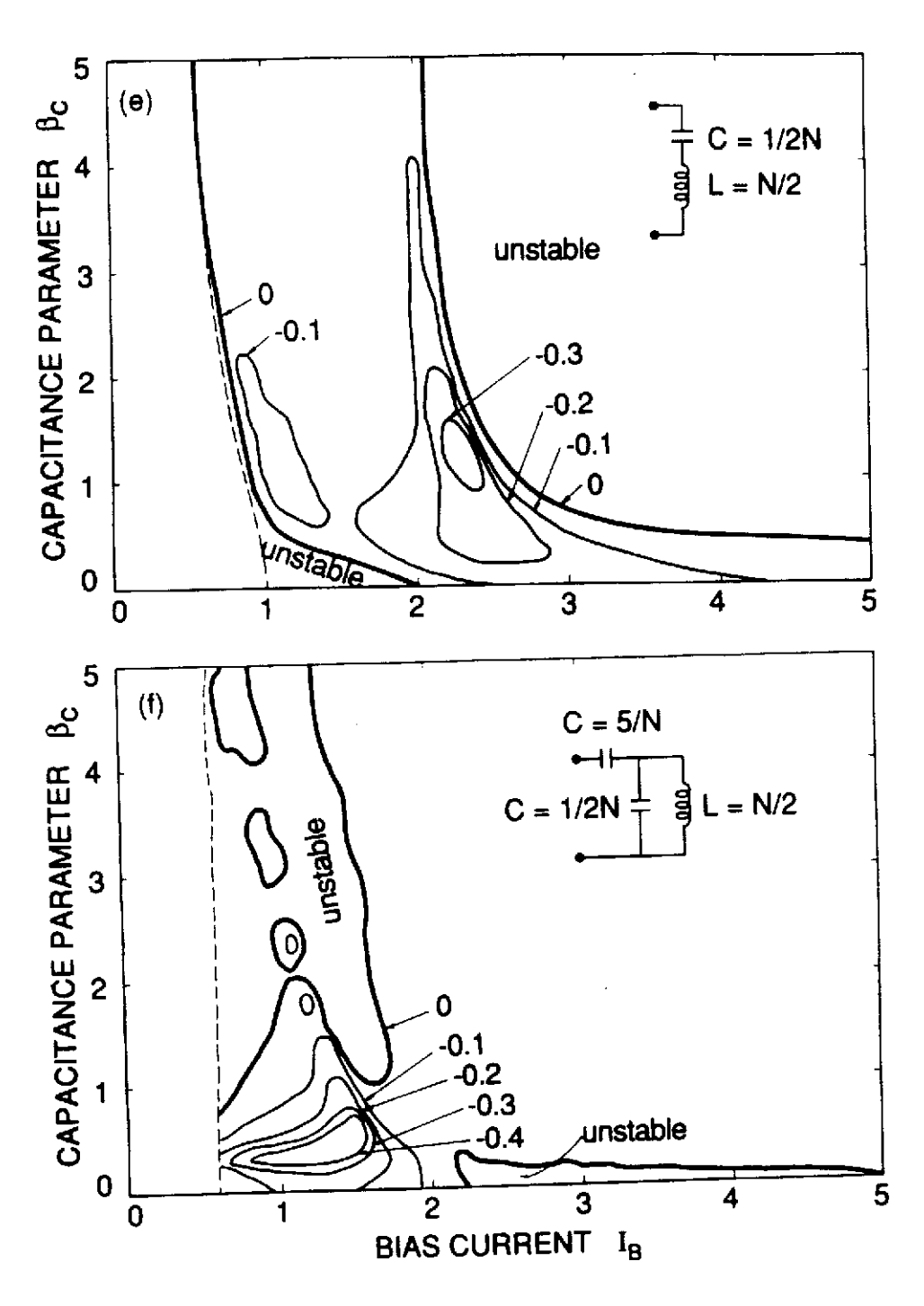


Fig. 4.1 continued - Contours of the largest real part of the Floquet exponents are plotted as a function of the junction capacitance,  $\beta_C$ , and the bias current,  $I_B$ . (4.1e) - Load is a series inductor-capacitor which passes through a resonance at a bias current of about 2, L=N/2, C=1/(2N). (4.1f) - Load is a parallel inductor-capacitor with a large blocking capacitor to prevent the inductor from shorting the junctions, L=N/2, C=1/(2N), blocking capacitor=5/N. This load also passes through a resonance at a bias current of about 2.

These stability plots show the range of parameters over which the in-phase solution is stable and they provide a quantitative measure of the stability. The heavy line is the Re(p)=0 contour and separates the stable and unstable regions. The dashed line corresponds to the transition to the zero voltage state. To the left of this line the junctions no longer oscillate and questions concerning coherent oscillations are moot. The in-phase solution is most stable for the regions where the exponents are most negative. For instance an exponent of -0.4 corresponds to the perturbations decreasing by a factor of about ten for every cycle of the in-phase oscillations. As the figures indicate we have observed stable in-phase oscillations in some region of the  $\beta_C$  -  $I_B$  plane for each type of load. Universally the strongest phase-locking occurs for  $\beta_C$  in the range 0-1 and  $I_B$  in the range 1-2. Lee and Schwarz found similar results for the optimum phaselocking regime based on calculations for two junction arrays.<sup>27</sup> These plots relate the stability of arbitrarily large arrays of junctions with a load that scales with the number of junctions. For instance Fig. 4.1a relates the stability of a series array of N junctions shunted by a resistor whose resistance is R=N in reduced units. The appropriate scalings for the other circuits are given in the figure caption.

Figures 4.1a and 4.1b show that in-phase oscillations are stable in most of the  $\beta_C$ -I<sub>B</sub> plane when the load is resistive or capacitive. The stability plots for the inductive loads, Fig. 4.1c -4.1d, are nearly the complement of the stability plot for the capacitive load or resistive load. (In the circuit of Fig. 4.1d a large capacitor is included in series with the inductor to block dc currents which would short the junctions, but the load appears inductive at all relevant frequencies.) Roughly speaking, the in-phase oscillations are stable for inductive loads in the regions where they were unstable for capacitive loads. As  $\beta_C$  or I<sub>B</sub> (or both) become large the real part of the Floquet exponent approaches zero in all of these plots implying that the in-

phase state approaches neutral stability. In this limit, arrays with a resistive or capacitive loads are stable and approaching neutral stability while arrays with inductive loads are unstable and approaching neutral stability. The numerical results agree with the limiting expressions presented above in all of the limits discussed.

The behavior of the stability of the in-phase solutions as the load goes through a resonance is shown in Fig. 4.1e-4.1f. For low bias currents the circuit in Fig. 4.1e has a capacitive impedance and the stability plot resembles that of the simple capacitive load, Fig. 4.1b. For high bias currents the circuit in Fig. 4.1e has an inductive impedance and the stability plot resembles that of the simple inductive load, Fig. 4.1c. Analogous statements can be made about the limiting regions in Fig. 4.1f. This shows how one can piece together the approximate stability plots of more complicated circuits by taking parts of simpler circuits in the appropriate limits.

#### Noise induced intermittent behavior

In several limiting cases we have shown that the in-phase solution is barely stable. If the in-phase solution is the only stable solution in these situations one would expect that this would lead to noisy or intermittent behavior. To test this idea, times series of the in-phase solution were recorded in a regime where the in-phase state was barely stable and a small amount of noise was added. These time series are shown in Fig. 4.2. Plotted on the vertical axis is a quantity called coherence where,

Coherence = 
$$\left(\sum_{k=1}^{N} \sin(\phi_k)\right)^2 + \left(\sum_{k=1}^{N} \cos(\phi_k)\right)^2$$
 4.8

When the array is in the in-phase state coherence=1. When the array is not in the in-phase state coherence<1. The four plots in Fig. 4.2 show the coherence plotted as a function of time for four different external noise

## Time Series of Coherence

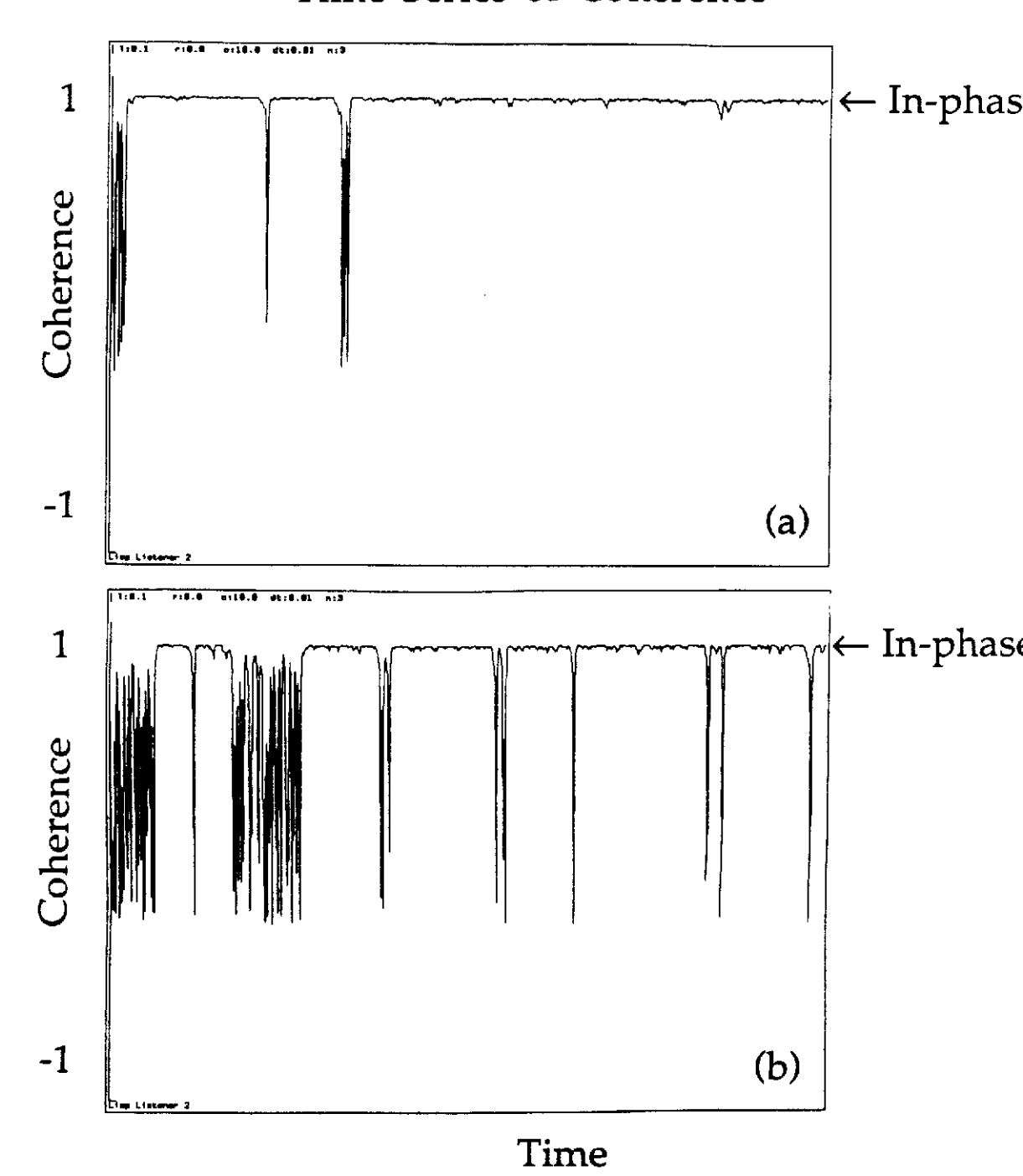


Fig. 4.2 - Coherence plotted against time for four different noise strengths. Coherence takes the value 1 when the array is in the in-phase state. These time series were made for a three junction array with a series LC load, L=0.1, C=10,  $\beta_c$ =0, I<sub>B</sub>=2. (4.2a) - Average noise strength=0.125. (4.2b) - Average noise strength=0.156.

# Time Series of Coherence

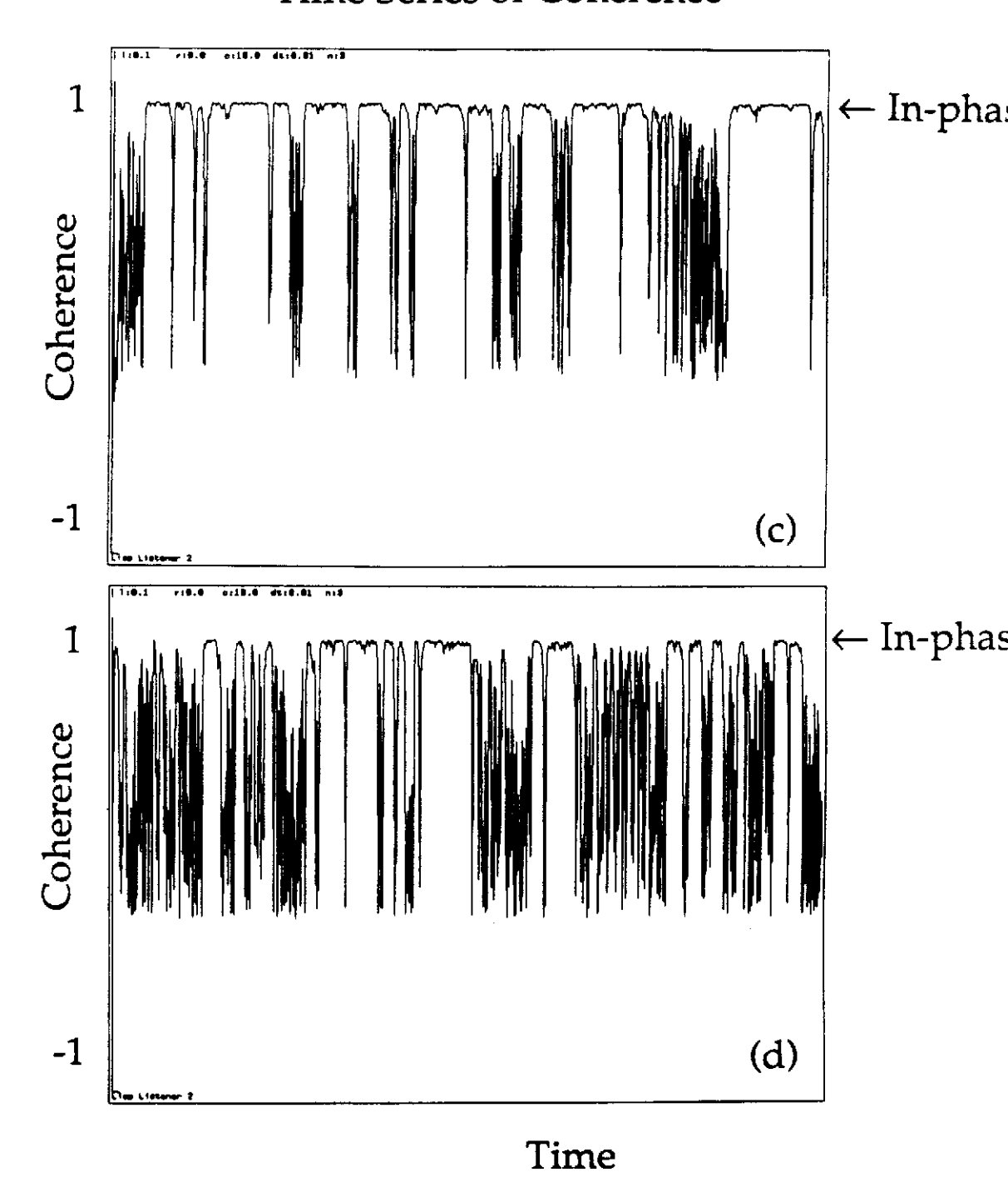


Fig. 4.2 continued - Coherence plotted against time for four different noise strengths. Coherence takes the value 1 when the array is in the in-phase state. These time series were made for a three junction array with a series LC load, L=0.1, C=10,  $\beta_c$ =0,  $I_B$ =2. (4.2c) - Average noise strength=0.187. (4.2d) - Average noise strength=0.25.

strengths. In the absence of any external noise, the array would remain in the in-phase solution and the coherence would be a constant line with a value of one. When a small amount of external noise is added the coherence hovers around a value of one but occasionally makes an excursion away from the in-phase state (see Fig. 4.2a). These excursions are much like the intermittent bursts described by Pomeau and Manneville.<sup>28</sup> As the noise level is increased the frequency and duration of the intermittent bursts increases (see Fig. 4.2b,c,d). Thus one should expect intermittent behavior form these arrays when they are biased in a regime where the in-phase state is the only solution and it is barely stable. The effects of noise will be discussed further in section 6.

Since the in-phase state is probably the most important dynamical state from a technological point of view we conclude this section with a discussion of the conditions under which the in-phase solution is most stable. Referring to the stability plots of Fig. 4.1 one can see that the in-phase state is almost universally most stable for  $\beta_{\text{C}}\approx 1$  and  $1<\text{I}_{\text{B}}<2$ . The in-phase state is either unstable or barely stable when  $\beta_{\text{C}}$  or  $I_{\text{B}}$  become large. In these limits when, the in-phase state is barely stable, intermittent behavior can be expected. The bias current,  $I_{\text{B}}$ , can easily be adjusted but  $\beta_{\text{C}}$  is fixed when the junctions are fabricated. Thus the most important design criterion to achieve stable, in-phase oscillations is to make junctions with  $\beta_{\text{C}}\approx 1$ . The next section builds on this analysis and considers what is happening right at the instabilities.

#### §5. Transitions between Solutions

When one of the solutions loses stability, the system makes a transition to another solution. This process is called a bifurcation. Some commonly known bifurcations such as symmetry breaking and period doubling appear in our arrays. The high symmetry of the Josephson junction arrays also results in some rather unusual bifurcations which will be discussed below.

In the previous section the stability of the the in-phase solution was examined. The arguments used there can be generalized to analyze the stability of any periodic solution. To linear order the perturbations to a periodic solution always obey a set of linear differential equation with periodic coefficients. The solutions to these equations have Floquet form,  $e^{\rho t}\chi(t)$ , where  $\chi(t)$  is a periodic function. A derivation of this result for the general case of a d-dimensional equation is given in appendix B. The periodic solution is stable as long as all of the Floquet exponents are negative. A bifurcation occurs if any one of the (complex) Floquet exponents crosses the imaginary axis so that its real part changes from negative to positive.

## Simple bifurcations

In the absence of special constraints or any underlying symmetry, there are only three ways in which the solution can lose stability as a single parameter is varied (see Fig. 5.1). The three possibilities are a saddle node bifurcation, where a single exponent crosses the imaginary axis at  $Im(\rho)=0$ ; a period doubling bifurcation, where a single exponent crosses the imaginary axis at  $Im(\rho)=\pi/T$ ; and a Hopf bifurcation, where a complex conjugate pair of exponents cross the imaginary axis anywhere else. Other bifurcations can appear when there is a symmetry present in the problem.<sup>29</sup>

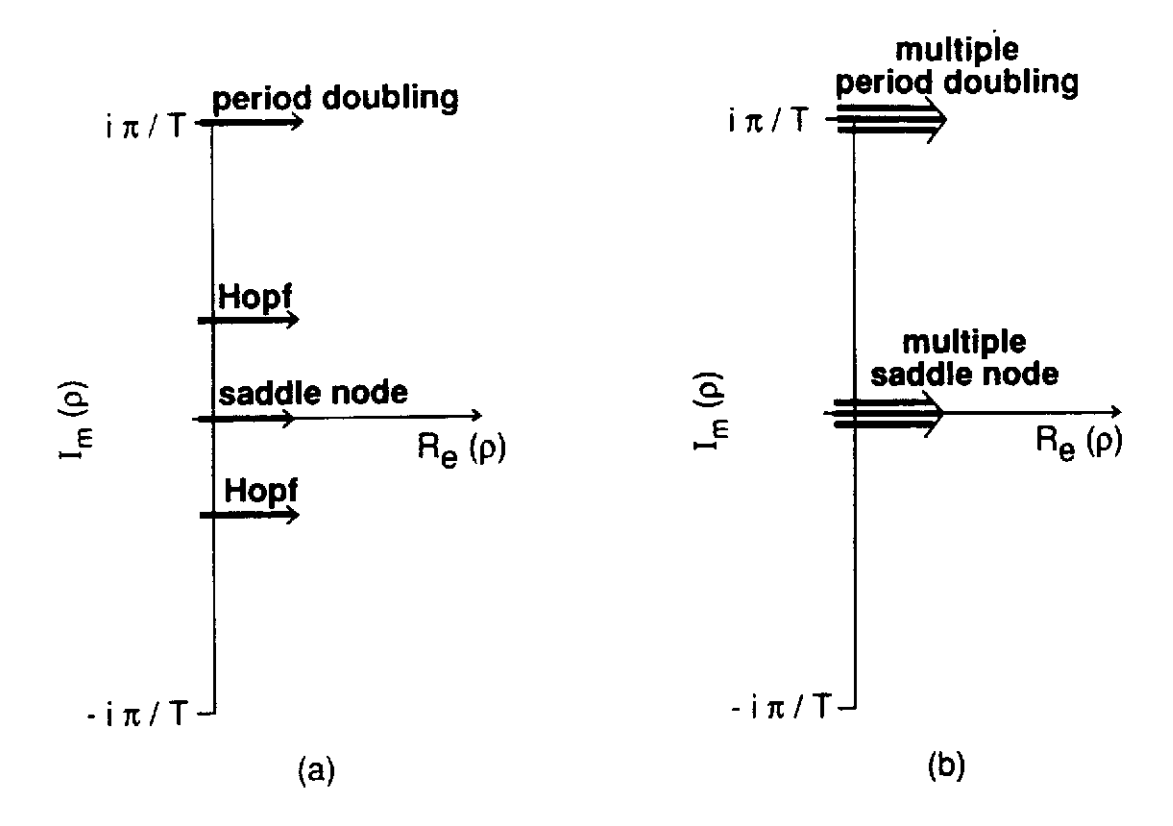


Fig. 5.1 (a) - The three generic, codimension-one bifurcations (period doubling, saddle-node, and Hopf) occur as a single Floquet exponent crosses the imaginary axis at  $i\pi/T$ , 0, and as a complex conjugate pair respectively. (b) - Two multiple bifurcations in which many Floquet exponents cross the imaginary axis together were observed at  $Im(\rho)=\pi/T$  and  $Im(\rho)=0$ .

These bifurcations generally manifest themselves as abrupt changes in the observables of the system. Figure 5.2 shows two current-voltage curves that were calculated for arrays with three junctions and  $\beta_{C}=0$ . The solid line in figure 5.2a is the calculated voltage as a function of current for the junction array shown in the inset. The dashed lines in the figure are the numerically determined in-phase solution and the approximation to the antiphase solution that was discussed in section 3. In this case the load is designed to be inductive at all of the relevant frequencies so the analysis of the last section tells us that the in-phase state should be stable. The figure agrees with this prediction. Figure 5.2b shows the same curves for a three junction array shunted by a capacitor. In this case the analysis of section 4 states that the in-phase state should be unstable. Again, the figure agrees with this prediction and shows that the antiphase solution is stable for high bias currents. However, for bias currents near the critical current the antiphase solution also becomes unstable and there is a kink visible in the current-voltage curve. This kink corresponds to a bifurcation.

By taking phase portraits of the motion on both sides of the kink we have determined that it signals a symmetry breaking bifurcation. The symmetry that is broken is a permutation symmetry; the equations are unchanged by the interchange of any two junctions. At the symmetry breaking bifurcation a Floquet exponent crosses the imaginary axis at  $Im(\rho)=\pi/T$ . This is the symmetry breaking bifurcation that must precede a period doubling bifurcation as Swift and Wiesenfeld described.<sup>30</sup> Figure 5.3 shows some phase portraits of the dynamics. In these portraits a closed trajectory corresponds to periodic motion. The sequence of phase portraits shows the symmetry breaking followed by a cascade of period-doubling bifurcations and eventually leading to chaos. At each period doubling a Floquet

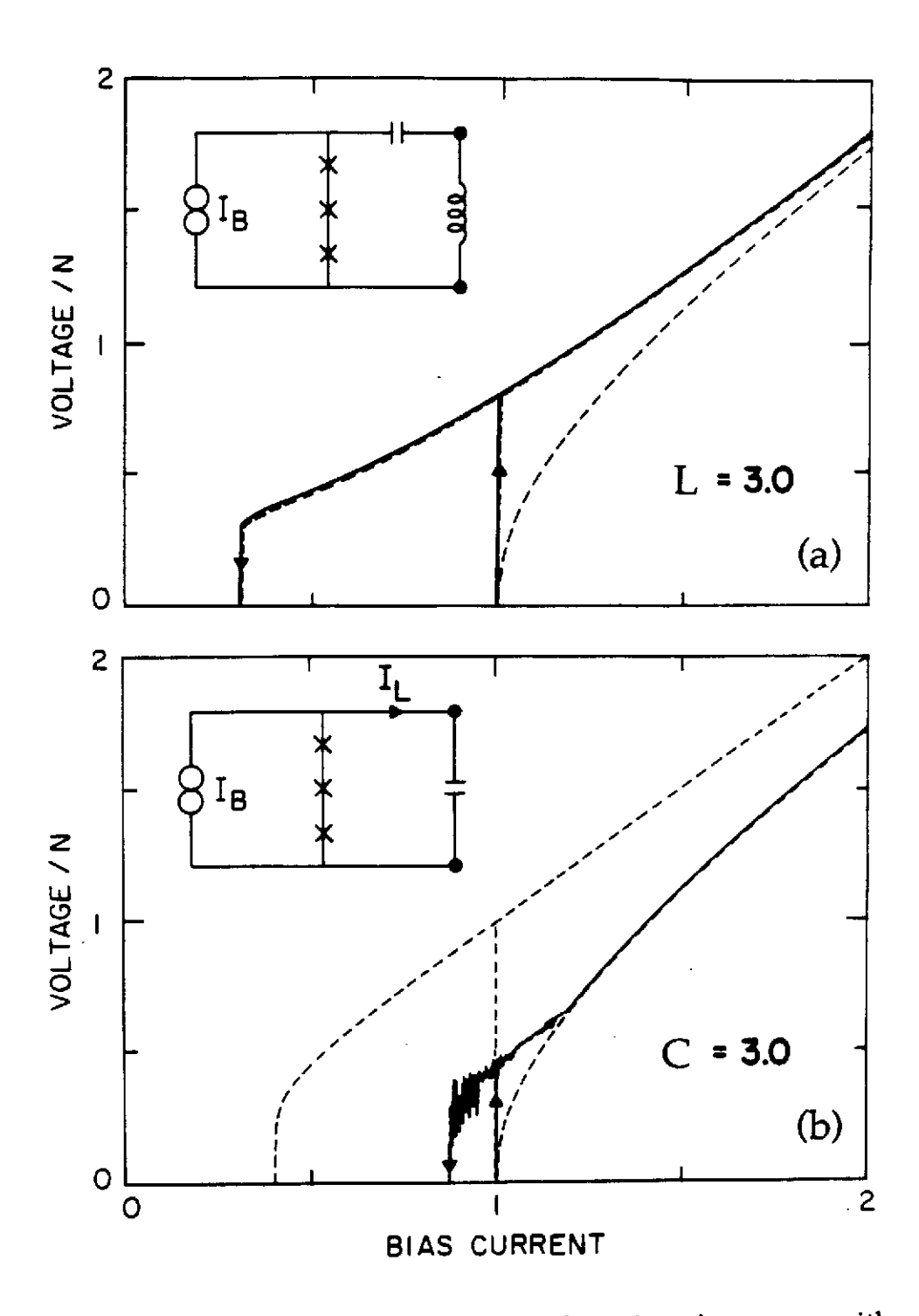


Fig. 5.2 (a) - Current-voltage curve for a three junction array with an inductive load, L=3, and a blocking capacitor, C=5. The dashed lines represent the in-phase and antiphase solutions. The curve shows that the in-phase solution is stable for an inductive load. (b) - Current-voltage curve for a three junction array with a capacitive load, C=3. This figure shows that the antiphase solution is stable at high bias for a capacitive load.

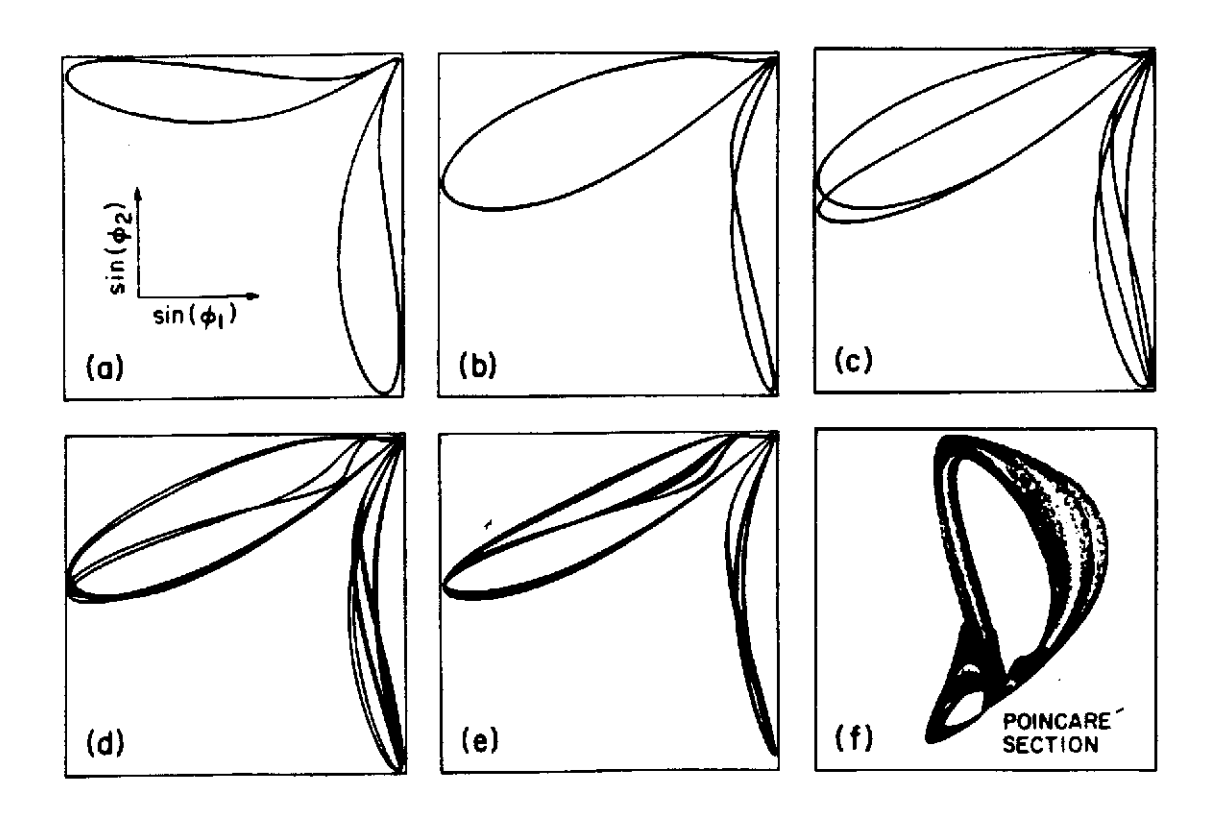


Fig. 5.3 Figures a-e are phase portraits of the motion, in the vicinity of the bifurcation seen in Fig. 5.2b, showing symmetry breaking followed by a period doubling cascade. The portraits are projections of the trajectory in phase space onto the  $\sin(\phi_1)$  vs.  $\sin(\phi_2)$  plane. Figure 2f is a Poincare section of chaotic motion showing the fractal structure of the strange attractor.

exponent crosses the imaginary axis at  $Im(\rho)=\pi/T$ . Figure 5.3f is a Poincare section of the chaotic motion that shows the fractal structure of the strange attractor.

When the array is shunted by a series LC load, the simulations show that the in-phase and anti-phase solutions exchange stability in a way that produces a hysteresis loop in the current-voltage curve, as shown in Fig. 5.4. The reactance of the load at the Josephson frequency goes from capacitive to inductive as the bias current is increased, causing the transitions. Beginning at low bias current the anti-phase solution remains stable, as the bias current is increased, until the fundamental Josephson frequency of the anti-phase solution exceeds the LC resonant frequency ( $\omega_R$ =(LC)-1/2) and the load becomes inductive. At that point a Floquet exponent crosses the imaginary axis at Im(p)=0 and the system jumps to the in-phase solution. This is a saddle node bifurcation. When the system jumps to the in-phase state, the fundamental Josephson oscillation jumps to a higher frequency. This makes the load look more inductive. The in-phase solution will thus remain stable until the bias current is decreased to the point at which the fundamental Josephson frequency of the in-phase is less than the LC resonant frequency, and the load looks capacitive once again. At this point the system suffers another saddle node bifurcation and returns to the antiphase state.

#### Memory cells

The hysteresis loop in Fig. 5.4 suggests that Josephson junction arrays could be used to construct a memory cell. The system would be biased so that both the in-phase solution and the antiphase solution are stable. A bit of information would be represented by whether the system was in the in-phase or antiphase state. To write the in-phase state the bias current would

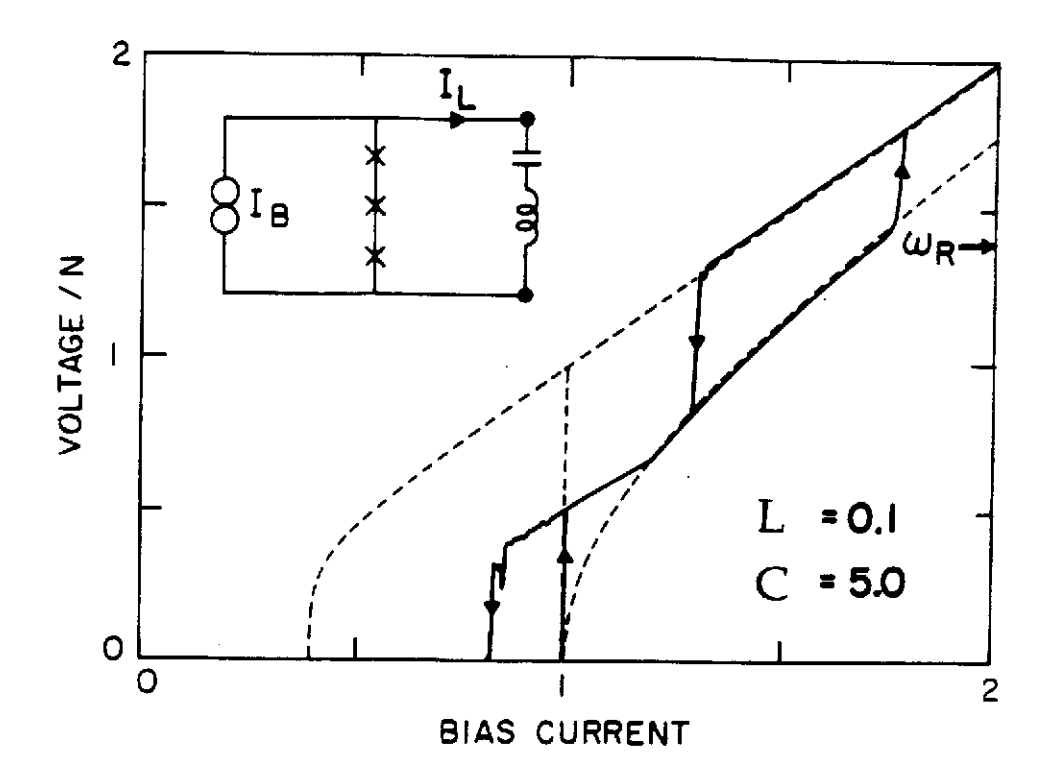


Fig. 5.4 Current-voltage curve for a three junction array shunted by a series LC circuit. C=5, L=0.1 The dashed lines represent the in-phase and the antiphase solutions. The arrow on the right indicates the value of  $\omega_R=(LC)^{-1/2}=\sqrt{2}$ . This figure shows the hysteresis between the in-phase and anti-phase solutions.

be temporarily increased above the point where the antiphase state loses stability and then decreased to the normal bias point where both solutions are stable. This would leave the system in the in-phase solution. Similarly the antiphase state could be written by temporarily decreasing the bias current. The memory cell could be read by either detecting the voltage across the array or by detecting the ac oscillations produced by the array. This would be an unusual memory cell in the sense that information would be stored in the form of a dynamical state instead of a static quantity.

#### Multiple bifurcations

The simple bifurcations are the ones you expect to find when there is no special symmetry in the problem. When a symmetry is present, there exists the possibility of a multiple bifurcation where several Floquet exponents cross the imaginary axis simultaneously.<sup>31</sup> In the present problem of series arrays, there is a permutation symmetry: any transformation of Eqn. 2.6 which exchanges two junctions leaves the circuit equations unchanged. It follows that if  $(\phi_1,\phi_2,...,\phi_j,\phi_k,...,\phi_N)$  is a solution then so is  $(\phi_1,\phi_2,...,\phi_k,\phi_j,...,\phi_N)$ , as are all of the other N! permutation related solutions. Of course, all of these solutions may not be distinct. If all N! permutations give the same solution, then this is a symmetric solution: this is just what we have been calling the in-phase solution. On the other hand, if a solution is not invariant with respect to all N! permutations of the  $\{\phi_k\}$ , then we call it a symmetry-broken solution. For instance, the antiphase solution and the split solution are symmetry-broken solutions.

In the analysis of the stability of the in-phase state we noted that the N-1 equations (4.2) that govern the relative coordinates are identical. This means that the N-1 associated Floquet exponents are all equal, and when the in-phase state loses stability these exponents all cross the imaginary axis

simultaneously. In our simulations multiple exponents have been observed crossing the imaginary axis at  $Im(\rho)=0$  and at  $Im(\rho)=\pi/T$  (see Fig. 5.1). When the in-phase state loses stability via a multiple bifurcation at  $Im(\rho)=0$  the array assumes a symmetry-broken, antiphase solution. At this point at least (N-1)! stable solutions simultaneously appear. When the in-phase solution loses stability via a multiple bifurcation at  $Im(\rho)=\pi/T$ , the array assumes a symmetry-broken split solution. Here  $N!/(\alpha!(N-\alpha)!)$  new, symmetry related solutions appear, where  $\alpha$  is the integer part of N/2. Thus the consequence of having many Floquet exponents cross the imaginary axis simultaneously seems to be a tremendous increase in the number of new solutions that appear. This phenomena seems to be a common occurrence in dynamical systems with many coupled degrees of freedom.

## §6. Noise Driven Fluctuations of the In-phase State

There is an interest in exploiting the high frequency oscillations of Josephson junctions to construct generators of millimeter wave radiation. Ideally, arrays of Josephson junctions oscillating in the in-phase state would generate a single, stable frequency. However, inevitable fluctuations in the circuit give the output a finite linewidth. This linewidth limits the practical utility of the arrays. The form of these fluctuations and the resulting linewidth are the focus of this section.

It has long been recognized that if the fluctuations at each junction of an array are independent, then the total fluctuations across the array are the incoherent sum of the fluctuations at the individual junctions. This leads to the result that the voltage fluctuations across an array scale like  $\sqrt{N}$ . <sup>21</sup> This narrowing of the linewidth in coherent arrays has been observed experimentally. <sup>32</sup> The upshot of this scaling is that the larger, more powerful arrays have a purer spectral output, which is a very desirable consequence from the practical point of view. Below a calculation of the form of the fluctuations in the limit of small external noise is presented. This calculation builds on the results obtained from the stability analysis of the in-phase state.

The response of the in-phase state to a small perturbation was calculated in section 4. It was shown there that a perturbation decays rapidly far away from any instability but that as an instability is approached perturbations decay more slowly. Right at the bifurcation perturbations take an infinitely long time to decay (Re(p)=0). In this section these results are extended to the case where the in-phase state is repeatedly perturbed by some external

noise source, such as thermal noise. The deviations from the in-phase state caused by the external noise are called the fluctuations of the system. Here the power spectrum of these fluctuations is calculated and it is shown that the fluctuations increase as a bifurcation is approached.

For a series array with a matched resistive load, the equations for the dynamics including noise are,

$$\beta_c \ddot{\phi}_k + \dot{\phi}_k + \sin(\phi_k) + \frac{1}{N} \sum_j \dot{\phi}_j = \xi_k(t) + \xi_L(t)$$
 k=1,...,N 6.1

Where the usual reduced units have been employed. The random terms  $\xi_{\mathbf{k}}(t)$  and  $\xi_{\mathbf{L}}(t)$  represent the noise generated in the kth junction and the load respectively. One unavoidable source of noise is the Johnson noise associated with the resistors in the equivalent circuit of the array. In this case the noise sources act independently at each resistor,  $\langle \xi_{\mathbf{k}}(t) \rangle = 0$ ,  $\langle \xi_{\mathbf{L}}(t) \rangle = 0$ ,  $\langle \xi_{\mathbf{k}}(t) \xi_{\mathbf{k}'}(t') \rangle = T_{\mathbf{B}} \delta_{\mathbf{k}\mathbf{k}'} \delta(t-t')$ ,  $\langle \xi_{\mathbf{L}}(t) \xi_{\mathbf{L}}(t') \rangle = T_{\mathbf{B}} \delta(t-t')/N$ , and  $\langle \xi_{\mathbf{k}}(t) \xi_{\mathbf{L}}(t') \rangle = 0$ , where  $T_{\mathbf{B}}$  is the normalized bath temperature,  $T_{\mathbf{B}} = 4ek_{\mathbf{B}}T/\hbar I_{\mathbf{C}}$ .

The in-phase solution,  $\phi_k = \phi_O$ , describes a closed trajectory (a limit cycle) in phase space. The fluctuations can either be along the in-phase trajectory (phase fluctuations) or transverse to the in-phase trajectory (transverse fluctuations). There is a fundamental difference between these two types of fluctuations. Deviations transverse to the trajectory decay with time because the in-phase trajectory is a stable solution. The transverse fluctuations are most pronounced when the in-phase state is least stable. Deviations along the trajectory do not decay because of a symmetry in the problem. This symmetry is the invariance of the system with respect to translations in time (this is an autonomous system). Fluctuations along the trajectory essentially shift the origin of time and do not decay. They

represent the diffusion of the system along the stable trajectory. As is shown below the power spectrum of these two types of fluctuations have a different form.

Both types of fluctuations can be visualized in the phase space for the dynamics. A representation of the 2N dimensional phase space is illustrated in Fig. 6.1. The closed curve represents the in-phase trajectory. Phase fluctuations,  $\psi$ , describe deviations tangent to this trajectory while transverse fluctuations, x, describe deviations in the 2N-1 directions transverse to the trajectory.

Since phase fluctuations correspond to shifts in the origin of time they alter an observable such as the voltage so that it takes the form,  $V(t)=V_O(t+\psi(t)), \text{ where } V_O(t) \text{ is the noise-free voltage and } \psi(t) \text{ are the phase fluctuations.}$  The effect that the phase fluctuations have on the linewidth can be seen by writing the noise-free voltage in a Fourier series,  $V_O(t)=\sum_{a}a_\omega e^{i\omega t}.$  With the phase fluctuations included V(t) becomes,  $V(t)=\sum_{a}a_\omega e^{i\omega(t+\psi)}.$  Here each Fourier component of the noise-free solution is multiplied by a fluctuating factor,  $e^{i\omega\psi}.$  Thus the lineshape of the Fourier component at frequency  $\omega$  is determined by the square of the Fourier transform of  $e^{i\omega\psi}.$  The consequence of this is that the phase fluctuations cause the array to generate a spread of frequencies instead of a single well defined frequency.

The second type of fluctuations come from the noise kicking the system transverse to the noise-free solution. Mathematically the transverse fluctuations are described by adding a term to the noise-free voltage,  $V(t) = V_O(t) + V_T(t).$  These fluctuations effect only the amplitude of the oscillations, not the frequency.

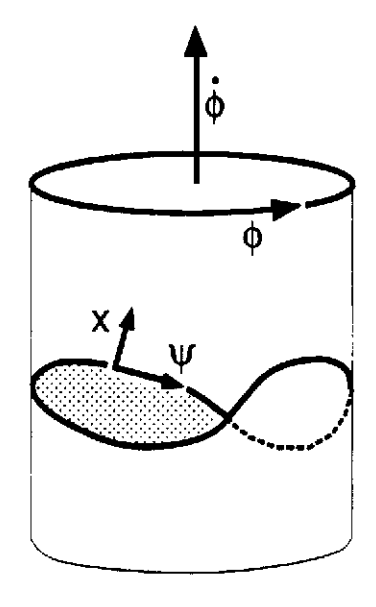


Fig. 6.1. - Representation of the in-phase solution in phase space indicating how the phase fluctuations and the transverse fluctuations describe the deviations from the in-phase solution. For this system the dynamics take place on an N dimensional cylinder where the variables  $\phi_k$  are periodic and the variables  $\phi_k$  can take on any value. The in-phase solution describes a closed trajectory on this N-cylinder. The phase fluctuations are the deviations tangent to the in-phase trajectory and the transverse fluctuations are the deviations transverse to the trajectory.

#### Small noise approximation

When the noise is small, the deviations from the in-phase solution are likewise small so consider a solution to Eqn. (1) of the form  $\phi_k = \phi_0(t) + \eta_k$ . The linearized equations for  $\eta_k$  are,

$$\beta \ddot{\eta}_{k} + \dot{\eta}_{k} + \cos(\phi_{0}) \eta_{k} + \frac{1}{N} \sum_{j} \dot{\eta}_{j} = \xi_{k}(t) + \xi_{L}(t)$$
 6.2

This approximation relies on linearizing the equations about a stable, noise-free solution. This implies that the results obtained here are only valid when the noise is sufficiently small that it does not perturb the system too far from the noise-free solution. For example, it has been reported that larger noise can lead to hopping between coexisting stable solutions.<sup>33</sup> The results presented here cannot account for such behavior.

Equation 6.2 can be simplified by once again taking advantage of the permutation symmetry. A transform is made to the natural coordinates of this system, which are the mean coordinate  $\vartheta=(1/N)\Sigma\eta_k$ , and the N-1 relative coordinates,  $\zeta_k=\eta_k-\eta_{k+1}$ . The linearized equations then become,

$$\beta_c \ddot{\vartheta}_k + \dot{\zeta}_k + \cos(\phi_o) \zeta_k = \xi_{k} - \xi_{k+1}$$
 6.3a 
$$\beta_c \ddot{\vartheta} + 2\dot{\vartheta} + \cos(\phi_o) \vartheta = \frac{1}{N} \sum_k \xi_k + \xi_L$$
 6.3b

As we have said before, this transformation decouples all N coordinates in the problem. Special attention should be given to  $\vartheta$  since it is the variable that describes the fluctuations across the entire array. These are the fluctuations that appear in a generator output.

Neglecting noise for a moment, consider the homogeneous solutions to Eqn. 6.3. These solutions describe how an impulse perturbation to the inphase solution evolves. Since Eqn. 6.3 is linear with periodic coefficients we know from Floquet theory that the homogeneous solutions have the form,

 $e^{\rho t}\chi(t)$ , where  $\chi(t)$  is a periodic function with the same period as  $\phi_0(t)$ . The Floquet exponent,  $\rho$ , specifies the rate of decay of an impulse perturbation. In particular the two homogeneous solutions to Eqn. 6.3b are,

$$\vartheta_{\parallel} = \dot{\phi}_{0}$$
 and  $\vartheta_{\perp} = \dot{\phi}_{0}(t) \int_{0}^{t} \frac{e^{-2t'/\beta_{c}}}{\dot{\phi}_{0}^{2}(t')} dt'$  6.4

Here  $\vartheta_{||}$  is periodic ( $\rho$ =0) and corresponds to a perturbation along the inphase solution. When a small perturbation of the form  $\epsilon\vartheta_{||}$  is added to the in-phase solution, the result is equivalent to translating the origin of time by the small quantity  $\epsilon$ ,  $\phi_0 + \epsilon \dot{\phi}_0 \approx \phi_0(t+\epsilon)$ . Because of this property  $\vartheta_{||}$  plays a special role in the analysis, namely, we identify the inhomogeneous solution of Eqn. 6.3b associated with  $\vartheta_{||}$  as the phase fluctuations. When the in-phase solution is stable all of the other homogeneous solutions to Eqn. 6.3 decay exponentially ( $\rho$ <0). These other inhomogeneous solutions of Eqn. 6.3 are then identified as the transverse fluctuations.

Solving for the inhomogeneous solutions to Eqn. 6.3 in terms of the homogeneous solutions, and inverting the transformation to the relative and mean coordinates, one obtains an approximate solution to Eqn. 6.1 of the form  $\phi_k = \phi_0(t+\psi) + x_k$  where

$$\Psi = -\int_{0}^{t} \frac{(\frac{1}{N}\sum_{k} \xi_{k} + \xi_{L})\dot{\phi}_{o}(t')}{\beta_{c}e^{-2t'/\beta_{c}}} \int_{0}^{t'} \frac{e^{-2t''/\beta_{c}}}{\dot{\phi}_{o}^{2}(t'')} dt'' dt'$$
 6.5a

$$x_{k} = \vartheta_{\perp} \int_{-\infty}^{t} \frac{(\frac{1}{N} \sum_{k} \xi_{k} + \xi_{L}) \dot{\phi}_{0}}{\beta_{c} e^{-2t'/\beta_{c}}} dt' - \frac{1}{N} \sum_{q=1}^{k-1} q \zeta_{q} + \frac{1}{N} \sum_{q=k}^{N-1} (N - q) \zeta_{q}$$
 6.5b

The details of this calculation appear in appendix C. Here  $\zeta_{\rm q}$  are the inhomogeneous solutions to Eqn. 6.3a which, unfortunately, must be calculated numerically. The procedure for doing this is described in appendix B.

Previously researchers have used a simpler approximation for the phase fluctuations,<sup>8</sup> namely,

$$\psi = \int \xi(t) dt$$
 6.6

where  $\xi(t)$  is random noise. This approximation arrives at the result that the phase fluctuations cause a spread in the oscillation frequency of the array with a Lorentzian lineshape but it completely neglects the dynamics. Equation 6.5 includes the dynamics of the system and it also describes the contribution of the transverse fluctuations which were previously neglected.

One experimentally accessible variable that exhibits both phase and transverse fluctuations is the voltage across any single junction of the array. In the normalized units this voltage is,  $V_{\mathbf{k}}(t)=\dot{\phi}_{0}(t+\psi)+x_{\mathbf{k}}$ . Phase fluctuations enter the voltage oscillations through the term,  $\dot{\phi}_{0}(t+\psi)$ , and cause a broadening of the linewidth of these oscillations. As was stated above the lineshape of the Fourier component of  $\dot{\phi}_{0}$  at frequency  $\omega$  is given by the square of the Fourier transform of the fluctuating function,  $e^{i\omega\psi}$ , where  $\psi$  is determined from Eqn. 6.5. All of the transverse fluctuations of this voltage have the same form. They are inhomogeneous solutions to noise driven equations whose homogeneous solutions are of Floquet form. Solutions of this sort were studied by Wiesenfeld.<sup>34</sup> He showed that these terms have a power spectrum that is the sum of Lorentzians whose shape is determined by the quantity  $\rho T$ , where  $\rho$  is the Floquet exponent of a homogeneous solution, and T is the period of the noise-free oscillations.

There is one Lorentzian contributed at each Fourier component of  $\phi_0$  by every homogeneous solution. The Lorentzian's width is proportional to  $\rho T$  and its amplitude is inversely proportional to  $\rho T$ . This means that features in the power spectrum will become tall and narrow whenever  $\rho T$  approaches zero. This happens near any bifurcation.

This phenomena, which has been observed experimentally in other systems (including chemical, electrical and optical experiments),<sup>35</sup> is called the noisy precursor to a bifurcation. It has been demonstrated that the power spectrum has certain universal scaling properties close to the bifurcation.<sup>34</sup> The bifurcations of the in-phase solution correspond to instabilities where all of the junctions no longer oscillate identically. At this instability the (N-1)! antiphase solutions appear. Thus the power spectrum of an individual junction of the array consists of a peaks that correspond to the basic oscillations of the junctions which have been broadened by phase fluctuations plus noise bumps which correspond to the decay of the transverse perturbations. As an instability is approached the noise bumps become more prominent in the power spectrum.

For an rf generator application it is most important to consider how the fluctuations effect the total voltage across the array. For small noise the voltage across the whole array is,

$$V(t) = N\dot{\phi}_{o}(t+\psi) + \dot{\vartheta}_{\perp}(t) \int_{0}^{t} \frac{(\frac{1}{N}\sum_{k} \xi_{k} + \xi_{L})\dot{\phi}_{o}(t')}{\beta_{c}e^{-2t'/\beta_{c}}} dt' \qquad 6.7$$

Note that the transverse fluctuations of the total voltage depend only on the mean coordinate,  $\vartheta$ . This leads to the surprising result that the noise bumps which correspond to instabilities where the array loses coherence

appear in the power spectrum of an individual junction of the array but do not appear in the power spectrum of the total voltage across the array. The power spectrum of the total voltage consists of two components. The first is the broadening of the linewidth of the oscillations due to phase fluctuations which was described above. The other component is the noise bump due to the transverse fluctuations. The transverse fluctuations contribute Lorentzians centered at the Fourier components of  $\dot{\phi}_{O}$  to the power spectrum. The amplitude and width of these Lorentzians are governed by the dimensionless quantity,  $\rho T$ , where  $\rho=-2/\beta_C$ . For small  $\beta_C$  and large T (large oscillation periods correspond to low bias currents), the noise bumps will be very broad so the transverse fluctuations contribute an essentially flat component to the power spectrum. In this case the linewidth will be due predominantly to the phase fluctuations. This is illustrated in Fig. 6.2a. For large  $\beta_{C}$  or large bias currents (small T), the transverse fluctuations contribute narrow Lorentzians at the Fourier components of  $\dot{\tilde{\phi}}_O(t)$  which add to the phase fluctuations to make up the linewidth (see Fig. 6.2b). A maximally stable in-phase state ( $\beta_C$ =0.75 and I<sub>B</sub>=2.3) produces a power spectrum qualitatively like that shown in Fig. 6.2a.

In summary, the total voltage across an array of coherently oscillating Josephson junctions exhibits two fundamentally different types of fluctuations, each of which makes its own characteristic type of contribution to the power spectrum. Phase fluctuations broaden the peaks in the power spectrum that correspond to the basic oscillations of the junctions and are primarily responsible for the linewidth of these oscillations. Transverse fluctuations contribute Lorentzian shaped noise bumps to the power spectrum at the fundamental and harmonics of the basic Josephson oscillations. These noise bumps become larger and narrower as  $T/\beta_C$  increases, making a contribution to the linewidth for large  $\beta_C$  and large bias

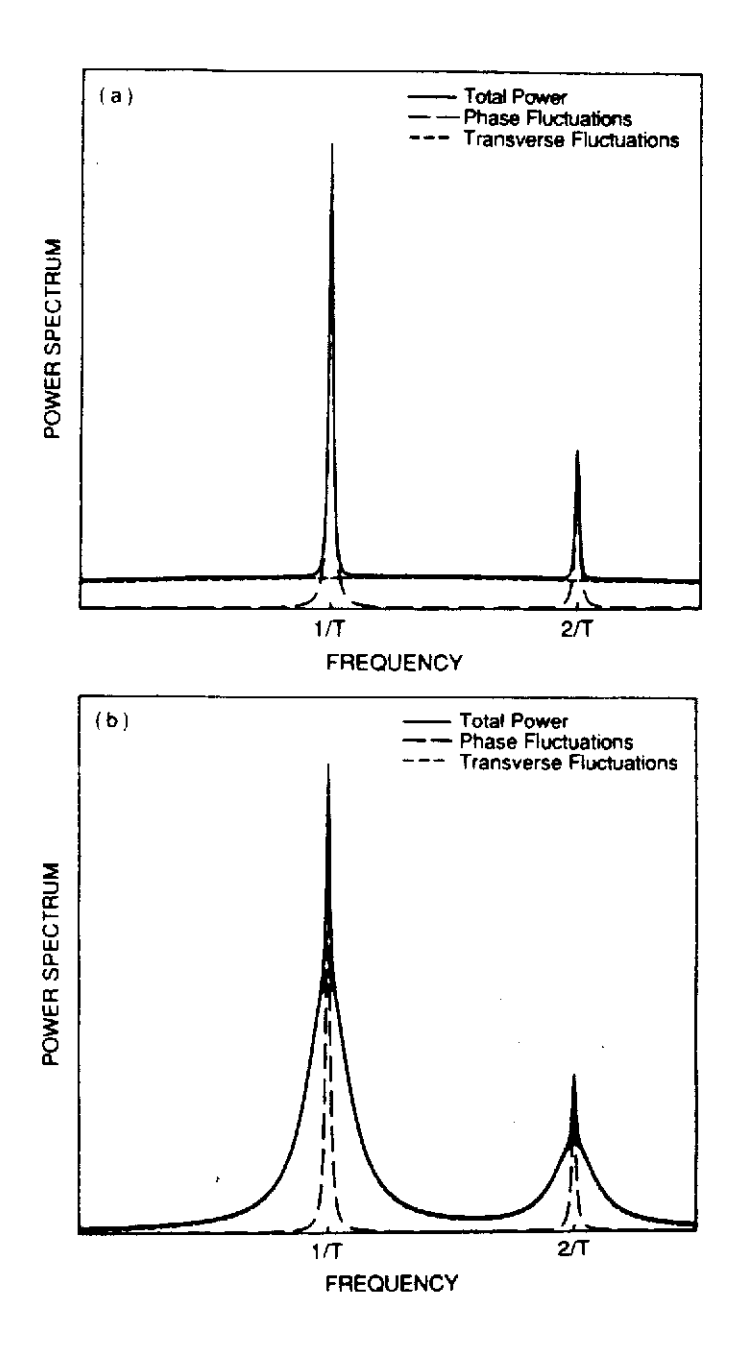


Fig. 6.2 - Power spectrum of the total voltage across the array showing the contributions of the phase and transverse fluctuations. (6.2a) - Large  $T/\beta_C$  where the transverse fluctuations make an nearly flat contribution to the power spectrum. (6.2b) - Small  $T/\beta_C$  where the contributions to the power spectrum are peaked around the fundamental and the harmonics of the basic Josephson oscillations.

currents. The approach of the instability which corresponds to the array losing coherence is responsible for the appearance of noise bumps in the power spectra of the individual junction voltages but the impending instability does not effect the power spectrum of the total voltage across the array. Finally it must be emphasized that all of this analysis has assumed that the in-phase solution was stable and that the noise was small. When either of these conditions are not met nonlinear effects will have to be taken into account.

# §7. Parametric Amplifiers

Modest parametric amplification using single Josephson junctions was first achieved in the sixties.<sup>36</sup> Later, researchers suggested that the performance of these amplifiers could be improved significantly by using series arrays of junctions in place of a single junction. Unfortunately, the gain of these amplifiers was disappointingly small and they exhibited a mysterious noise rise phenomena. Here we suggest that the limited success of the arrays as parametric amplifiers might be understood in terms of the array dynamics. This section concludes with a proposal for a high gain parametric amplifier.

Parametric amplification is a nonlinear interaction by which power is transferred from a "pump" oscillation to a "signal" oscillation. Recently Bryant, Wiesenfeld, and McNamara recognized that the process of parametric amplification can be usefully described in the language of bifurcation theory. The advantage of approaching the problem this way is that certain universal properties, which have to do with the type of bifurcation involved, become apparent in this approach. In these terms a parametric amplifier consists of a pump oscillation that is tuned near a bifurcation. To linear order, perturbations to the pump have Floquet form,  $e^{\rho t}\chi(t)$ . Since the pump is near an instability, some of these perturbations decay very slowly ( $\rho \approx 0$ ). The system is tuned so that the signal has the correct frequency to excite these slowly decaying perturbations. This causes the perturbations to grow and in response to the applied signal which is the basis of the amplification.

In 1975 Feldman, Parrish, and Chiao suggested that series arrays of Josephson junctions could be used to build a high gain, low noise

parametric amplifier.<sup>38</sup> In the analysis that they presented, they assumed that all of the junctions remained in the in-phase state. Other solutions such as the antiphase solution were not considered. When the experiments did not agree with their predictions they suggested that, for some unexplained reason, only a fraction of the junctions were active in producing the nonlinear effects. Our analysis of the stability of the in-phase state suggests they may have been operating in a regime where the in-phase state was unstable. This would make it appear as if not all the junctions were participating. If the in-phase state can be stabilized then the high gain, low noise amplifier that they envisioned might be realized.

In order to design a parametric amplifier it is important to understand the nature of the bifurcation that provides the amplification. Some bifurcations are more suitable for parametric amplifier applications than others. To achieve the greatest amplification it is important to use an instability that causes a large voltage response at the output of the array. The multiple bifurcations described in section 5 would make a rather poor amplifier because in that case the phases of the junctions tend to cancel out, resulting in very small response at the output of the array.

The best bifurcation to use for an amplifier would be one in which all of the junctions oscillate identically throughout the bifurcation. The response at such a bifurcation would be greater because all of the the junctions would contribute constructively to the response. This kind of "coherent bifurcation" would be one where only a single Floquet exponent crosses the imaginary axis and where the in-phase state would be stable on both sides of the bifurcation. After a bit of searching, bifurcations of this sort were observed for ac driven arrays with a capacitive load.

The circuit diagram for the array which exhibits these bifurcations is shown in Fig. 7.1. It is a series array of N junctions driven by an ac current (the pump) and shunted by a capacitor. In normalized units the equations that describe the dynamics of this circuit are

$$\beta_c \ddot{\phi}_k(t) + \dot{\phi}_k(t) + \sin(\phi_k(t)) + c\dot{v} = A\cos(\omega t)$$
  $k=1,2,...,N$  7.1a  $v = \sum_{j=1}^{N} \dot{\phi}_j$  7.1b

This is essentially the same circuit as that studied by Feldman et al. except here  $\beta_{\boldsymbol{C}}$  and the shunt capacitor have been chosen to stabilize the in-phase state. Numerical simulations of these equations show that there are two different coherent bifurcations were observed for this system with the parameter values  $\beta_{C}$ =1,  $\omega$ =0.5, and c=6/N. One is a period doubling bifurcation which occurs at A~4. By tuning the system close to this bifurcation one could construct a parametric amplifier that operates in the conventional three photon mode.37 This would amplify signals with a frequency near  $\pi/T$ . The other coherent bifurcation is a symmetry breaking bifurcation which occurs at A~3.2. This bifurcation could be used to operate an amplifier in the recently described six photon mode.<sup>37</sup> In this case signals with a frequency of  $2\pi/T$  would be amplified. In between these two bifurcations this system exhibits a virtual Hopf phenomena where a complex conjugate pair of Floquet exponenets travel just to the left of the imaginary axis from  $\text{Im}(\rho)=0$  to  $\text{Im}(\rho)=i\pi/T$ . The virtual Hopf phenomena is nearly a Hopf bifurcation and might be used to construct a parametric amplifier at frequencies between  $\pi/T$  and  $2\pi/T$ .

Finally there is the question of noise rise in parametric amplifiers. The noise rise has been attributed to noise driven hopping among solutions. In this picture external noise kicks the system among one of several stable solutions. This hopping results in a Lorentzian shaped noise bump

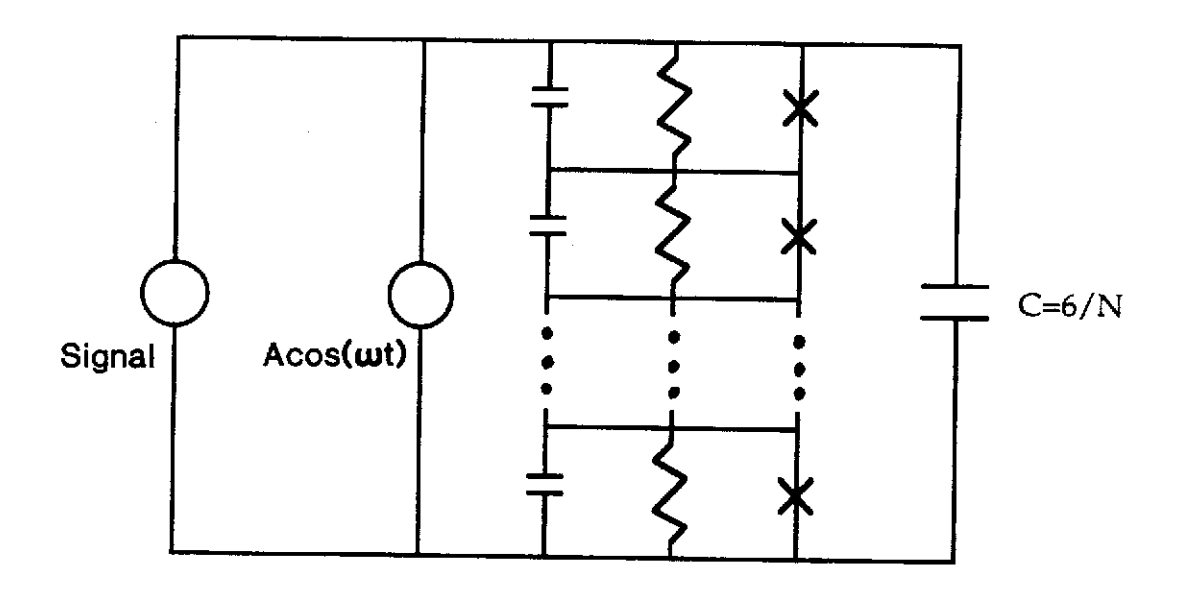


Fig. 7.1 - Circuit diagram of the proposed high gain, low noise parametric amplifier. Here  $\beta_C$ =1,  $\omega$ =0.5, A=3.2, and c=6/N where N is the number of junctions.

centered at zero frequency in the power spectrum of the dynamics. In the case of a period doubling bifurcation there are two branches of the same solution and the external noise causes the system to hop from one branch to the other. For the coherent symmetry breaking bifurcation the two symmetry broken solutions are disjoint in phase space so the hopping takes place over larger distances. If these arguments about the noise rise are correct then this implies that there would be less of a noise rise at the symmetry breaking bifurcation than at the period doubling bifurcation. Since the amplifier described above exhibits both bifurcations it could be used to test this noise rise theory.

### §8. Nonidentical Junctions

Thus far we have dealt with the idealized case of identical junctions. This simplification was made in order to make the problem tractable for arrays with arbitrarily large numbers of junctions. Of course, in any real array, all of the junctions would have slightly different critical currents, shunt resistances, and capacitances. The hope is that when these deviations are small that the results presented above remain qualitatively valid.

To gain some insight into the effect that nonidentical junction parameters have on the in-phase oscillations we have performed simulations of 100 junction arrays. When all of the junctions are identical the in-phase state of the array is stable with a Floquet exponent of -0.4. The parameters of the junctions are then altered so the junctions are not identical and the simulations are run again. Figures 8.1a-8.1e are movies of nonidentical junction arrays in which we have introduced flat distributions of 0%, 5%, 10%, 15%, and 20% in the critical currents, the shunt resistances and the capacitances of the junctions. The lengths of the lines that show the positions of the phases are proportional to the critical currents of the junctions. Thermal noise was also included in the simulations. When the noise terms are included in Eqn. 2.6 we have,

$$\beta_{c}\ddot{\phi}_{k}(t) + \dot{\phi}_{k}(t) + \sin(\phi_{k}(t)) + I_{L}(t) = I_{B} + \xi_{k}(t)$$

$$V(t) = \sum_{k=1}^{N} \dot{\phi}_{k}(t) = F(I_{L}(t))$$
8.1a
8.1b

where  $\xi_k(t)$  are the uncorrelated noise currents,  $\langle \xi_k(t) \xi_{k'}(t') \rangle = (4/\gamma) \delta_{kk'} \delta(t-t')$ , and  $\gamma = \hbar I_C/(ek_BT) = 1150$ . This level of thermal noise corresponds to critical currents of  $10^{-4}$  Amps and an operating temperature of 4.2°K. Notice that the oscillations remain largely in-phase when a 15% spread in the

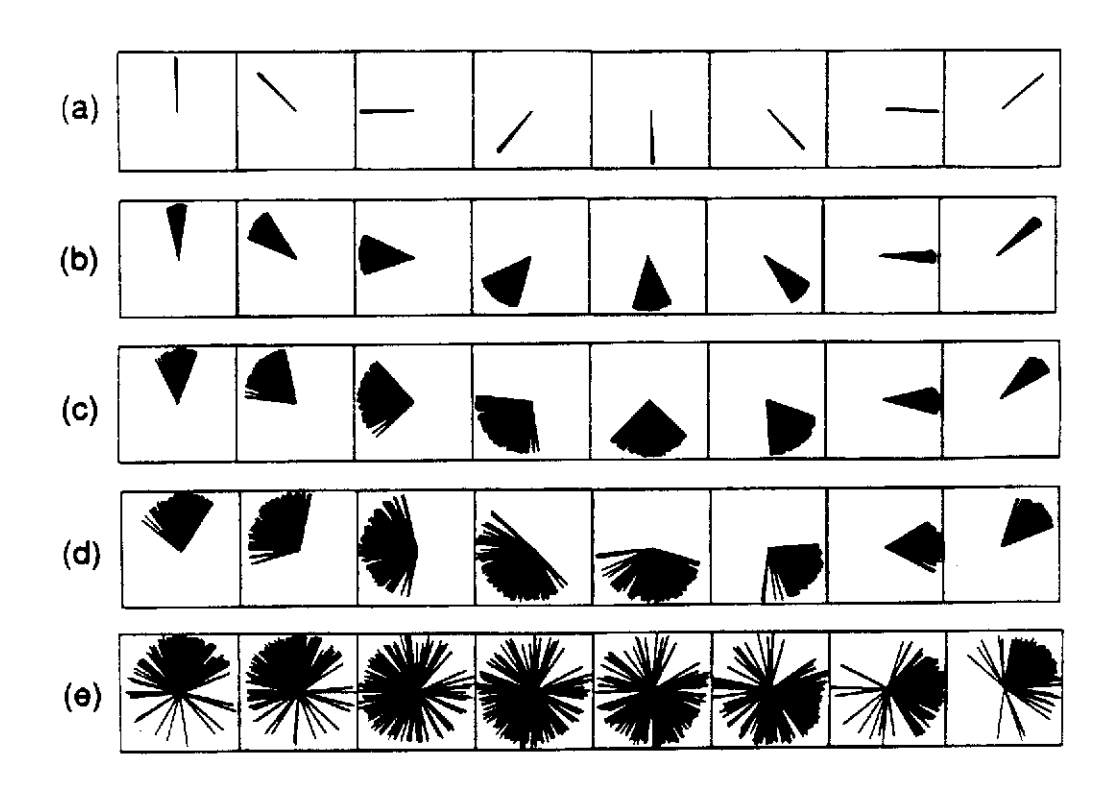


Fig. 8.1 - Movie of the solution for 100 junction arrays with nonidentical parameters and a matched resistive load, R=N. Each sequence has a different percentage spread in the junction parameters (critical current, capacitance, and shunt resistance). (7a) - 0% spread in the junction parameters. (7b) - 5%. (7c) - 10%. (7d) - 15%. (7e) - 20%. In each case  $I_B=2.3$ ,  $\beta_C=.75$ , and  $\gamma=1150$ .

junction parameters is introduced. These simulations show that the inphase solution can remain stable when modest junction mismatches and thermal noise are included.

Calculating the stability of the mismatched junction arrays is more laborious than it was for the identical junction arrays. This is because we can no longer use the symmetry to reduce the problem the way we did in section 4. Nevertheless the stability calculation could be done using the method described in appendix B. This involves numerically determining the solution to the array equations over one cycle and then constructing a return map. The Floquet exponents are proportional to the logarithm of the eigenvalues of the return map so the in-phase state is stable when all of the eigenvalues have a magnitude less than one. When all of the junctions are identical there are many degenerate Floquet exponents. When the junctions are slightly different this degeneracy is broken and one expects the exponents to be scattered around the degenerate, identical junction values. One can use the following theorem (due to Gershgorin)<sup>39</sup> to estimate the largest eigenvalue of the return map in the nonidentical junction case.

$$|\lambda_{\max}| \le \max(\sum_{i} |A_{ij} + \delta_{ij}|)$$
 8.2

where  $A_{ij}$  are the matrix elements for an array with identical junctions and  $\delta_{ij}$  represent the deviations. On average the deviations have a random nature and add incoherently. This would tend to increase the largest eigenvalue and thus make the in-phase state less stable. The greater the number of junctions, the more deviations there would be to add in Eqn. 8.2 so the greater the largest exponent would likely be. Thus the stability of the in-phase state would decrease as the mismatches between the junctions increases and as the number of nonidentical junctions increases. The

simulations agree with this picture qualitatively but a quantitative numerical study of this effect has not been made.

There are two main consequences of having nonidentical junctions. The first is that the power that an array can deliver decreases as the mismatches increase. This can be seen in Fig. 8.1 where the destructive interference of the junctions increases as the spread in parameters increases. The other consequence of using nonidentical junctions is that the fluctuations increase. As we discussed in section 6, the fluctuations depend on the Floquet exponents. These exponents come closer to the critical value  $(Re(\rho)=0)$  as the mismatches increase and as the number of junctions increase. This causes the fluctuations to increase. Thus, for the local oscillator and parametric amplifier applications it is advantageous to make the junctions as identical as possible.

# §9. Coupled 1-d, 2-d, and 3-d arrays

In this section the stability of the in-phase state for more complex arrays are discussed. Examples of these arrays include coupled 1-d arrays (Fig. 9.1a), 2-d arrays (Fig. 9.1b), and 3-d arrays (Fig. 9.1c). In each of these cases it will be assumed that all of the junctions of an array are identical and that no magnetic field is applied. For this configuration, each junction is coupled to every other junction just as they were for the series arrays. Ironically it is easier to determine the stability of these arrays than it was for the series arrays that were discussed in section 4. This is because we can use symmetry arguments to show that the in-phase state is not linearly stable.

First consider the coupled 1-d array of Fig. 9.1a. This array has been proposed as a microwave generator. Here we assume that the junctions are spaced far enough apart that radiative and quasiparticle coupling mechanisms can be neglected. The resistors are included in the circuit to break the quantum interference and thereby to reduce the magnetic field dependence of the circuit. The equations that conserve current at every junction are

$$\beta_c \ddot{\phi}_{ij} + \dot{\phi}_{ij} + \sin(\phi_{ij}) = I_j$$
 9.1

where i=1,2,...N, j=1,2,...M, and  $I_j$  is the current flowing through the jth column. In addition to these equations are the equations that equate the voltage across every column and the equation that conserves the total current.

$$V = \sum_{i} \dot{\phi}_{ij} + I_{j}R \qquad j=1,2,...,M$$
 9.2 
$$I_{B} = \sum_{i} I_{j}$$
 9.3

Equations 9.2 and 9.3 can be used to eliminate the variables  $I_j$  and V. The dynamics of the array are then described by

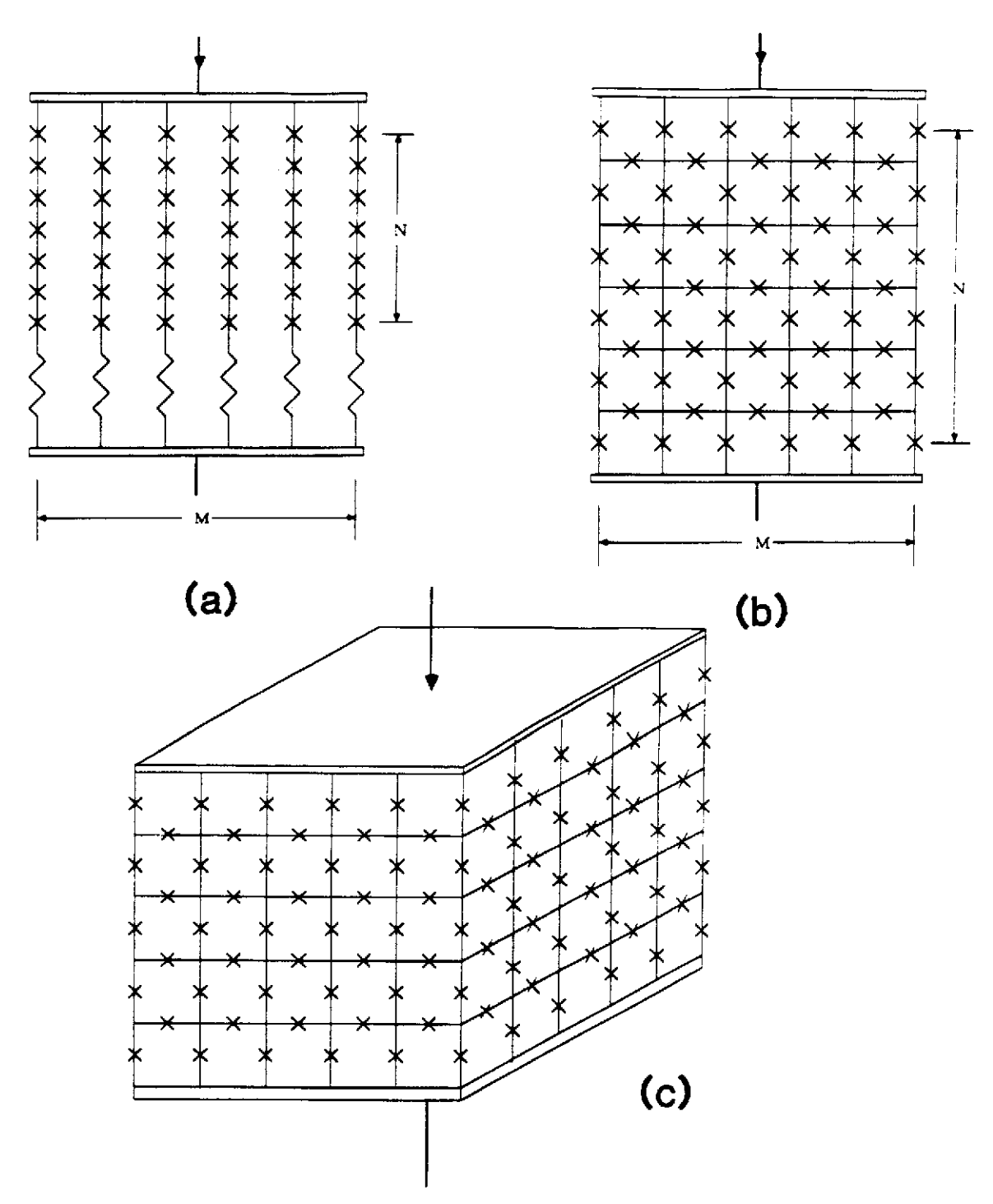


Fig. 9.1 - More complex Josephson junction arrays. (9.1a) Coupled 1-d array. (9.1b) 2-array. (9.1c) 3-d array. Here each x represents an entire junction, not just the supercurrent component.

$$\beta_c \dot{\phi}_{ij} + \dot{\phi}_{ij} + sin(\phi_{ij}) - \frac{\sum\limits_{i,j} \dot{\phi}_{ij} + I_B R}{MR} + \frac{\sum\limits_{i} \dot{\phi}_{ij}}{R} = 0 \qquad \qquad 9.4$$

This equation shows that every junction is coupled to every other junction. In order for this array to function as a microwave generator each junction must oscillate identically,  $\phi_{ij} = \phi_0$ . In this case Eqn. 9.4 reduces to

$$\beta_c \ddot{\varphi}_0 + \dot{\varphi}_0 + \sin(\varphi_0) = I_B/M$$
 9.5

This equation is equivalent to the one that describes the dynamics of a single junction biased with a current of  $I_B/M$ . To calculate the stability of this in-phase solution one adds a small perturbation to the in-phase solution,  $\phi_0+\eta_{ij}$ , and then solves for the linear equations that describe the evolution of the perturbations. The linearized equations for the perturbations are

$$\beta_{c}\dot{\eta}_{ij} + \dot{\eta}_{ij} + \eta_{ij}cos(\phi_{o}) - \frac{\sum_{i,j} \dot{\eta}_{ij}}{MR} + \frac{\sum_{i} \dot{\eta}_{ij}}{R} = 0$$
9.6

We make two successive transformations of this equation. The first is to the relative coordinates,  $\zeta_{ij}=\eta_{ij}-\eta_{i+1,j}$  (i=1,2,...,N-1, j=1,2,...M), and the mean column coordinates,  $\vartheta_j=\sum_i \eta_{ij}$  (j=1,2,...M). This transformation results in the following equations,

$$\beta_c \ddot{\zeta}_{ij} + \dot{\zeta}_{ij} + \zeta_{ij} \cos(\phi_0) = 0$$
 9.7

$$\beta_{c}\ddot{\vartheta}_{j} + \dot{\vartheta}_{j} + \vartheta_{j}cos(\varphi_{o}) - \frac{\sum_{k} \dot{\vartheta}_{k}}{MR} + \frac{\dot{\vartheta}_{j}}{R} = 0$$
9.8

Next we transform Eqn. 9.8 to the relative column coordinates,  $\gamma_j = \vartheta_j - \vartheta_{j+1}$  (j=1,2,...,M-1), and the total mean coordinate,  $\Phi = \Sigma \vartheta_k$ .

$$\beta_{c}\ddot{\zeta}_{ij} + \dot{\zeta}_{ij} + \zeta_{ij}\cos(\varphi_{o}) = 0$$
 9.9

$$\beta_c \dot{\Phi} + \dot{\Phi} + \Phi \cos(\phi_0) = 0 \qquad 9.10$$

$$\beta_c \dot{\gamma}_j + \frac{1+R}{R} \dot{\gamma}_j + \gamma_j \cos(\phi_0) = 0$$
 9.11

These are the equations that need to be solved to determine the stability of this array. For the series arrays we solved equations like these numerically.

In this case, however, some of the solutions can be determined without any numerical calculation. By differentiating Eqn. 9.5 one finds,

$$\beta_{c}\ddot{\phi}_{o} + \ddot{\phi}_{o} + \dot{\phi}\cos(\phi_{o}) = 0$$
9.12

Thus one of the solutions to Eqn. 9.9 and Eqn. 9.10 is  $\zeta_{ij} = \Phi = \dot{\phi}_0$ . The Floquet exponent that describes the decay of this solution is zero. Since Eqn. 9.9 is a set of (N-1)M identical equations, there are (N-1)M+1 degenerate Floquet exponents all equal to zero. We also know from Floquet theory that the exponents must satisfy the condition  $\rho_1 + \rho_2 = -1/\beta_c$ . Therefore there must also be (N-1)M+1 Floquet exponents equal to  $-1/\beta_c$ . If all of the other Floquet exponents are less than zero then the in-phase solution of the coupled 1-d array is (linearly) neutrally stable. If any of the other Floquet are greater that zero then the in-phase solution is unstable. In either case, the in-phase solution is not linearly stable.

Notice that it was possible to make a statement about the stability of the solution without specifying the particular characteristics of the junctions and without performing any numerical calculations. The essential feature of this argument is that it is possible to find a transformation that makes some of the equations that describe the perturbations to the in-phase solution equivalent to an equation that describes the evolution of a perturbation to the solution of an autonomous system. Autonomous systems always have at least one zero Floquet exponent because they are invariant with respect to translations in time. The autonomous system in this case is Eqn. 9.5 which describes the dynamics of a single junction.

In order to stabilize the in-phase oscillations one must alter the solution so that it no longer maps onto an autonomous system. For instance adding a load across the array alters the structure of the in-phase solution (see Fig.

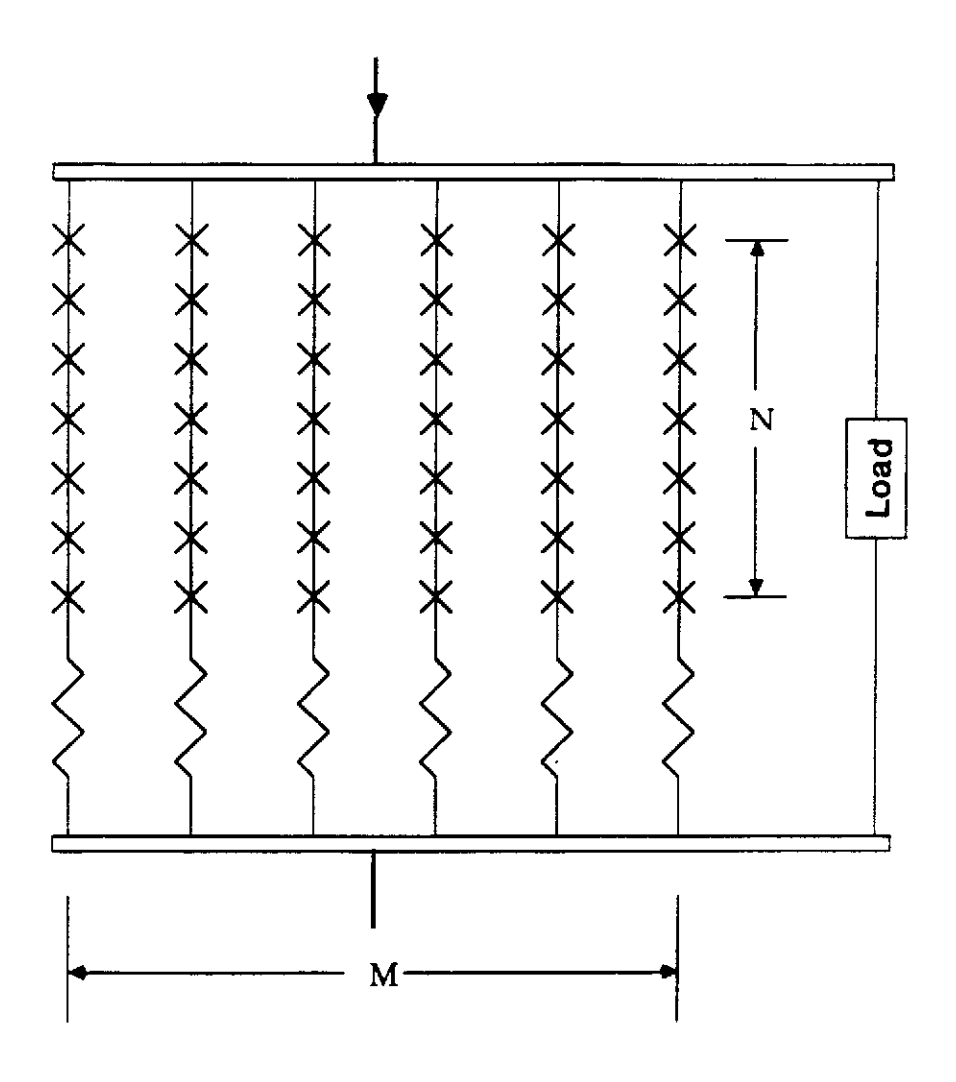


Fig. 9.2 - The coupled 1-d array of Fig. 9.1a is altered by adding a shunt impedance. This changes the structure of the in-phase solution so that it no longer decouples into independent subsystems. The shunt may stabilize the in-phase oscillations.

9.2). With the load included, Eqn. 9.9 is unchanged but the in-phase solution is now defined by,

$$M(\beta_c \ddot{\varphi}_0 + \dot{\varphi}_0 + \sin(\varphi_0)) + I_L = I_B$$
 9.13

where  $I_L$  is the current that flows through the load. In this case  $\dot{\phi}_O$  no longer solves Eqn. 9.9 and a full numerical calculation of the stability is required. This leaves open the possibility that regimes can be found where the in-phase solution is stable.

Before the load was added the array was symmetric in the sense that every path that the bias current could choose to follow was identical. In this case we found that the symmetric (in-phase) solution was not linearly stable. After the load was added a symmetry was broken because not all of the paths that the bias current could choose were equivalent. Once this symmetry is broken it is possible that the symmetric solution can be linearly stable.

Next consider the 2-d array of Fig. 9.1b. This system has been studied extensively for low bias currents where it can be described by the 2-d X-Y model. Here we consider higher bias currents which cause oscillations to arise in the junctions due to the ac Josephson effect. In particular, we examine the stability of the phase-locked solution where all of the junctions which lie along the direction of the bias current oscillate identically. This will be a zero temperature, zero applied magnetic field analysis, and all of the junctions will be assumed to be identical. Even with these simplifying assumptions the system still displays complex dynamics.

It is convenient to work with the phases of the superconductors in this case rather that the phase differences across the Josephson junction. Figure 9.3 shows an array of junctions and the two superconducting electrodes

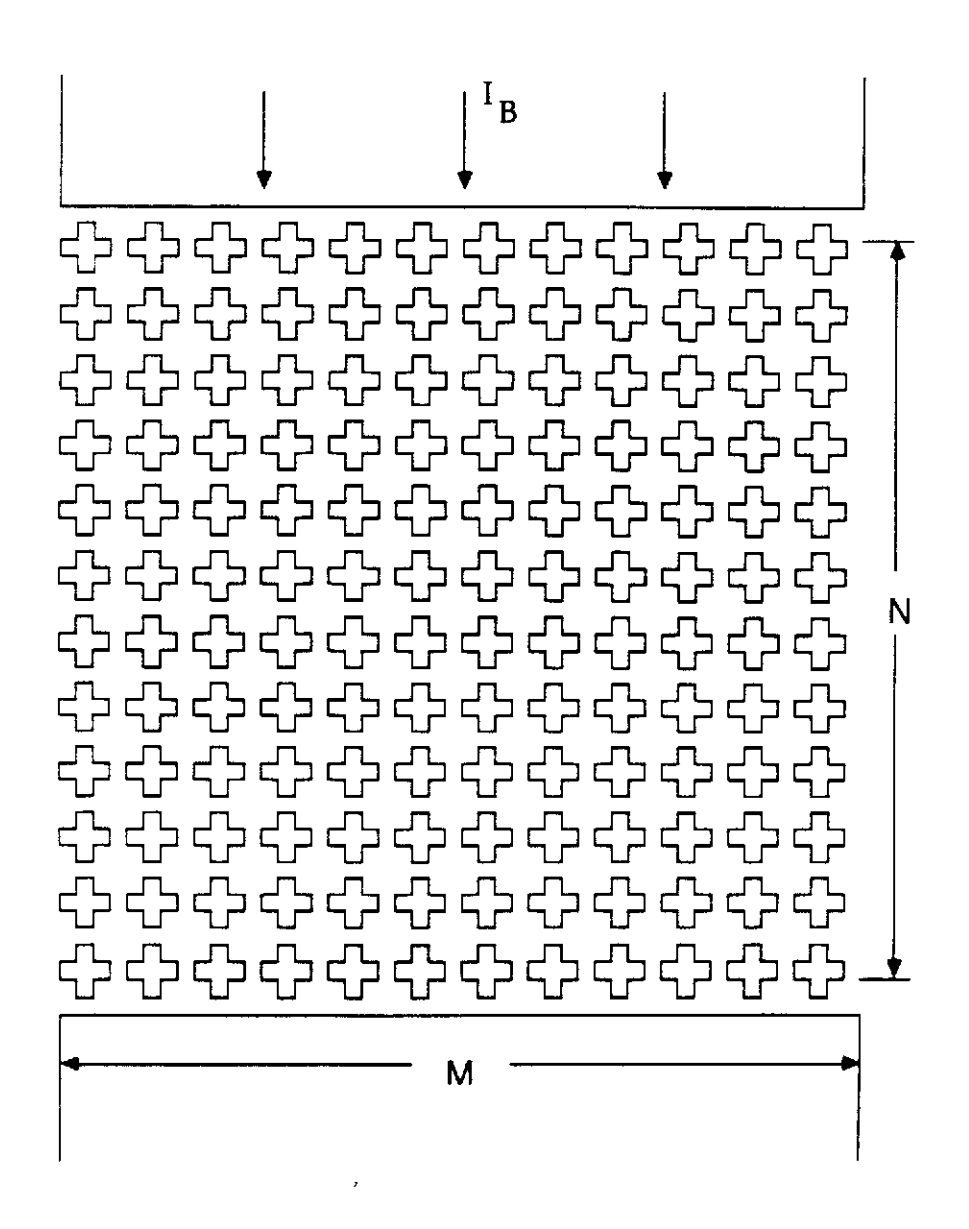


Fig. 9.3 A 2-d array of Josephson junctions. The cross shaped regions represent islands of superconductors.

which the supply the bias current. The array consists of cross shaped islands of superconductors. There are M islands in each row and N islands in each column. Josephson junctions are formed at the boundaries of the islands where the superconductors are weakly coupled. For simplicity we will describe the state of each island and each electrode by a single phase,  $\gamma$ . We will choose the phase of the upper electrode to be zero. The equations for the array can then be written as

$$\sum_{kl=n,n,\ of\ ij} \beta_c(\ddot{\gamma}_{ij} - \ddot{\gamma}_{kl}) \ + \ (\dot{\gamma}_{ij} - \dot{\gamma}_{kl}) \ + \ sin(\gamma_{ij} - \gamma_{kl}) \ = \ 0 \qquad \qquad 9.14a$$

$$\sum_{j} \beta_{c}(\dot{\gamma}_{1j}) + (\dot{\gamma}_{1j}) + \sin(\gamma_{1j}) = -I_{B}$$
9.14b

where the first equation is the statement of the conservation of current at each island (the sum is over the nearest neighbors of the island at position i,j) and the second equation states that the bias current, I<sub>B</sub>, must be equal to the total current flowing through the array (the sum is over the first row). There is one second order equation for every superconducting island, and one more second order equation for the unspecified electrode.

There is a symmetric, phase-locked solution to these equations where a current of  $I_B/M$  flows through each column of the array and each junction along the columns oscillates identically. We will call this solution the inphase solution for a 2-d array. The currents that flow through the junction depend on the difference of the phases of the adjacent superconductors so the statement that the current flowing through every column is the same is equivalent to saying that the phase difference between any pair of junctions along a column is the same,  $\gamma_{ij}$ - $\gamma_{(i-1)j} = \gamma_{kl}$ - $\gamma_{(k-1)l} = \phi_0$ . In the in-phase solution the junctions perpendicular to the direction of the applied bias current do not oscillate at all  $(\gamma_{ij} = \gamma_{i(j+1)})$ . The equation for  $\phi_0$  is,

$$\beta_c(\ddot{\varphi}_o) + (\dot{\varphi}_o) + \sin(\varphi_o) = I_B/M \qquad 9.15$$

The stability of the in-phase solution can be studied by considering small perturbations to it. The linearized equations for the evolution of these perturbations are,

$$\sum_{k|=n,n,\text{ of }ij} \{\beta_{c}(\hat{\eta}_{ij} - \hat{\eta}_{kl}) + \hat{\eta}_{ij} - \hat{\eta}_{kl}\} + \sum_{k=n,n,\text{ of }ij} (\eta_{ij} - \eta_{kj}) \cos(\phi_{0}) + \sum_{l=n,n,\text{ of }ij} (\eta_{ij} - \eta_{il}) = 0$$
9.16a

$$\sum_{i} \beta_{c} \ddot{\eta}_{1j} + \dot{\eta}_{1j} + \eta_{1j} \cos(\phi_{0}) = 0$$
 9.16b

These are linear differential equations with periodic coefficients. Again, from Floquet theory we know that the solutions to these equations have the form,  $e^{\rho t}\chi(t)$ , where  $\rho$  is the Floquet exponent and  $\chi(t)$  is a periodic function.

It is convenient to eliminate one column of the  $\eta$  coordinates in favor of a row coordinate,  $\vartheta_i = \sum_j \eta_{ij}$ . When this transformation is made, N of the linear equations that must be solved have the form

$$\beta_c \ddot{\vartheta}_i + \dot{\vartheta}_i + \vartheta_i \cos(\varphi_0) = 0 \qquad i=1,2,...,N \qquad 9.17$$

These are a special subset of the equations for the evolution of the perturbations because they can be readily solved. We observe that one of the solutions to Eqn. 9.17 is  $\vartheta_i = \mathring{\phi}_0$ . (One can check this by differentiating Eqn. 9.15) This is a periodic solution so the Floquet exponent is zero. In fact, this same solution solves all N of the above equations [9.17] so there are N Floquet exponents equal to zero. These N zero Floquet exponents imply that each row of the array acts as an autonomous subsystem.

In experiments on 2-d arrays performed at Delft by van der Zant, Muller, Geerlings, Harmans, and Mooij there is evidence that the rows do indeed act independently.<sup>41</sup> In these experiments the current-voltage (I-V) characteristics of carefully constructed 2-d arrays of Josephson junctions were measured. As the bias current was increased, steps in the voltage appear (see Fig. 9.4). There seem to be as many voltage steps as there are rows in the arrays. This implies that each row acts as a unit and starts oscillating independently. Here we suggest that one could further test the idea that the rows act as units by shunting these 2-d arrays with a series inductor-capacitor (LC) load. If the rows act as units then a shunted 2-d array of junctions would behave like a series array, and a hysteresis loop will appear in the I-V curve as the system makes transitions from the inphase to the antiphase state.

The stability analysis above does not tell us what the observed solution of a 2-d array will be, it only tells us that the in-phase solution is not linearly stable. Since the in-phase solution is the only solution with the full symmetry of the equations, the observed solution must be a symmetry broken solution. Symmetry broken solutions are always degenerate so the observed solution cannot be unique.

It may possible to modify the 2-d array, by shunting it with a load, so that the in-phase solution is linearly stable. Note that if the 2-d array is shunted by a load, then  $\phi_0$  will no longer be a solution to Eqn. 9.17 and the N Floquet exponents that were shown to be zero above could have any value. This allows for the possibility that all of the Floquet exponents could be less than zero and the in-phase solution could be linearly stable. In order to determine which load will stabilize the in-phase state of the 2-d array one

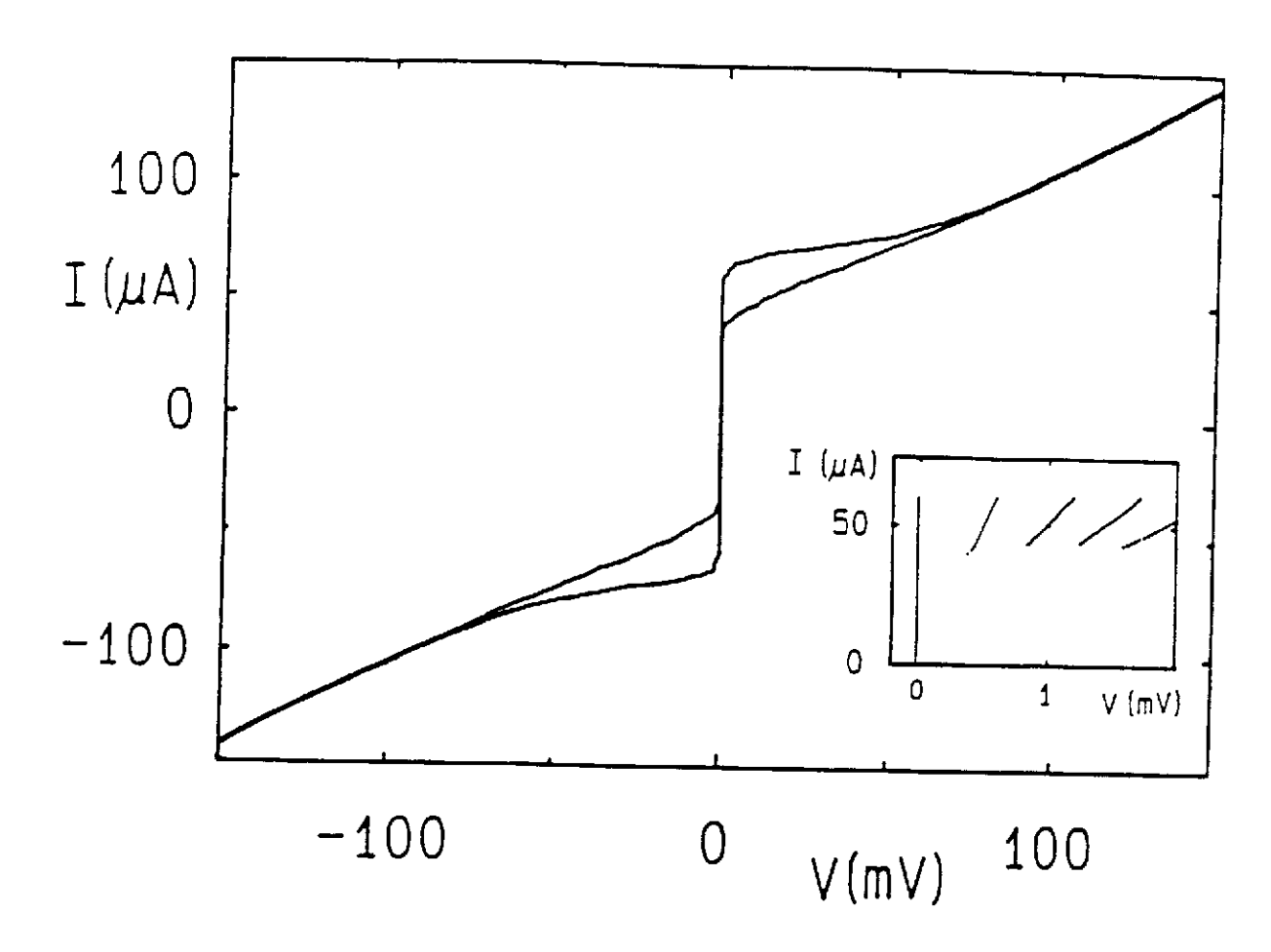


Fig. 9.4 Current-voltage curve showing steps in the voltage that suggest that the rows of a 2-d array act as independent units. (From van der Zant, Muller, Geerlings, Harmans, and Mooij.)

would have to go through the same sort of computer calculations that were described in section 4.

By arguments similar to those given above one can show that the inphase state of a 3-d array shown in Fig 9.1c is not linearly stable. In this case the plane coordinates,  $\Phi_k=\Sigma\phi_{ijk}$ , can be used to map the linearized stability equations onto an autonomous single junction problem. There are as many zero Floquet exponents as there are planes in the array and one expects the planes to act as independent subsystems.

The essential feature of the argument that shows that the in-phase solution is not stable is that the bias current must be divided equally among identical elements. If some nonidentical elements such as a shunt across the array are included in the system, then the argument fails and the in-phase solution might be stable. Thus, if the array is perfectly symmetric then the symmetric (in-phase) solution is not linearly stable but if the array is not perfectly symmetric then the in-phase solution can be linearly stable.

### §10. Conclusions

The dynamics of Josephson junction arrays is a topic that lies at the intersection of the fields of nonlinear dynamics and Josephson junction technology. Such arrays are high dimensional nonlinear systems of a type for which little was previously known. Numerical simulations were used to examine this system and several unusual dynamical states were discovered. Three distinct types of periodic solutions to the array equations were observed as well as period doubled and chaotic solutions. One of the periodic solutions is the symmetric in-phase solution where all of the junctions oscillate identically. The other two periodic solutions are symmetry-broken solutions where all of the junctions do not oscillate identically. The symmetry-broken solutions are highly degenerate. As many as (N-1)! stable solutions can coexist for an array of N junctions. These many stable solutions crowd phase space and make the system sensitive to noise. Understanding the stability of the several solutions and the transitions between them is vital to the design of useful devices.

From the technological point of view the most useful dynamical state of Josephson junction arrays is the in-phase state where all of the junctions oscillate identically. A detailed analysis of the stability of the in-phase state was given and the fluctuations about the in-phase state were described. The transitions among the periodic solutions was also discussed in terms of the language of bifurcation theory. This system exhibits both simple and multiple bifurcations. Using this analysis, the conditions for maximal stability of series junction arrays intended as mm-wave generators were established. The most important design criterion is that  $\beta_{C}\approx 1$  for stable in-phase oscillations. The other technological application that was discussed is parametric amplification. It was shown that parametric amplifiers basically

exploit the dynamical instabilities of the system. Here a proposal is made for the design of a high gain parametric amplifier that uses a previously undocumented bifurcation. Finally more complex arrays than series arrays were considered. For symmetric arrays consisting of only identical junctions the symmetric (in-phase) solution is not linearly stable and symmetry broken solutions must be observed. The symmetric solution can be stable only if the array is not perfectly symmetric.

## Appendix A: The nature of chaos

Chaotic solutions look complicated; there seems to be no simple way to specify a chaotic solution. In fact, Shaw showed that as a chaotic solution evolves it is constantly generating information. Thus to describe the entire evolution of a chaotic solution would require an infinite amount of information. However, in order to specify a solution all one needs to do is give a differential equation along with a set of initial conditions. To see where the infinite amount of information is lurking when a chaotic solution is specified by a differential equation we need to examine both the nature of the equations and the initial conditions. We proceed by discussing two seemingly unrelated subjects: random number generators and uncomputable numbers.

#### Random number generators

When people are trying to model a random process they usually use a random number generator. A simplistic, though commonly used random number generator, is the linear congruential generator,<sup>20</sup>

$$x_{k+1} = ax_k + c \pmod{m}$$
 A1

This recurrence relation takes the seed  $(x_k)$ , multiplies it by a large constant (a), adds another constant (c), and then maps the result into the interval (0,m). When the constants are properly chosen this relation produces an apparently random string of numbers between 0 and m. Better random number generators exist but this one has the two essential features of all random number generators. These two features are stretching (multiplying by a large constant) and folding (mapping the result into a compact region).

The stretching and folding make the random number generator sensitive to the initial seed  $(x_0)$  that is chosen. This sensitivity to initial conditions is illustrated in Fig. A1. The two dots in the first frame of the figure represent two slightly different initial choices. At each stretching these two solutions move farther and farther apart. No matter how close the two dots start out they eventually diverge.

Sometimes nature constructs crude random number generators of its own. The same processes of stretching and folding can then make these natural systems sensitive to initial conditions. Naturally occurring random number generators are called chaotic systems. Figure A2 shows the chaotic dynamics exhibited by a Josephson junction array. There is no apparent pattern to this solution. By taking a cross section of the solution we can see its delicate layered structure (see Fig. A3). This looks similar to the cross section of a croissant since both are produced by the same type of stretching and folding.

## Uncomputable numbers

A number is computable if there exists a finite computer program to compute that number. For instance, 7,  $\pi$ , e, and  $\sqrt{2}$  are computable numbers since you can write finite computer programs to calculate these numbers. Indeed every number that has ever been specified, and every number that will ever be specified is computable by definition. This leaves one wondering if there are any uncomputable numbers. The existence of the uncomputable numbers can be demonstrated by an argument that roughly parallels the proof of Gödel's famous incompleteness theorem.<sup>43</sup> The incompleteness theorem states that there are truths in any formal system of reasoning that are not theorems of that system of reasoning. The parallel argument is the following.

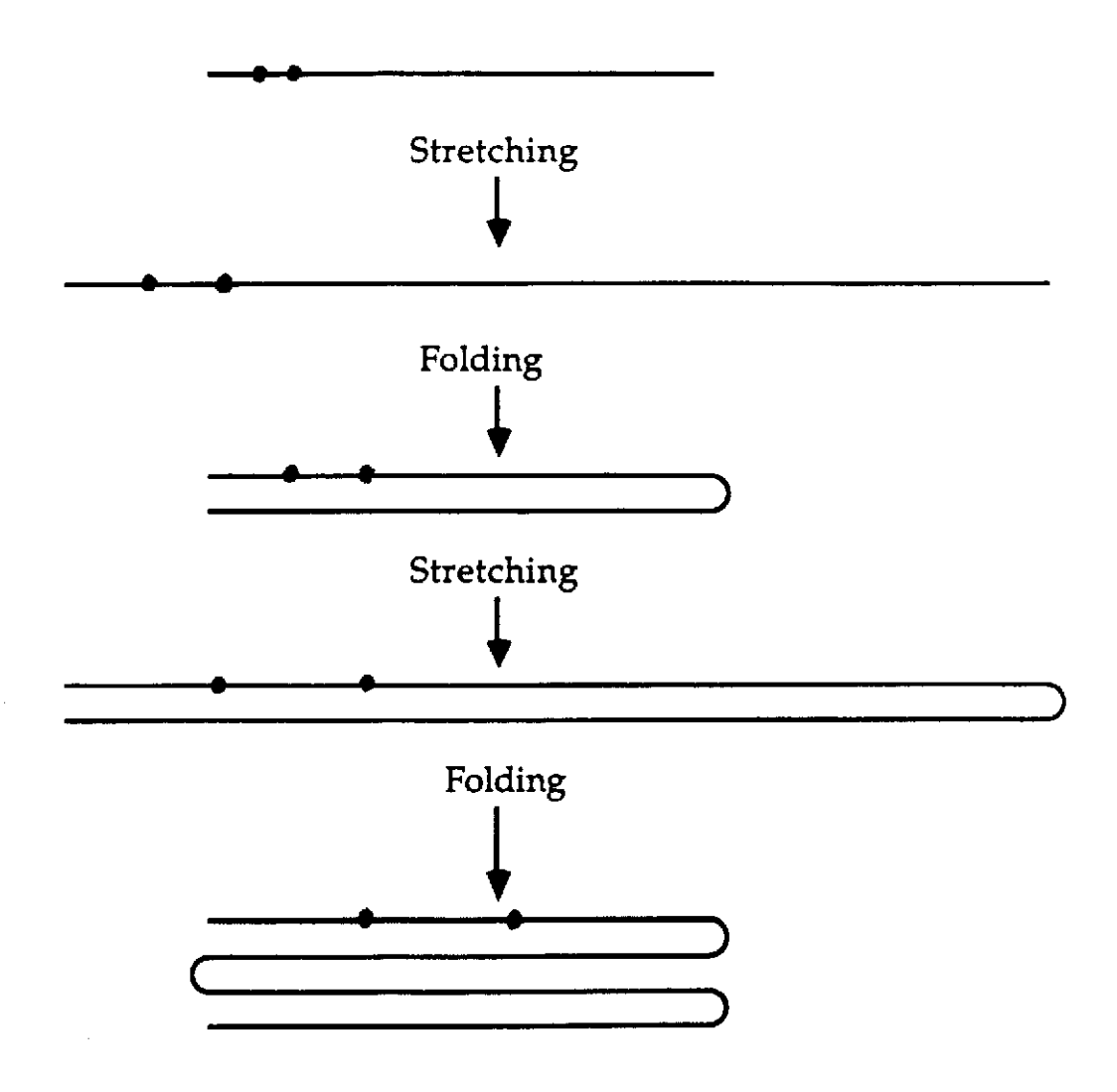


Fig. A1 - Random number generator use stretching and folding to produce an apparently random sequence. Sensitivity to the initial conditions is illustrated by the two dots in the figure. They start out close together but as the stretching and folding proceeds the dots diverge.

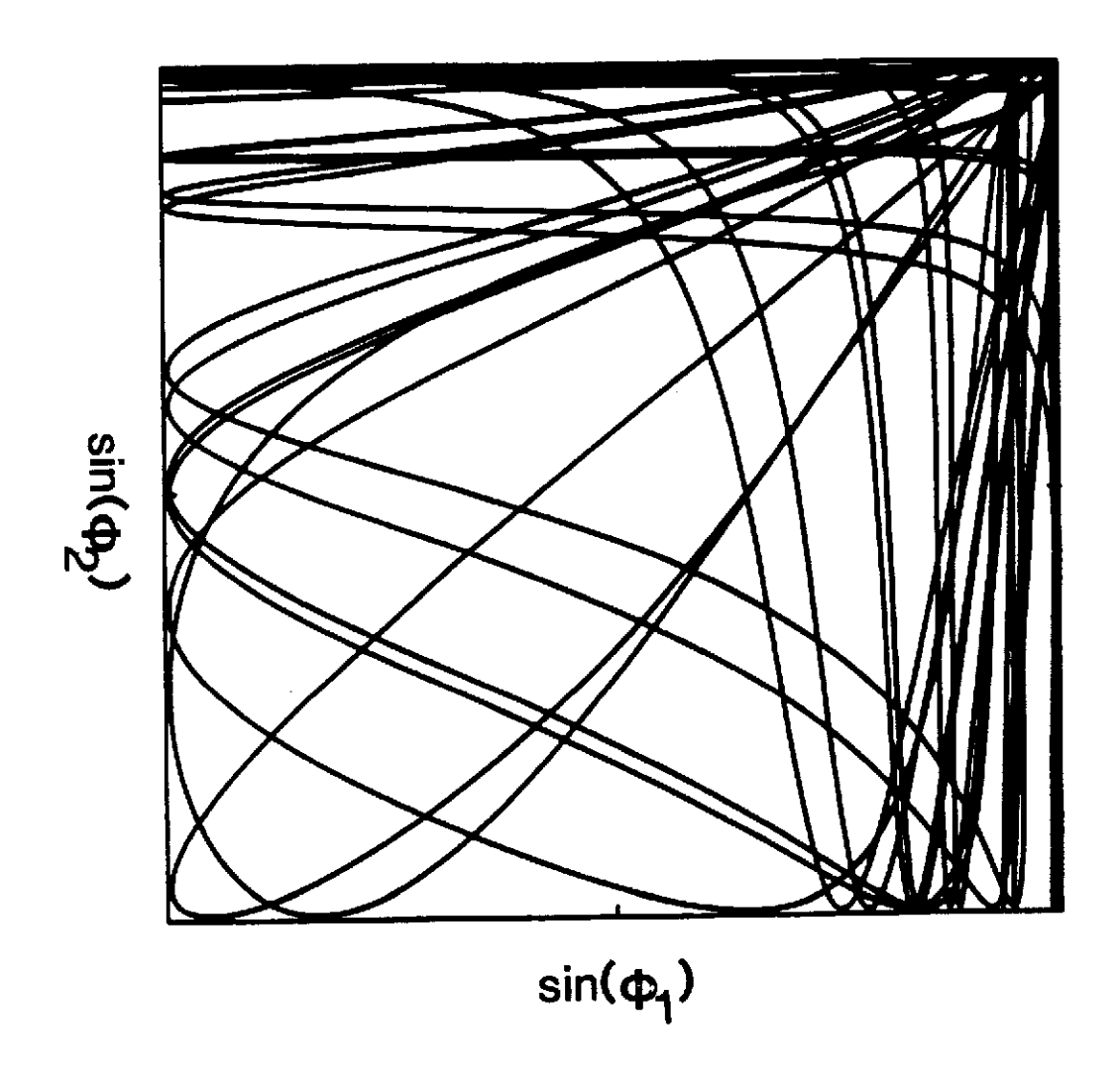


Fig. A2 - Chaotic solution of a two junction series array,  $\beta_{\text{C}}\text{=-}1,\,I_{\text{B}}\text{=-}1.2$ 

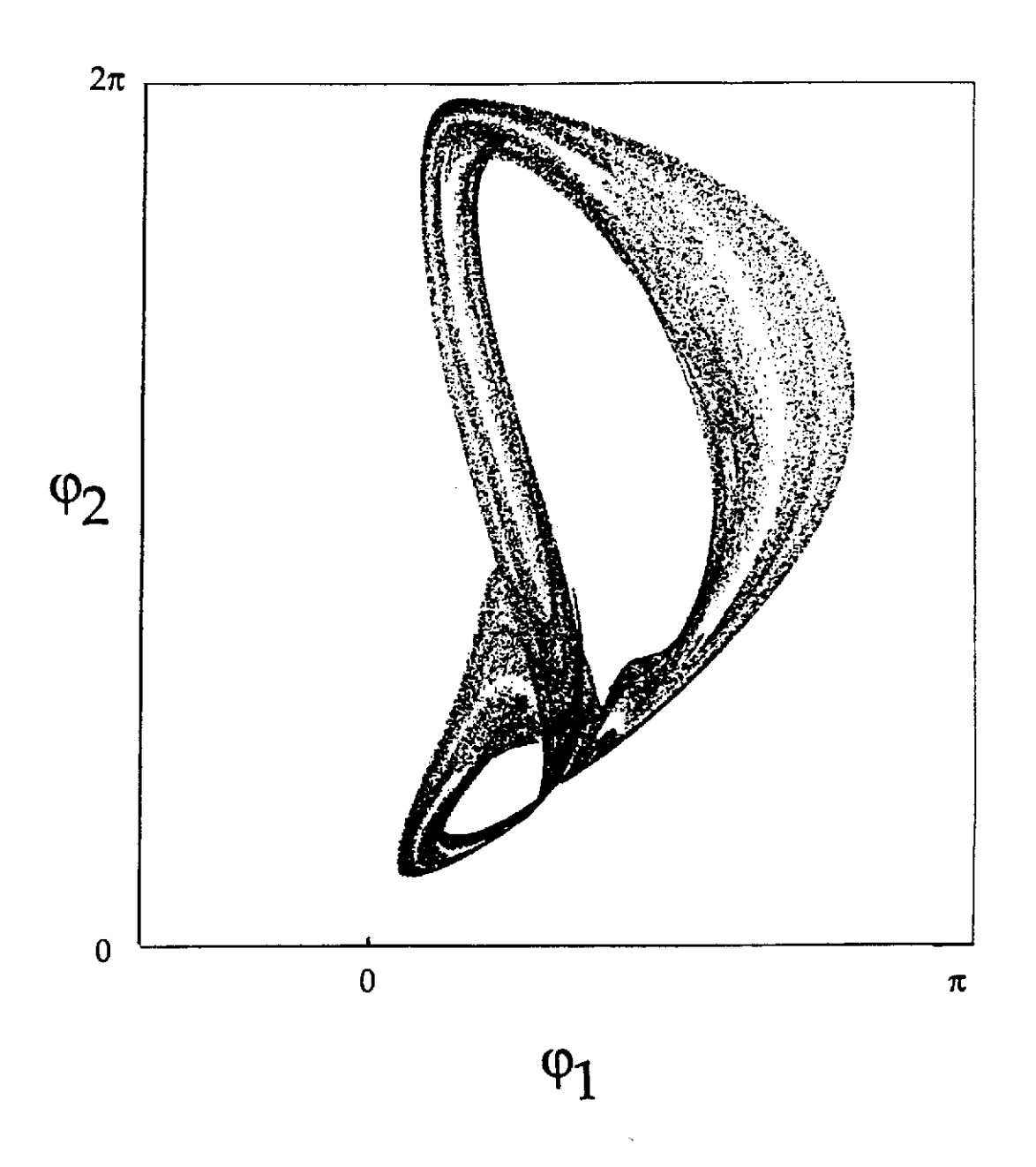


Fig. A3 - Cross section of a chaotic solution (often called a Poincare section) showing the layered (fractal) structure of the solution.

Suppose that a certain computer understands 100 instructions. Give each instruction a two number code, 00 through 99. Then any program can be represented as an integer which is just the two number instruction codes strung together. If a number is computable then it can be computed on our hypothetical computer by Church's thesis.<sup>43</sup> So for every computable number there is a computer program, and for every computer program there is an integer. Since the integers form a set of measure zero on the real axis, the computable numbers must also form a set of measure zero. This means that almost every number is uncomputable and cannot be specified with a finite amount of effort.

A consequence of the existence of uncomputable numbers is the existence of uncomputable functions. A function can be described by a differential equation along with a set of initial conditions. If the initial condition contain an uncomputable number (and almost every number is uncomputable) then since no finite computer program exists which can specify the initial condition, no finite computer program exists that specifies the solution. Thus, almost every function described by differential equations is uncomputable. Normally this does not cause a problem because regular equations are not sensitive to the initial conditions. Changing the initial conditions slightly only changes the solution slightly. Chaotic solutions, however, are sensitive to the initial conditions. Changing the initial conditions of a chaotic solution slightly, however, eventually changes the solution dramatically. The consequence of all this is that anything that is sensitive to initial conditions will have chaotic solutions that cannot be specified with a finite amount of effort.

The existence of these uncomputable, chaotic solutions creates a problem for anyone wishing to calculate a solution using perturbation theory. A perturbation theory is a finite algorithm for finding corrections to a known solution. The finite algorithm and the known solution can be specified by a finite computer program so the end product of any perturbation theory is a computable function. Thus chaotic solutions can not be found by perturbation theory. We usually say the perturbation theory "breaks down" before the chaotic solution is reached.

# Appendix B: Stability of N-dimensional periodic solutions

This appendix describes how to analyze the stability of a periodic solution of a N-dimensional equation. We assume that we already have the vector solution, x, to some nonlinear N-dimensional equation.

$$\dot{x} = F(x,t)$$
 B1

To find the stability of this solution we add a small perturbation, v, to x and then linearize the Eqn. B1. This results in a linear system with periodic coefficients.

$$\dot{v} = f(t)v$$
 B2

where v is an N component column vector and  $f(t)=\partial F_i/\partial x_j$  is the Jacobian matrix of first partial derivatives of F. Because x is periodic, f is also periodic, f(t)=f(t+T). Equation B2 can be analyzed with an extension of standard Floquet theory to the N-dimensional case. For further discussion of this topic see *Nonlinear Oscillations* by Nayef and Mook.<sup>25</sup>

From the theory of linear differential equations we know that there is a complete set of N linearly independent vector solutions,  $\mathbf{v}_j(t)$  j=1,2,...,N, to this equation. In general it is difficult to calculate the complete solutions,  $\mathbf{v}_j(t)$ , analytically. It is straightforward, however, to calculate the solutions numerically and then use return maps to analyze their stability. To do this first we note that if  $\mathbf{v}_j(t)$  is a solution then so is  $\mathbf{v}_j(t+T)$ . Since the functions  $\mathbf{v}_j(t)$  form a complete set we can write,

The matrix, A, is called a return map. It specifies how the  $v_j(t)$ 's evolve in time. A return map can be constructed by taking any linearly independent set of column vectors,  $v_j$ , as initial conditions, and numerically integrating

the equations over one period. The initial vectors,  $v_j(t=0)$ , and the final vectors,  $v_j(T)$ , can then be arranged into matrices that are related by the expression,

$$\left(\left(\begin{array}{c} v_1(T) \end{array}\right) \dots \left(\begin{array}{c} v_N(T) \end{array}\right) = A \left(\left(\begin{array}{c} v_1(0) \end{array}\right) \dots \left(\begin{array}{c} v_N(0) \end{array}\right) \right)$$
 B4

It is convenient to choose the initial vectors so that they form the identity matrix. Then the return map is simply

$$A = \left( \left( v_1(T) \right) \dots \left( v_N(T) \right) \right)$$
 B5

In general when we construct A in this way it will not be in diagonal form. If the eigenvalues are all distinct we can put A into its diagonal form, B, by applying a transformation P.

$$B = P^{-1} AP$$
 B6

Both B and P can be determined numerically. Once we have B and P we can define a new set of vectors, uk, by the transformation,

$$v_i(t) = Pu_i(t)$$
. B7

The matrix B tells us how these new variables evolve in time,

$$u_{j}(t+T) = Bu_{j}(t).$$
 B8

Since B is diagonal, we can write this in component form,

$$u_j(t+T) = \lambda_j u_j(t),$$
 B9

where the  $\lambda_j$  are the eigenvalues of B. Let  $\lambda_j = e P_i^T$ , and multiply the last equation by  $e^{-p(t+T)}$ , then we have,

$$e^{-\rho(t+T)} u_j(t+T) = e^{-\rho_j t} u_j(t)$$
. B10

This equation tells us that the function,  $e^{-\rho_i t} u_j(t)$ , is periodic with period T. Let's call this periodic function  $\chi_j(t)$ . Now we can write the N linearly independent solutions to Eqn. 1 in the traditional form of Floquet theory,

$$u_j(t) = e^{\rho t} \chi_j(t)$$
. B11

where the  $\rho_{\boldsymbol{j}}$  are the Floquet exponents,

$$\rho_j = \ln(\lambda_j)/T,$$
B12

and the  $\chi_{\hat{\boldsymbol{j}}}(t)$  are periodic functions,

$$\chi_{j}(t) = e^{-\rho_{j}t} P^{-1} v_{j}(t).$$
 B13

Now that the perturbations to the original solution have been put into Floquet form we can say that the periodic solution, x, will be stable when all of the Floquet exponents are negative.

#### Appendix C: Some mathematical details

This appendix describes how one solves inhomogeneous differential equations such as those encountered in the section on fluctuations. The equation that must be solved is,

$$\beta_c \ddot{\vartheta} + 2\dot{\vartheta} + \cos(\varphi_o)\vartheta = \frac{1}{N} \sum_{k} \xi_k + \xi_L$$
 C1

where  $\phi_0$  solves the nonlinear equation,

$$\beta_c \ddot{\varphi}_o + 2\dot{\varphi}_o + \sin(\varphi_o) = I_B$$
 C2

By differentiating Eqn. C2 one can see that one of the homogeneous solutions to Eqn. C1 is  $\phi_0$ . Once one homogeneous solution is known the other can be found by the method of reduction of order.<sup>44</sup> Briefly this method consists of assuming a solution to Eqn. C1 of the form  $y(t)\phi_0$ . Substituting this into the equation results in a first order equation for y(t) which can be solved by separation of variables. The two homogeneous solutions to Eqn. C1 are then,

$$\vartheta_{\parallel} = \dot{\phi}_{o}$$
 and  $\vartheta_{\perp} = \dot{\phi}_{o}(t) \int_{0}^{t} \frac{e^{-2t'/\beta_{c}}}{\dot{\phi}_{o}^{2}(t')} dt'$  C3

The inhomogeneous solution to Eqn. C1 can be constructed from the homogeneous solutions. First write Eqn. C1 in matrix form as a coupled set of first order equations in the form,

$$\dot{X} = AX + \Xi$$
 C4

where x is a vector and A is a Matrix. The solution to any set of coupled first order equations in this form is

$$x = \Phi \Phi^{-1} = dt$$
 C5

where  $\Phi$  is a matrix whose columns are the vector solutions to the homogeneous equation

$$\dot{x}_0 = Ax_0$$

Using these concepts one can show that the inhomogeneous solution to Eqn. C1 is,

$$\vartheta = \dot{\phi}_{0} \int_{-\frac{1}{N}}^{t} \frac{(\frac{1}{N} \sum_{k} \xi_{k} + \xi_{L}) \dot{\phi}_{0}(t')}{e^{-2t''/\beta_{c}}} \int_{-\frac{1}{N}}^{t'} \frac{e^{-2t''/\beta_{c}}}{\dot{\phi}_{0}^{2}(t'')} dt'' dt'$$

$$+ \dot{\phi}_{o} \int_{t}^{t} \frac{(\frac{1}{N} \sum_{k} \xi_{k} + \xi_{L}) \dot{\phi}_{o}(t')}{e^{-2t'/\beta_{c}}} dt' \int_{t}^{t} \frac{e^{-2t'/\beta_{c}}}{\dot{\phi}_{o}^{2}(t')} dt'$$

This inhomogeneous solution can be separated into phase fluctuations and transverse fluctuations.

If the noise were to somehow only to perturb the system along the inphase trajectory then the inhomogeneous solution would be

$$\vartheta = \vartheta_{\parallel} \int \frac{\xi_{\parallel}}{\vartheta_{\parallel}} dt$$
 C8

where  $\xi_{11}$  is the noise that only perturbs the system only the trajectory. These are the phase fluctuations. Furthermore, if the noise were only to perturb the system transverse to the in-phase trajectory then the inhomogeneous solution would be

$$\vartheta = \vartheta_{\perp} \int \frac{\xi_{\perp}}{\vartheta_{\perp}} dt$$

where  $\xi_{\perp}$  is the noise that only perturbs the system transverse to the trajectory. These are the transverse fluctuations.

The noise terms given in Eqn. C1 constitute the noise along and the noise transverse to the trajectory,  $\xi_{1|}+\xi_{\perp}=(1/N)\sum_{k}\xi_{k}+\xi_{L}$ . Using this constraint and comparing Eqn. C8 and Eqn. C9 with Eqn. C7 we see that the phase fluctuations,  $\psi$ , and the transverse fluctuations, x, associated with Eqn. C1 are,

$$\psi = -\int^{t} \frac{(\frac{1}{N}\sum_{k} \xi_{k} + \xi_{L})\dot{\phi}_{o}(t')}{\beta_{c}e^{-2t'/\beta_{c}}} \int^{t'} \frac{e^{-2t''/\beta_{c}}}{\dot{\phi}_{o}^{2}(t'')} dt''dt'$$
C10

$$x = \vartheta_{\perp} \int_{0}^{t} \frac{\left(\frac{1}{N} \sum_{k} \xi_{k} + \xi_{L}\right) \dot{\phi}_{0}}{\beta_{c} e^{-2t'/\beta_{c}}} dt'$$

$$C \quad 1 \quad 1$$

#### References

- 1. B. D. Josephson, Phys. Lett. <u>1</u> 251 (1962).
- P. W. Anderson and J. M. Rowell, Phys. Rev. Lett. <u>10</u> 230 (1963);
   Shapiro, Phys. Rev. Lett. <u>11</u> 80 (1963);
   J. M. Rowell, Phys. Rev. Lett. <u>11</u> 200 (1963).
- 3. B. A. Huberman, J. P. Crutchfield, and N. Packard, Appl. Phys. Lett. <u>37</u> 750 (1980); R. C. Kautz, J. Appl. Phys. <u>52</u> 624 (1981).
- 4. E. Fermi, Collected Papers Vol. II (University of Chicago Press, Chicago, 1965) p. 978.
- 5. A. J. Lichtenberg and M. A. Lieberman, Regular and Stochastic Motion (Springer-Verlag, New York, 1983).
- B. V. Chirikov, Phys. Rep. <u>52</u> 265 (1979); T. Hogg and B. A. Huberman,
   Phys. Rev. A <u>29</u> 275 (1984); J. Keeler and J. D. Farmer, Physica <u>23D</u> 413 (1987);
   P. N. Strenski and S. Doniach, J. Appl. Phys. <u>57</u> 867 (1985).
- 7. R. L. Kautz, C. A. Hamilton, F. L. Lloyd, IEEE Trans. <u>MAG-23</u> 883 (1987); IEEE Trans. IM-36 258 (1987).
- 8. A. K. Jain, K. K. Likharev, J. E. Lukens, and J. E. Sauvageau, Phys. Rep. <u>109</u>, 310 (1984).
- 9. P. Hadley and M. R. Beasley, Appl. Phys. Lett. <u>50</u> 621 (1987).
- 10. P. Hadley and M. R. Beasley, Jap. J. of Appl. Phys. 26 1419 (1987).
- 11. P. Hadley, M. R. Beasley and K. Wiesenfeld, Appl. Phys. Lett. <u>52</u> 1619 (1988).
- 12. P. Hadley, M. R. Beasley and K. Wiesenfeld, Phys. Rev. B 38 8712 (1988).
- 13. P. Hadley, M. R. Beasley and K. Wiesenfeld, IEEE Trans. Mag. (to be published).

- 14. W. C. Stewart, Appl. Phys. Lett. <u>12</u> 277 (1968); D. E. McCumber, J. Appl. Phys. <u>39</u> 3113 (1960).
- 15. K. K. Likharev, Dynamics of Josephson Junctions and Circuits (Gordon and Breach Science Publishers, New York, 1986).
- 16. T. Van Duzer and C. W. Turner, Principles of Superconductive Devices and Circuits (Elsevier, New York, 1981), p.170.
- 17. S. Shapiro, Phys. Rev. Lett. 11 80 (1963).
- 18. J. J. Stoker, Nonlinear Vibrations in Mechanical and Electrical Systems (Interscience Publishers, Inc., New York, 1950).
- 19. D. R. Tilley, Phys. Lett. 33A 205 (1970).
- 20. W. H. Press, B. P. Flannery, S. A. Teukolsky, and W. T. Vetterling, *Numerical Recipes* (Cambridge University Press, New York, 1986).
- 21. T. D. Clark, Phys. Lett. 27 585 (1968).
- 22. T. F. Finnegan and S. Wahlsten, Appl. Phys. Lett. <u>21</u> 541 (1972).
- 23. K. Wiesenfeld and P. Hadley, (to be published).
- 24. M. J. Feigenbaum, J. Stat. Phys. <u>19</u> 25 (1978); <u>21</u> 669 (1979).
- 25. A. H. Nayfeh and D. T. Mook, *Nonlinear Oscillations* (Wiley, New York, 1979); W. Magnus and S. Winkler, *Hill's Equation* (Dover, New York, 1979).
- 26. N. N. Bogoliubov and I. A. Mitropolskii, Asymptotic Methods in the Theory of Nonlinear Oscillations (Hindustan Pub. Corp., Delhi, 1961).
- 27. G. S. Lee and S. E. Schwarz, J. Appl. Phys. <u>55</u> 1035 (1984).
- 28. Y. Pomeau and P. Manneville, Commun. Math. Phys. 74 189 (1980).
- 29. J. Guckenheimer and P. Holmes, Nonlinear Oscillations, Dynamical Systems, and Bifurcations of Vector Fields (Springer-Verlag, New York, 1983).

- 30. J. W. Swift and K. Wiesenfeld, Phys. Rev. Lett. <u>52</u> 705 (1984).
- 31. See for example, M. Golubitsky and J. Guckenheimer, eds., *Multiparameter Bifurcation Theory*, Contemporary Mathematics <u>56</u>, (American Mathematical Society, Providence, 1986).
- 32. C. Varmazis, R. D. Sandell, A. K. Jain, and J. E. Lukens, Appl. Phys. Lett. <u>33</u> 357 (1987).
- 33. R. F. Miracky, J. Clarke, and R. H. Koch, Phys. Rev. Lett. <u>50</u>, 856 (1983).
- 34. K. Wiesenfeld, J. Stat. Phys. <u>38</u> 1071 (1985).
- 35. K. Wiesenfeld, "Period Doubling Bifurcations, What Good Are They Anyway?" *Noise in Nonlinear Dynamical Systems* F. Moss ed. (Cambridge University Press, Cambridge, 1988).
- 36. H. Zimmer, Appl. Phys. Lett. <u>10</u> 193 (1967); A. S. Clorfeine, Proc. IEEE <u>52</u> 844 (1964).
- 37. P. Bryant, K. Wiesenfeld, and B. McNamara, J. Appl. Phys. 62 2898 (1987).
- 38. M. J. Feldman, P. T. Parrish, and R. Y. Chiao, J Appl. Phys. 46 4031 (1975).
- 39. J. H. Wilkinson, *The Algebraic Eigenvalue Problem* (Oxford University Press, New York, 1965).
- 40. C. J. Lobb, D. W. Abraham, and M. Tinkham, Phys. Rev. B 27 150 (1983).
- 41. H. S. J. van der Zant, C. J. Muller, L. J. Geerligs, C. J. P. M. Harmans, and J. E. Mooji, Phys. Rev. B <u>38</u> 5154 (1988).
- 42. R. Shaw, Zeitschrift für Naturforschung 36a 80 (1981).
- 43. G. S. Boolos and R. C. Jeffrey, Computability and Logic (Cambridge University Press, New York, 1980).
- 44. C. M. Bender and S. A. Orszag, Advanced Mathematical Methods For Scientists and Engineers (McGraw-Hill, New York, 1978).